EMULSION-BASED SYNTHESIS AND CHARACTERIZATION OF BIPHASIC JANUS PARTICLES FOR DUAL DRUG DELIVERY

by

Jennifer Sherri Winkler

A dissertation submitted to the

Graduate School-New Brunswick

and

The Graduate School of Biomedical Sciences

Rutgers, The State University of New Jersey

In partial fulfillment of the requirements

For the degree of

Doctor of Philosophy

Graduate Program in Biomedical Engineering

Written under the direction of

Professor M. Silvina Tomassone

And approved by

_____

_____

_____

_____

New Brunswick, New Jersey

May 2016

ABSTRACT OF THE DISSERTATION

Emulsion-Based Synthesis and Characterization of Biphasic Janus Particles for Dual Drug Delivery

by JENNIFER SHERRI WINKLER

Dissertation Director:

Professor M. Silvina Tomassone

Janus particles exhibit many unique chemical, optical, electrical, and physical properties due to their two chemically distinct surfaces. They are highly sought after for diverse applications across many fields including electronics, energy, catalysis, and emulsion stabilization. Janus particles also hold great promise in the field of biomedical engineering as drug delivery vehicles, theranostic platforms, and components of biosensors. As drug delivery vehicles, they offer a platform for co-encapsulating drugs with widely disparate solubility as well as independent release kinetics. However, large-scale synthesis methods are needed before Janus particles can realize their full potential in biomedicine. A novel technique based on the phase separation of two immiscible polymers and/or lipids within single O/W and double W/O/W emulsion droplets is presented for the production of Janus particles. The effects of various formulation and process variables on final Janus particle properties including particle size, stability, morphology, and encapsulation efficiency are studied. A wide range of Janus particle morphologies were synthesized, including acorn-like, spherical, crescent moon, and two nearly separated droplets. From a purely thermodynamic perspective, particle shape is a function of the interfacial tensions between the two polymers, as well as the interfacial tensions between each of the polymers and the

aqueous phase containing surfactant. These interfacial tensions are adjusted by changing the type and concentration of surfactant in the water phase, making a wide range of morphologies accessible. In order to quantifiably describe the influence of interfacial tension on particle morphology, a thermodynamic model for the prediction of Janus particle morphology was developed. The model is derived from first-principles, in which the exact shape of a Janus particle is extracted via total free energy minimization of Janus particles modeled as two overlapping semicircles. In reverse, particle geometry measurements obtained from microscopy can be applied to the model in order to explicitly calculate the volume ratio and the surface tension of each of the three interfaces. The ability to control Janus particle shape is of fundamental importance for many potential applications, as function depends on structure. Janus particles were applied to a case study involving the treatment of lung cancer with doxorubicin, a broad spectrum chemotherapeutic, and curcumin, a bioflavanoid with antioxidant, anti-inflammatory, and antitumor effects. The Janus particles containing doxorubicin and curcumin completely inhibited tumor growth over a four-week treatment period, attesting to the advantages of bicompartmental Janus carriers for dual drug delivery of synergistic compounds.

DEDICATION

In loving memory of my brother, Steven Ryan Winkler (1990-2013)

ACKNOWLEDGEMENTS

This dissertation was made possible by the unwavering support of all the phenomenal people who I am so very lucky to call my family, friends, and colleagues. First and foremost, I would like to express my deepest gratitude to my advisor, Professor M. Silvina Tomassone, for her constant support of my research, as well as her encouragement, enthusiasm, and patience. She believed in me from the very beginning, which gave me the confidence I needed to grow and flourish as a scientist. She has been not only my research advisor but also a great friend and role model who has helped me through many hardships I faced during this journey. I would also like to thank the other members of my thesis committee, Prof. Nina Shapley, Prof. Fernando Muzzio, and Prof. Bo Michniak, for their support and guidance. And I would be remiss if I didn't acknowledge a few extraordinary teachers who have made a lasting impact on me along the way – to Mrs. Pamela Hunter and Mrs. Heather Morningstar, thank you both for inspiring me and continuing to root for my success even though it's been ten years since I graduated from high school.

I am eternally grateful to Dr. Frank Romanski for taking me under his wing and being the best mentor I could ever ask for. Frank, I've always looked up to you and I hope you are proud of all the work I've done for the projects that you laid the groundwork for. I am also thankful to my labmates (past and present): Kurt Smith, Dr. Michael Clark, and Dr. Yangyang Shen. I've gained so much from their insight, ideas, and generous help over the years. I would like to express my gratitude to fellow graduate students Brittany Taylor, Dr. Kristin Steeley, and Dr. Krizia Karry, who I could always count on to brighten my day. I am honored to have had the privilege to mentor many undergraduate students in the lab and I would like to especially thank Jonathan Gerszberg for his significant contribution to

the nanosuspension project. I thoroughly enjoyed working with Jonathan for the past three years and I look forward to seeing his continued success as he embarks on his PhD studies.

I was fortunate enough to come to Rutgers alongside two of my classmates from the University of Rochester, Dr. Renea Faulknor and Margot Zevon. Renea, the most fortuitous random assignment of my entire life was getting you as a roommate freshman year. My best memories from both UR and RU were with you, and I will always have some really good stories from our time together. I would also like to thank the other two "Giggle heads" from our cohort, Ana Gomez and Dan Myers. You guys made me actually look forward to going to class. Our Six Flags trips, 5k races, and ski trips helped me escape from the stress of demanding coursework. Finally, I would like to thank Jill Melchior, who has been one of my closest friends since middle school. I definitely appreciated all those pool days and shopping trips whenever I needed a break from working.

Most importantly, I would like to express my gratitude to my family who made this dream possible with their unending support. I would like to thank my mom, Ellen Winkler, for being my best friend and biggest supporter. She has always been there for me through every up and down I've ever had in my life, and I am grateful that I get to celebrate this major milestone with her by my side. I am also extremely thankful for my grandparents, Betty and Arnold Abramowitz, for always believing in me and pushing me to succeed. From as far back as I could remember, my grandfather always emphasized the importance of education. His lessons of perseverance and dedication were not lost on me, and I owe a great deal of my success to him. My grandmother used to frequently ask me if I was almost done with school yet, and I wish she could be here to see the day that I can finally say I am done with school. Her kind soul and unconditional love are sorely missed. I would also like

to express my gratitude for my brother, Steven Winkler, who was my best friend growing up. I will always cherish our childhood memories of snowboarding, sledding in the backyard, playing with Legos, and playing basketball outside. I would like to thank my sister, Debbie Winkler, and my nephews, Joshua and Jordan Anderson, who I've been able to maintain a close relationship with despite the distance that separates us. I've enjoyed my yearly holiday trips to visit you guys and I hope it's a tradition that we can continue. To Josh and Jordan, I hope that when you see me walk across the stage at graduation it will inspire you to set high goals for yourselves and follow your dreams.

Table of Contents

LIST OF TABLES

LIST OF FIGURES

CHAPTER 1: INTRODUCTION

1.1 Background and Motivation

The concept of Janus particles was first introduced by P.G. de Gennes in his 1991 Nobel Laureate speech [1]. Named after the two-faced Roman god Janus, Janus particles contain two distinct surfaces with different chemistries, functionalities, and/or polarities. Janus particles can be produced from a wide variety of materials including: polymeric, inorganic, organic-inorganic, or polymeric-inorganic materials [2, 3]. In addition, Janus particles may be produced into a multitude of different morphologies, such as spheres, rods, dumbbell-like, snowman-like, acorn-like, raspberry-like, cylindrical, and disk-like [3, 4]. Strictly speaking, however, a Janus particle has two opposing surfaces of comparable surface area. This unusual structural dichotomy of Janus particles gives rise to amphiphilic, magnetic, catalytic, optical, and electric properties [3]. Due to these unique properties, Janus particles have attracted considerable attention for their propensity to serve as potential colloidal surfactants, building blocks for self-assembly into complex macrostructures, biosensors, catalysts, components of electronic paper, and drug delivery systems [5-8].

Biocompatible Janus particles have the potential to solve fundamental problems in drug delivery by offering multiple functionalities such as staggered release profiles, simultaneous delivery of chemically dissimilar compounds, and compartmentalization of multiple therapeutic or diagnostic agents. Thus, there exists a critical need to develop integrative approaches for the synthesis of biocompatible, biodegradable Janus particles for drug delivery, tissue engineering, self- assembly of biomaterials, and countless other biomedical applications. Current manufacturing techniques fail to produce anisotropic particles in quantities large enough to meet the massive demand present in the

pharmaceutical and biomedical fields. Despite significant advances in the nanotechnology field, multicompartmentalization in micro- and nanoparticles has not yet been achieved. Furthermore, due to the complex nature of colloidal systems, little is known about the functionality of Janus particles and the assessment of *in vitro* and *in vivo* benefits of Janus particles in drug delivery. This dissertation was designed to address the dearth of research focused on the design and application of Janus particles in drug delivery.

1.2 Nanotechnology-Based Drug Delivery Systems

Poor aqueous solubility is a problem faced by an increasing number of new chemical entities as well as current drug compounds [9, 10]. It is estimated that more than 40% of new chemical entities are practically water insoluble [11]. Nanotechnology-based drug delivery systems such as polymer nanoparticles, solid lipid nanoparticles, inorganic nanoparticles, liposomes, dendrimers, micelles, and nanosuspensions have traditionally been used to enhance the bioavailability of poorly soluble compounds through increased dissolution rate and increased dissolved drug levels [12]. Over the past few decades, “smart” materials have enabled targeted delivery, controlled release, and stimuli-responsive drug delivery [13]. Moreover, stealth coating of nanocarriers by hydrophilic polymers such as PEG or polysaccharides prolongs circulation time in vivo by preventing macrophage recognition and RES clearance. The attachment of targeting ligands such as antibodies, peptides, aptamers, or small molecules (i.e., folic acid) allows for cell-specific targeting. Next-generation nanotechnology drug delivery systems will likely combine therapeutics and diagnostics in a single platform. Multifunctional drug delivery vehicles will enable live tracking of treatment, image-guided therapy, co-delivery of synergistic agents, and multilevel targeting for enhanced cell/tissue specificity. Nanoparticle-based

combination therapy is an effective tool with widespread clinical applications. However, many challenges associated with nanocarriers need to be overcome before they can be fully introduced into the market.

1.3 Current Approaches to Combination Therapy Using Nanotechnology

The goal of combination treatment is to improve therapeutic efficacy while mitigating adverse side effects by utilizing multiple drugs to combat the same condition. Drug combinations are chosen based on their complementary mechanisms of action. Effective combinations inhibit disease progression by targeting multiple cellular pathways and molecular targets. Combination therapy is advantageous when using drugs with high levels of toxicity, as smaller dosages of each drug are generally needed to elicit the desired therapeutic effect.

Owing to the complex nature of cancer, combination therapy has shown great promise where monotherapies have consistently failed. Cancer cells develop chemoresistance over time after prolonged exposure to chemotherapeutic agents, and eventually, the chemotherapy is no longer effective. This phenomena accounts for most of the failed cases in cancer therapy [14]. Combination therapy has demonstrated vastly improved clinical therapeutic efficacy and reduced systemic toxicity compared to single-drug therapy, particularly in combating chemoresistance due to the fact that different chemotherapy drugs attack cancer cells at varying stages of their growth cycles [15, 16]. Another strategy for overcoming chemoresistance is to combine chemotherapy drugs with antiangiogenic agents, chemosensitizers, or small interfering RNA.

Current approaches to nanoparticle-based combination therapy include administering a cocktail of single-drug nanoparticles, co-encapsulation of multiple drugs

into a single nanoparticle core, conjugating one drug to the particle surface while encapsulating the other inside of the core, and covalently conjugating multiple drugs to the same polymer backbone. While innovative, these strategies suffer many drawbacks that hinder their performance as drug delivery vehicles. For instance, administering a cocktail of nanocarriers containing different drugs could lead to inadequate or unbalanced drug levels due to varying pharmacokinetics [17]. Co-encapsulation of multiple drugs into a single carrier is only suitable for drugs with similar chemical properties and may result in drug interactions. Layered nanocapsules have low drug loading capacity and only enable sequential drug release [18-21]. None of these methods provide co-delivery of two drugs with strongly dissimilar water solubility, segregation of potentially reactive drug compounds, and sequenced drug release all simultaneously.

1.4 Advantages of Janus Particles in Drug Delivery

Biphasic Janus particles hold great promise as sophisticated drug delivery systems with the potential to solve many fundamental problems in drug delivery. Co-encapsulating two synergistic drugs in a single particle is the only way to ensure co-localization of both drugs at the same time. The ability to deliver multiple therapeutic agents in a single platform with independent release kinetics allows for unprecedented control over the order and rate at which each compound is released. As with other nanocarriers, the rate and onset of drug release is determined by the degradation behavior of the polymer matrix. Janus particles can also deliver both a therapeutic agent and an imaging modality to enable real-time tracking of treatment. Compartmentalization prevents undesired reactions, interactions, or destruction prior to administration [22].

The incorporation of stimuli-responsive polymers imparts an even greater degree

of flexibility in the design of Janus particles; for example, one or both compartments could be designed to degrade in a pH-dependent manner so as to prevent degradation or drug loss during various stages of digestion, or, alternatively, to trigger drug release in an acidic tumor microenvironment [23]. Furthermore, zero-order release has been demonstrated with a hemi-spherical particle that only allows degradation on the face [24]. Therefore, Janus particles comprised of one biodegradable polymer and one non-biodegradable polymer (i.e., PLGA and PMMA) could potentially mimic this system, enabling zero-order release. Due to the difference in chemical composition of the two halves, each compartment will intrinsically exhibit a unique release profile.

1.5 Role of Particle Shape in Drug Delivery

Particle shape has been shown to affect circulation, biodistribution, phagocytosis, cellular internalization, and intracellular transport [25-27]. For example, particle shape dictates flow patterns throughout the vasculature, with disc-like particles remaining in the center of flow alongside red blood cells and rod-like particles drifting toward the vessel wall [28]. While in circulation, particles with complex local geometries are capable of preventing initial contact with incoming macrophages, thereby evading RES clearance. The probability of phagocytosis initiation is largely determined by local particle shape and the corresponding angle of contact from the perspective of the approaching macrophage [25]. Surface curvature also affects targeting ligand adsorption, as well as the degree to which particles fit in the contours of target cell membranes [24]. Nonspherical particles may be beneficial in passive targeting due to their presentation of diverse shapes, sizes, and surfaces [28]. The distinct surfaces presented by Janus particles can each be decorated with different targeting ligands or a combination of targeting ligands and hydrophilic

moieties such as PEG for prolonged circulation time and improved targeting ability. Shape is a fundamental design parameter that could be exploited to prolong circulation time, improve targeting, enhance cellular uptake, and tailor drug release profiles.

1.6 Janus Particle Synthesis

The three main synthetic schemes for obtaining Janus particles are self-assembly, masking, and phase separation of a heterogeneous mixture [29]. Triblock copolymers undergo direct self-assembly in solution into Janus micelles. In masking, homogeneous precursor particles are immobilized for toposelective surface modification then released. Phase separation occurs when a mixture of two incompatible separates upon solvent removal within emulsion droplets. In this work, we employ self-assembly. A summary of the methods is shown in Figure 1 and brief descriptions of each are provided in the subsequent sections.

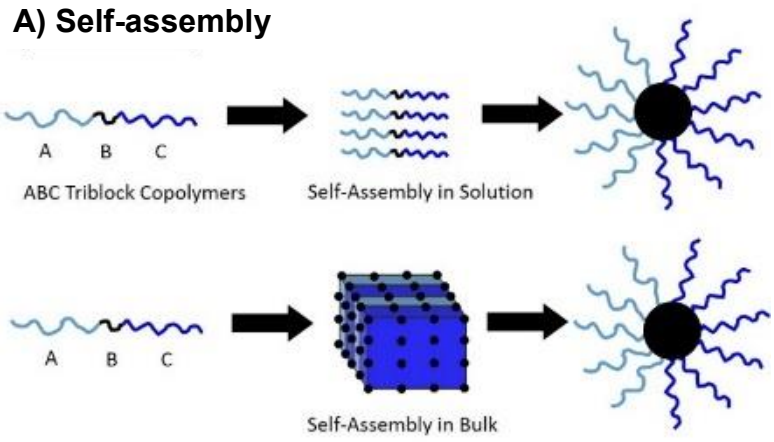

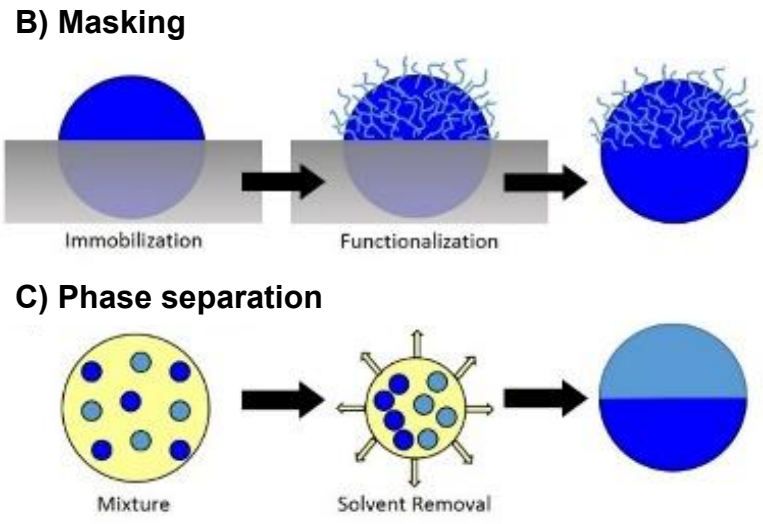

Figure 1: Overview of Janus particle synthesis by A) self-assembly, B) masking, and C) phase separation.

1.6.1 Self-Assembly of Block Copolymers

Self-assembly of block copolymers from solution or bulk structures was among the early techniques for preparing Janus particles [30]. Block copolymers are known to segregate into distinct phases in selective solvents or in the bulk [31]. Solution-based self-assembly of two diblock copolymers AB and BC (or ABC triblock copolymers) involves the crosslinking of incompatible blocks A and C to a mutually compatible block B followed by precipitation during solvent evaporation. The end result is a Janus-type polymeric micelle with a central block B forming the core, and blocks A and C extending outwards in opposite directions. The central block, specifically its weight fraction, plays a crucial role in determining particle morphology. A variety of different polymers can be used as long as their A and C blocks are incompatible and they are both soluble in a suitable solvent. Unfortunately, reaction mixtures are typically far too dilute for the large-scale production of Janus particles [31].

Self-assembly of triblock copolymers into terpolymers via film casting and subsequent dissolution gives rise to Janus spheres, cylinders, or disks [30]. Ultimately, the

final particle morphology can be manipulated by changing the molecular weight of the blocks, block lengths, block ratios, and dissolution method of the intermediate bulk terpolymer. Narrow particle size distributions and very small sizes down to the tens of nanometers are attainable through self-assembly [32]. There is a virtually limitless array of chemical functionalities that can be imparted to the particle surface, and the inner structure is compartmentalized. The self-assembly process is generally well-controlled, leading to highly uniform structures. However, this is not the case at high copolymer concentrations, thus limiting scalability [30]. Therefore, self-assembly is only feasible for combinations of polymers with distinctly different properties, such as polystyrene (PS)-polyisoprene (PI) or poly(ethylene oxide) (PEO)-poly(propylene) oxide copolymers [33, 34]. It should be noted that the synthesis of block copolymers traditionally comes at high cost [35].

1.6.2 Masking

One of the most common approaches for the preparation of Janus particles is toposelective surface modification, or masking. Masking involves protection of one portion of a particle surface during functionalization so that only the unmasked surface is modified, resulting in Janus particles anisotropic in surface and in bulk. Immobilization of a monolayer of particles for surface modification is carried out by entrapping the particles at a solid surface or in a fluid interface such as one formed by a Pickering emulsion. A Pickering emulsion is a special type of emulsion where the droplet interface is stabilized by small colloidal particles rather of surfactants. The emulsion droplet then serves as a template for Janus particle synthesis, where precursor particles are immobilized at the solid/liquid interface upon solidification. In one example utilizing wax, one hemisphere is suspended in the wax, and thus protected, while other side is chemically modified. After

chemical modification of the exposed surface, the wax is dissolved by organic solvent to release the newly-formed particles. Pickering emulsions are capable of producing large quantities of Janus nanoparticles as small as 100 nm with controllable surface geometries [36]. However, weakly attracted particles have a tendency to drop from the solid/liquid interface during chemical modification, thus resulting in a mixture of functionalized Janus particles and unfunctionalized precursor particles, potentially lowering the yield of the process [37]. In addition, due to the low melting point of wax, as well as the propensity of the wax to dissolve in most common solvents, there are a limited number of treatments that can be used. Moreover, the functionalization must be performed from an aqueous phase, which may require a series of chemical reactions at various yields in order to implement.

If greater versatility in terms of functionalization is desired, planar solid substrates may be used instead of Pickering emulsions for particle immobilization. A monolayer of homogeneous precursor particles is deposited on or partially embedded in the substrate to allow for selective functionalization of the exposed surface. The substrate is typically comprised of an inert material such as polymer, glass, or silicone. Substrate thickness determines the relative surface area that is exposed for modification. If necessary, the template is removed through dissolution, calcination, or etching to liberate the newly-formed Janus particles. It is worth noting that a multistep, complicated protocol is required for the modification of both surfaces, which could limit scalability and effective yield. Although the use of solid substrates offers good control over surface geometry, only milligrams of particles are produced in a single batch, further limiting the possibility of commercial-scale production [38]. While Janus particles synthesized via toposelective surface modification techniques can exhibit unique biochemical interactions, they

ultimately are not bicompartmental since only the surfaces of the homogeneous precursor particles are altered.

1.6.3 Droplet-Based Phase Separation

Microfluidics and electrohydrodynamic co-jetting are frequently used in the preparation of biodegradable Janus particles [8, 39]. In general, the experimental setup consists of two side-by-side channels that merge into a single channel and are fed into a nozzle where droplet formation occurs. If the microfluidic device is used for emulsion formation, additional side channels may be required to introduce the aqueous solution containing an emulsifier. Microfluidic devices may serve as a template for Janus particle formation via single emulsion, oil-water-oil double emulsion, or polymerization of monomers in aqueous solution [8, 40].

On the other hand, Janus particles prepared by electrohydrodynamic co-jetting are generally based on aqueous solutions of polymers rather than emulsions. Both microfluidics and electrohydrodynamic co-jetting employ laminar flow of two parallel streams of monomers or polymer solutions. Yet, as its name implies, electrohydrodynamic co-jetting relies on electric forces to move the fluids through the channels. Because laminar flow occurs at low Reynolds numbers, there is no convective transport across the interface between the two streams [41]. This prevents even miscible fluids from mixing within the capillary channel. In fact, the two fluids must be miscible in order to maintain a stable interface independent of location and time [40]. Once the stream exits the nozzle, the two fluids coalesce into a unified droplet. Rapid solidification of the droplets results in biphasic Janus particles with a distinctive interface. For microfluidics, the composition of the droplets determines the method by which they are solidified. Droplets can solidify upon

cooling, solvent evaporation from dissolved polymer or through photo/thermal polymerization. If solidification is contingent on a polymerization reaction, the precursor monomers must be either photo- or thermocurable. In electrohydrodynamic co-jetting, solidification occurs via electrospraying. Since the output is one single particle at a time, these devices can only produce a few tens of grams per day [42]. Though microfluidic techniques offer high monodispersity, particle size has yet to approach the submicron regime due to the relatively large size of the fluid channels [43]. Conversely, submicron sized Janus particles have been fabricated using electrohydrodynamic co-jetting, but with a fairly broad size distribution [44]. Microfluidics and electrohydrodynamic co-jetting are both well-defined processes that yield particles with uniform shape, surface geometry, and compartmentalization. Janus particles produced by capillary-based methods are largely spherical because the templating droplets are almost always spheres, however rods and discs have also been produced by simply varying process parameters such as flow rate and polymer solution viscosity [8, 45]. Electrohydrodynamic co-jetting is mainly applied to water-soluble polymers but has recently been demonstrated with organic solutions containing hydrophobic polymers such as poly(lactide-co-glycolide) (PLGA) [45, 46]. Microfluidics can be utilized for either hydrophilic or hydrophobic polymers, but generally not at the same time if the particles are templated from a single emulsion, and each must ultimately be dissolved in adequate proportions within the dispersed droplet phase. There are also special conditions for droplet formation that limit the types of materials that can be used in microfluidic devices. For example, only fluids with low viscosity, negligible viscoelastic response, and moderate interfacial tension meet the criteria for drop formation [47]. The use of two immiscible fluids to produce a double emulsion further expands the

selection of materials that can be used for each side of the particle [40]. Organophilic-hydrophilic Janus particles have been formed in this way [40]. In addition to having different surface properties, the bicompartmental nature of the Janus particles produced via microfluidics and electrohydrodynamic co-jetting enables segregation of two encapsulated materials. For instance, a metallic component can be included for diagnostic imaging or photothermal therapy in one compartment, while the other compartment can hold a drug compound [8].

1.6.4 Seeded Polymerization

Controlled nucleation and growth of two immiscible or incompatible polymers or a polymer and an inorganic material also may be utilized to produce Janus particles. Due to the fact that many polymers are immiscible with each other and inorganic materials may readily be functionalized to be further incompatible with polymers, the direct phase separation method is suitable for a wide range of materials [30]. It should be noted that in the following techniques, it is important for some molecular affinity between the dissimilar polymers in order to maintain an adequate particle interface. Direct seeded polymerization in solution can lead to a plethora of different architectures, such as dumbbell, acorn, popcorn-like, ice cream cone-like, and raspberry-like [7]. Seeded polymerization was originally used for the production of core-shell particles. However, it was discovered that under the right conditions and with sufficient incompatibility of the monomer and seed polymer, heterogeneous nucleation becomes favorable. In this approach, cross-linked polymer seed particles are swollen with polymerizable monomer. The monomer is polymerized upon heating. The cross-linked polymer network then shrinks and ejects the monomer solution, forming a bulge on the particle surface [7, 48]. The monomer

polymerizes and grows on the original seed, forming a heterodimer. The size of the seed particles, monomer concentration, crosslinking density of the seed polymer, and hydrophilicity of the cross-linked particle surface all contribute to the final morphology of the resultant particles [49, 50].

A special type of seeded polymerization is called seeded emulsion polymerization. In a seeded emulsion polymerization, solvent evaporation induces phase separation. Seeded emulsion polymerization is most frequently applied to organic-inorganic hybrid anisotropic particles that incorporate silica or iron oxide along with a polymer such as polystyrene (PS) [7, 51, 52]. Typically, these structures have one major component and one minor component [3]. High yields of Janus particles in the nano-scale particle size range have been synthesized using the seeded polymerization methods [7, 53]. Controlled heterogeneous nucleation requires precise knowledge of and control over system thermodynamics and kinetics in order to arrive at the desired Janus morphology and avoid the formation of core-shell particles.

1.6.5 Emulsion Solvent Evaporation Method

A far simpler approach is based on the oil-in-water emulsion-solvent evaporation method commonly used to prepare polymeric micro- and nanoparticles. The preparation of polymeric micro- and nanoparticles via emulsification solvent evaporation has been explored extensively over the past 35 years along with the influence of various process parameters [54-60]. In order to apply the technique to the production of Janus particles, a binary mixture of two incompatible polymers is dissolved in a common solvent to form the oil phase. The oil phase is added to an aqueous phase consisting of water and a surfactant, and an oil-in-water emulsion is created by the application of shear through various means

such as homogenization. The shear forces result in dispersion of the oil phase into discrete droplets stabilized by the surfactant molecules at the interface between the phases. The solvent may first diffuse into the aqueous medium before it can be removed by evaporation from the air/water interface. During solvent diffusion and evaporation, the polymers do not blend together but instead phase separate due to their immiscibility. Upon complete solvent removal, the composite particles harden and an aqueous dispersion of biphasic Janus particles is obtained. Emulsion-solvent evaporation is a simple, one-pot technique suitable for producing large quantities of Janus particles from a wide range of polymers and other biodegradable materials. Furthermore, it is easy to scale up and requires little processing equipment. Recently, our group has demonstrated the production of novel PLGA/PCL and PLGA/Precirol® Janus particles from O/W emulsions[61].

1.7 Dissertation Objectives and Organization

The importance of shape in drug delivery and vast applicability of Janus particles have been summarized in the preceding sections. Current synthesis methods fail to produce Janus particles in quantities large enough to meet the high demand present in the pharmaceutical industry. Although masking and self-assembly are capable of producing monodisperse, submicron Janus particles, they are not bicompartmental. Microfluidics and electrohydrodynamic co-jetting result in monodisperse Janus particles that are bicompartmental; however, these techniques suffer from low yield and material constraints. Thus, there is a critical need to develop a scalable technique for manufacturing monodisperse, multicompartmental Janus particles.

Despite considerable progress in the way of Janus particle synthesis in recent years, research examining the functionality of Janus particles is lagging far behind. Based on the

literature available through 2011, in excess of 60% of current research on Janus particles is devoted to synthesis and characterization, while only a mere 8% is focused on their application [62]. To address this, a significant portion of this work is devoted to assessing the *in vitro* and *in vivo* benefits of Janus particles in drug delivery. The goals of this dissertation are achieved through the completion of the following aims:

Specific Aim 1: Synthesize and characterize a platform of Janus particles from biodegradable polymers and lipids using emulsions as templates.

Specific Aim 2: Design and evaluate Janus particle-based drug delivery systems for various case studies demonstrating simultaneous encapsulation of hydrophilic and hydrophobic drugs or two hydrophobic drugs in Janus particles.

Specific Aim 3: Develop a theoretical model to describe phase separation behavior and to predict Janus particle morphology as a function of interfacial tensions.

With an overview of current Janus particle synthesis methods and the advantages of anisotropic particles in drug delivery presented in Chapter 1, the remainder of this dissertation focuses on novel synthesis, application, and thermodynamic modeling of biodegradable Janus particles.

Chapter 2 describes emulsion-based synthesis of Janus particles from biodegradable polymers and lipids. Results from comprehensive physicochemical characterization of the Janus particles are presented. Chapter 3 discusses three strategies employed to simultaneously encapsulate hydrophobic and hydrophilic payloads into PLGA/PCL Janus particles: single O/W emulsion using a partially water-miscible solvent, single O/W emulsion using a co-solvent, and double W/O/W emulsion. Chapter 4 contains a case study in which PLGA/Precirol® Janus particles loaded with doxorubicin and

curcumin are applied to lung cancer treatment. *In vitro* and *in vivo* results highlight the advantages of using Janus particles to achieve unified biodistribution and simultaneous release of synergistic drug pairs. In Chapter 5, a thermodynamic model for the prediction of Janus particle morphology based on interfacial tensions is presented. The model allows for explicit calculation of Janus particle geometry given the volume ratio and the surface tension of each of its interfaces. In reverse, the model can be utilized to calculate the interfacial tension between two solid polymers given Janus particle geometry measurements obtained from standard microscope measurements. Chapter 6 builds upon the knowledge and expertise of emulsions, surfactants, and solvents gained in the formation of Janus particles and applies it to the production of pharmaceutical nanosuspensions by the emulsion-diffusion method. The effects of surfactant HLB, surfactant synergism, and solvent properties on the size and stability of ibuprofen, indomethacin, and fenofibrate nanosuspensions are explored. Conclusions of this work and recommendations for future work are provided in Chapter 7.

CHAPTER 2: EMULSION-BASED SYNTHESIS OF BIOEDGRADABLE JANUS PARTICLES

Part of the data in this chapter has been published:

Romanski, F.S., **Winkler, J.S.**, Riccobene, R.C., Tomassone, M.S. Production and Characterization of Anisotropic Particles from Biodegradable Materials. Langmuir 2012 (28) 3756-3765.

2.1 Introduction

The emulsion solvent evaporation method is widely used in the preparation of nanoparticles. It has been studied extensively over the past few decades, and the influence of process variables on final particle characteristics are well documented [55, 63-65]. The oil-in-water (O/W) single emulsion technique is effective for entrapping hydrophobic compounds. The first step is to add the oil phase, a water-immiscible organic solvent consisting of the dissolved drug and polymer, to an aqueous phase containing surfactant. The crude emulsion is passed through a high pressure homogenizer for size reduction. As the solvent diffuses out of the droplets and evaporates, the polymer precipitates and particles are formed.

There are several formulation and preparative variables that affect final particle characteristics including size, stability, entrapment efficiency, and release behavior. Generally, increasing the concentration of surfactant in the water phase, decreasing the polymer concentration in the oil phase, and increasing the shear level during homogenization all lead to a reduction in the particle size [66, 67]. However, once the surfactant concentration exceeds the critical micelle concentration (CMC), adding more surfactant will not assist in achieving smaller particle size because there is no further reduction in interfacial tension. In terms of encapsulation efficiency, increased polymer concentration, increased outer aqueous phase volume, and decreased inner aqueous phase

volume (in the case of the double emulsion) result in higher encapsulation efficiencies [19, 20, 68]. Solvent type has also been shown to affect particle size and encapsulation efficiency [69, 70].

While microfluidics and electrohydrodynamic co-jetting have been pursued in the past few years as templates for producing biodegradable Janus particles, droplet-based techniques suffer from low yield and offer little flexibility in particle geometry. The constraints of fluidic devices severely restrict or exclude the use of lipid-based biodegradable materials commonly used in pharmaceutical products. Toposelective surface modification techniques do not yield compartmentalized Janus particles, and self-assembly of block copolymers is restricted to a limited set of materials. Emulsion-solvent evaporation of two immiscible polymer species (or polymer and lipid) has emerged as a versatile synthesis method for large-scale production of biodegradable Janus particles. One of the most well-studied systems for Janus particle preparation via emulsion-solvent evaporation is the PS/poly(methyl methacrylate) (PMMA) oil-in-water emulsion with toluene as the dispersed phase [49, 50, 71, 72]. However, PS and PMMA are not biodegradable and therefore not acceptable for use in pharmaceutical formulations. Recently, we demonstrated the preparation of Janus particles from various binary combinations of biodegradable materials such as poly(lactic-co-glycolic) acid (PLGA), polycaprolactone (PCL), glyceryl distearate (Precirol® ATO 5), and glyceryl behenate (Compritol® 888 ATO) via emulsion solvent evaporation [61]. Particles and scaffolds comprised of PLGA/PCL blends have been reported in the literature, but they have not been used in the formation of biphasic Janus particles up until this point [73, 74].

2.2 Materials and Methods

2.2.1 Materials

Biodegradable polymers: PLGA and PCL are FDA-approved, biodegradable polymers frequently used in drug delivery and tissue engineering [75-77]. PLGA is a copolymer of poly lactic acid (PLA) and poly glycolic acid (PGA). PGA is highly crystalline, while PLA is semi-crystalline. PLGA is classified as semi-crystalline, but its overall crystallinity is determined by the ratio of glycolide to lactide units. Copolymers having a higher glycolide content generally degrade faster, allowing for control over degradation rate [75, 78]. Owing to its high crystallinity and hydrophobicity, PCL provides a slower degradation rate over a period of more than one year [79-81]. The PCL is more hydrophobic than PLGA and may provide greater drug capacity for more hydrophobic drugs [82]. Poly(2-hydroxyethyl methacrylate), poly(acrylic acid), poly(*N*-vinylpyrrolidone), poly(methyl methacrylate), and poly(*tert*-butyl methacrylate) were also tested.

Biodegradable lipids: Glyceryl palmitostearate (Precirol®) and glyceryl behenate (Compritol®) was used as the lipid. Precirol® and Compritol® are fatty esters with long acid chains. They are FDA-approved lipids that are frequently used in the production of solid lipid nanoparticles or as excipients. Lipids offer greater retention of very hydrophobic drugs and also allow for incorporation of hydrophilic drugs [83-87]. Core-shell type hybrid PLGA-lipid nanoparticles have demonstrated greater serum stability, enhanced bioavailability, and greater drug retention [88-90]. By including a lipid component, drugs with vastly different chemical properties and disparate solubility can be encapsulated within a single particle.

Surfactants: Surfactants play a vital role in the formation and stabilization of emulsions. Nonionic surfactants are preferred for pharmaceutical applications due to their very low toxicity levels. The nonionic surfactants studied here represent three major chemical classes: synthetic polymers (polyvinyl alcohol, PVA) sorbitan esters (Spans and Tweens), and linear block copolymers (poloxamers). Spans are fatty acid esters of sorbitol. Tweens are ethoxylated derivatives of Spans. Poloxamers comprise a central hydrophobic chain of polypropylene oxide (PO) units surrounded by two hydrophilic blocks of polyethylene oxide (EO) units [91]. Spans, Tweens, PVA, and poloxamers are all approved for use as inactive ingredients in oral suspensions and other pharmaceutical products by the FDA [92]. For W/O emulsions, surfactants and surfactant mixtures with very low HLB values (3-6) such as Span 80 were used. PVA is frequently used as a stabilizer in the formation of PLGA nanoparticles by the emulsion solvent evaporation method [66, 93, 94]. Ionic surfactants such as sodium dodecyl sulfate (SDS), sodium dodecylbenzenesulfonate (SDSB), and cetyltrimethylammonium bromide (CTAB) were also studied. Although ionic surfactants generally give smaller emulsion droplets and therefore smaller particles, they are rarely used in pharmaceutical products due to their harmful side effects [95].

Organic solvents: Solvents used in the preparation of particles by the emulsion solvent evaporation method should have negligible miscibility with water, high volatility, and a low boiling point. Additionally, both the polymer and the drug(s) must have high solubility in the chosen solvent. Dichloromethane (DCM), tetrahydrofuran (THF), toluene, and chloroform were employed in this work. They are frequently used in emulsion solvent evaporation due to their ease of evaporation. Although these solvents are designated as Class 2 based on their toxicity, the residual amount left after solvent evaporation is not

expected to exceed the concentration limits set forth by the FDA and ICH. Partially water-miscible solvents are preferred for pharmaceutical applications due to their low toxicity profiles. The ICH has set forth limits of 60, 600, and 5000 ppm for the concentration of residual chloroform, DCM, and ethyl acetate, respectively in pharmaceutical formulations [96]. While ethyl acetate is less toxic, its low volatility makes it more difficult to remove by evaporation. Previous studies have shown that the amount of residual dichloromethane remaining in nanoparticles prepared using the solvent evaporation method is negligible (<15 ppm) [66, 97-99]. In some cases, co-solvents such as methanol or acetone are used to increase the solubility of the drug in the oil phase. Less toxic solvents such as ethyl acetate can be used in conjunction with or in replacement of Class 2 solvents. However, the high solubility of ethyl acetate in water can lead to drug loss to the continuous phase and rapid solvent diffusion.

2.2.2 Preparation of Janus Particles by the Single Emulsion Method

The oil phase was created by dissolving 2.5% w/v of each PLGA (lactide:glycolide=65:35, M.W.=40,000-75,000) and polycaprolactone (PCL, M.W.=42,500-65,000) in 4 mL of DCM. Separately, a 10 mL solution of 1% w/v PVA in deionized water was prepared. The oil phase was added to the water phase and emulsified. The O/W emulsion was further homogenized using either an Ultra Turrax T-25 rotor-stator, probe-tip sonicator, or Avestin Emulsifex C-3 piston-gap high pressure homogenizer (Avestin Inc., Ottawa, Canada), depending on the desired particle size. Post-homogenization, the O/W emulsion was magnetically stirred and kept at 40 °C in an open beaker to allow for solvent evaporation. Upon complete solvent removal, particles were harvested by centrifugation at 20,000 rpm for 30 minutes. The supernatant was discarded

and the remaining powder bed was washed with deionized water. Particles were stored in a vacuum desiccator for further analysis. A schematic of the general experimental procedure is shown in Figure 2.

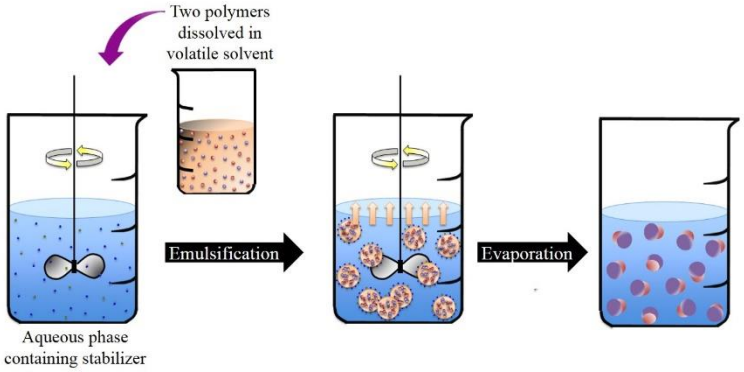

Figure 2: Overview of the emulsion solvent evaporation method used to prepare Janus particles.

Formulation variables such as surfactant type, surfactant concentration, polymer concentration, polymer type, solvent type, and O/W phase volume ratio were varied in order to study their effect on final particle characteristics. Process variables such as homogenization method and evaporation rate were also explored.

2.2.3 Optical and Scanning Electron Microscopy

Janus particles were visualized using a Celestron 44350 LCD Digital LDM Biological Microscope. The digital microscope also has video recording capabilities. Liquid samples are mounted on glass slides and immobilized by coverslips. The Amray 1830 I scanning electron microscope (SEM) was used when higher resolution is necessary. To prepare SEM samples, aluminum stubs are covered by double-sided adhesive carbon tape. A 5 mm x 7 mm silicon wafer is then placed atop the circular carbon tape. The sample is pipetted onto the silicon wafer, and excess liquid is removed by a vacuum desiccator. Samples were sputter coated with carbon prior to imaging using a Bal-Tech MED-020 coating system.

2.2.4 Particle Size Analysis

The mean particle size and size distribution of particles in suspension was measured by laser diffraction using a Beckman-Coulter LS-13 320. In laser diffraction, a monochromatic laser beam is passed through the sample, which results in a scattering pattern. The scattering pattern is converted into a volume equivalent sphere size distribution using the Fraunhofer and Mie optical models. Particle size is reported as volume-weighted mean diameter and standard deviation. Samples were analyzed based on obscuration and polarization intensity differential scattering. Refractive indices of 1.467 and 1.333 were used for the polymers and dispersion medium, respectively.

2.2.5 Zeta Potential

Zeta potential is an important indicator of colloidal stability. Zeta potential is a measure of electric charge at the surface of particles used to predict the physical stability of colloids. Particles in solution inherently possess a surface charge and are surrounded by a layer of strongly bound ions known as the Stern layer. An outer layer of loosely associated counterions known as the diffuse layer forms adjacent to the Stern layer to neutralize the particle surface charge. The electrical potential at the boundary between the ions in the diffuse layer and the Stern layer is the zeta potential. The zeta potential of the particles was determined using a Malvern Zetasizer Nano ZS90. Prior to analysis samples were diluted 1:10 with ultra-purified water. Measurements were repeated three times and the mean and standard deviations are reported.

2.2.6 X-Ray Diffraction

Every crystalline substance exhibits a unique x-ray diffraction (XRD) pattern, making it possible to identify the chemical composition and relative amounts of each component of a mixture, as well as an estimate of the bulk crystallinity of the sample. XRD

is the equivalent of a “fingerprint” for a compound, as each element emits x-rays at a unique set of fixed wavelengths. It can be used to identify an unknown crystal material by comparing the diffraction pattern of the sample to that of a reference. When an x-ray is passed through a crystalline sample, it diffracts in a pattern unique to the crystal structure. Interatomic distances are calculated from incident x-ray wavelengths at different angles using Bragg’s law. The result is a spectrum of diffraction intensity as a function of angle. XRD analysis was carried out using a Phillips X’Pert Powder X-ray Diffraction unit. Samples were tested from 10° to 90° at a sensitivity of 0.01.

2.2.7 Raman Spectroscopy

Raman spectroscopy is often used in conjunction with XRD in order to gather more information on the crystalline structure of a material. Raman spectroscopy is a non-destructive characterization technique based on the inelastic scattering of monochromatic light by the specimen under study. Raman spectroscopy analysis was carried out using a Renishaw inVia Raman Microscope. Samples were mounted onto a glass microscope slide and covered with a coverslip. The spectrometer uses a 633 nm laser with a peak power of 150 mW. Data was acquired and processed using Windows-based Raman Environment (WiRE) software.

2.3 Results and Discussion

2.3.1 PLGA/PCL Janus Particles via Single Emulsion

Biphasic Janus particles were formed from a binary mixture of PLGA and PCL using 0.3% w/v PVA and 0.1% w/v SDBS as surfactants. Two separate compartments can be clearly seen in microscope images of micron-sized particles, shown in Figure 3 below.

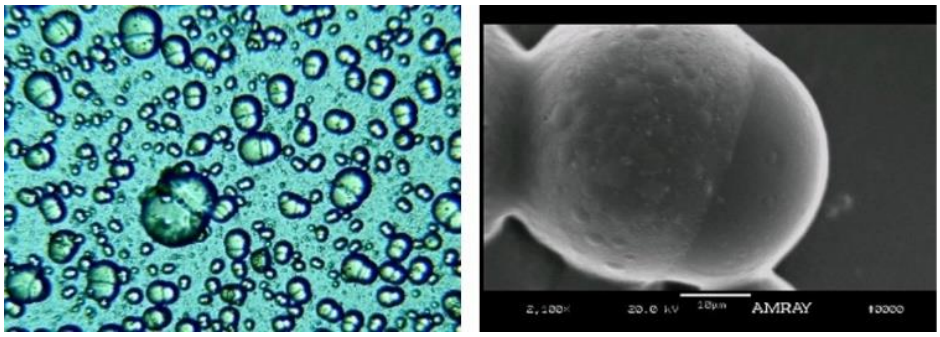

Figure 3: Optical and scanning electron microscope images of PLGA/PCL Janus particles.

Based on previous studies with individual PLGA and PCL particles, it was determined that PLGA is the smaller compartment and PCL is the larger compartment due to PLGA's smooth surface and PCL's rough surface. The higher solubility of PCL in DCM results in the solvent partitioning more into the PCL phase than the PLGA phase, leading to greater swelling of PCL [100, 101].

PLGA/PCL Janus particles were prepared under low, moderate, and high shear levels using a high pressure homogenizer (HPH), rotor-stator, and manual shaking, respectively. Resulting particle size distributions are shown in Figure 4. Sonication is an alternative to HPH which also gives submicron particles. Emulsions formed by manual shaking resulted in particles approximately 100 microns in diameter, whereas HPH resulted in particles in the nano regime. These results are expected for an emulsion-based process, where the amount of energy applied to the system determines the emulsion droplet size.

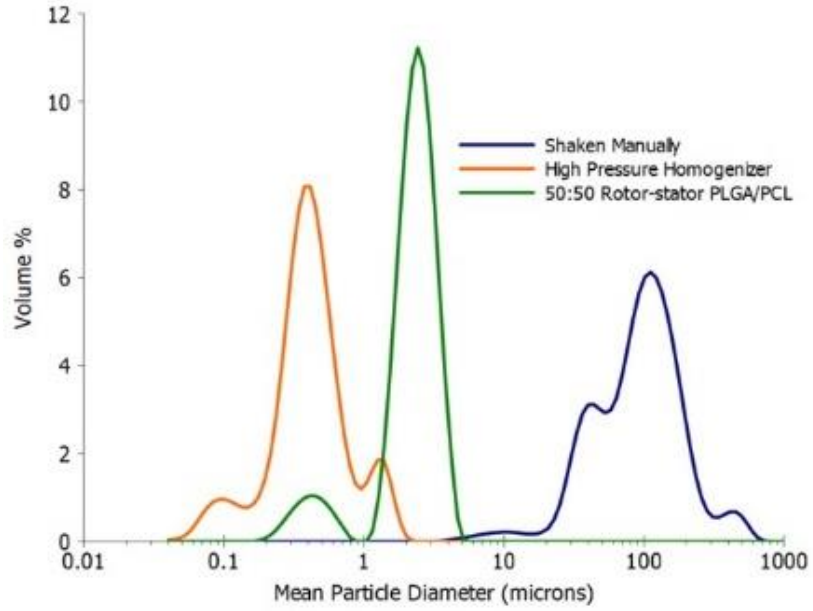

Figure 4: Particle size distributions of PLGA/PCL Janus particles homogenized using HPH (orange), rotor-stator (green), and manual shaking (blue).

2.3.2 The Feasibility of Different Polymer Combinations

The PLGA/PCL combination was our initial choice and starting point for Janus particle production due to the biocompatibility and biodegradability of these two polymers. In an effort to establish a working library of polymer combinations that lead to Janus particles, the following polymers listed in Table 1 were also tested:

Polymers	Average Molecular Weight, M_w	Functional Groups
Poly(2-hydroxyethylmethacrylate)(poly HEMA)	20,000; 300,000	H-bond donors and acceptors
Polymethacrylic acid (poly-MAA)	8,000; 19,000	
Poly(*N*-vinylpyrrolidone) (poly-VP)	10,000(PVP10); 40,000 (PVP40)	H-bond acceptors, with tertiary amide and amine groups
Poly(4-vinylpyridine) (poly-4VP)	60,000; 160,000	
Poly(methylmethacrylate) (poly-MMA)	8,000; 10,000	H-bond acceptors with ester groups
Poly(*tert*-butyl methacrylate) (poly-*t*-BuMA)	10,000; 170,000	
Poly(lactic-co-glycolic acid) (PLGA)	30,000 - 60,000	H- bond donors and acceptors, including *block*-copolymers
	50,000 - 75,000	
Polycaprolactone (PCL)	10,000; 45,000	

Table 1: Various polymers tested in Janus particle synthesis and their properties.

Combinations were chosen based on their functionalities and propensity to interact with one another via hydrogen bonding, ionic interactions, or donor-acceptor interactions.

It was found that no other combinations aside from PLGA/PCL resulted in biphasic Janus particles. The three combinations that formed particles, PVP/PTBMA, PLGA/PMMA, and PCL/PMMA, are shown in Figure 5 alongside PLGA/PCL particles. PVA was used as the surfactant in all studies.

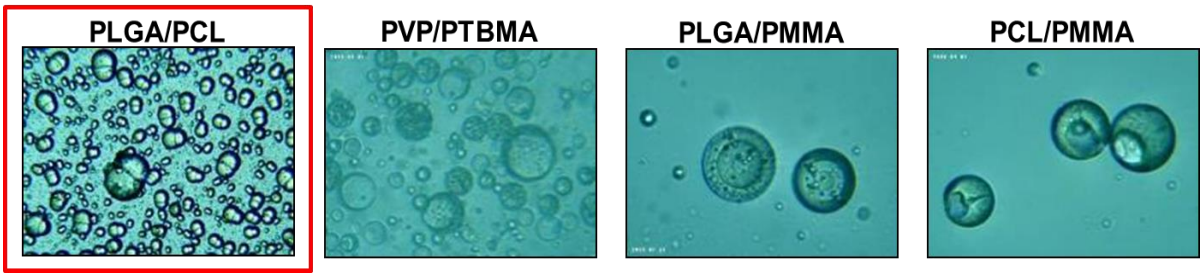

Figure 5: Particles resulting from different polymer combinations

The phase separation of two chemically similar polymers into Janus particles was explored in the context of solubility parameters. The Hildebrand solubility parameter provides an estimation of the degree of interaction between a polymer and a solvent, or between two polymers, based on van der Waals forces, hydrogen bonding, and polar interactions. Generally speaking, two compounds are considered immiscible if the difference between their solubility parameters is greater than 10 $MPa^{1/2}$, and miscible if the difference is smaller than 7 $MPa^{1/2}$ [102]. The solubility parameter difference of the combinations tested are shown in Table 2. Combinations that led to phase-separated particles are shown in red, and combinations that resulted in blended or separated particles are shown in black.

Polymer Combination	Δδ ($MPa^{1/2}$)
PLGA/PCL	3.14
PLGA/PMMA	3.05
PCL/PMMA	0.09
PVP/PTBMA	1.90
HEMA/P4VP	7.93
PMAA/PVP	7.00
PMAA/PMMA	0.60
PLGA/Compritol	3.61

Table 2: Solubility parameter difference of polymers tested.

The general miscibility rules did not apply to Janus particle production. Instead, we observed that Janus particle formation occurs when 1 $MPa^{1/2} < \Delta\delta < 7$ $MPa^{1/2}$. This is an important result because it is a starting point for material selection in the synthesis of Janus particles by phase separation. There needs to be enough interaction to form an interfacial network between the two polymers, yet not enough interaction to form a miscible blend.

PCL and PMMA resulted in blended, bowl-shaped particles, suggesting they are readily miscible. Although the other polymer combinations did not form biphasic Janus particles like PLGA and PCL, PVP/PTBMA and PLGA/PMMA produced phase separated particles. These particles have an inner compartment nearly completely surrounded by an outer shell. Such core-shell type configurations occur when the surface tension of one polymer with water is significantly higher than that of the other polymer with water, which is the case with PVP/PTBMA. In this case, the polymer having the lower surface tension (PTBMA) would surround the polymer with the higher surface tension (PVP) in order to lower the overall surface energy of the system. Another potential cause of this is heterogeneous surfactant adsorption such as that observed with SDS in PS/PMMA systems

[115]. The role of surfactant will be discussed in Section 2.3.6.

2.3.3 Polymer/Lipid Janus Particles via Single Emulsion

By replacing PLGA/PCL with a 3:1 mixture of PLGA/Precirol®, we observed the formation of novel ice cream cone shaped polymer-lipid Janus particles. Figure 6 shows PLGA/Precirol® Janus particles prepared using either 0.3% PVA and 0.1% SDBS or 0.3% SDS and 0.1% SDBS. When SDS was used, the particles exhibited a longer lipid tail.

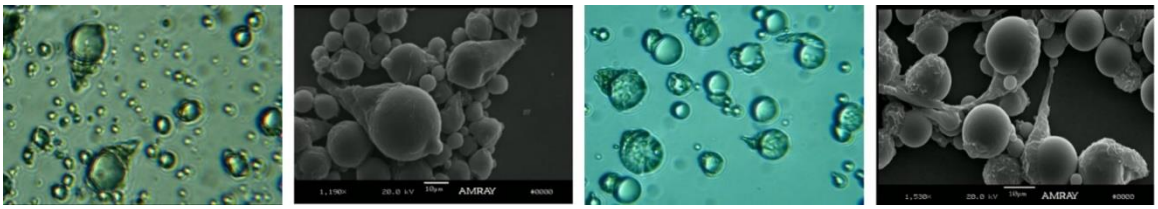

Figure 6: Optical and SEM images of PLGA/Precirol Janus particles prepared using (a,b) 0.3% PVA and 0.1% SDBS, (c,d) 0.3% SDS and 0.1% SDBS.

Similar structures were obtained when PCL was used in place of PLGA or Compritol® was used in place Precirol®.

2.3.4 Formation Kinetics

The low entropy of mixing makes it thermodynamically unfavorable for most high molecular weight polymers to form homogeneous mixtures [116]. Heterogeneous Janus particles are the direct result of the intrinsic immiscibility of polymer blends. Slow solvent evaporation is critical for complete phase separation of the PLGA and PCL. The importance of solvent evaporation rate was studied by varying the temperature and the surface area of the evaporation vessel; results are shown in Figure 7.

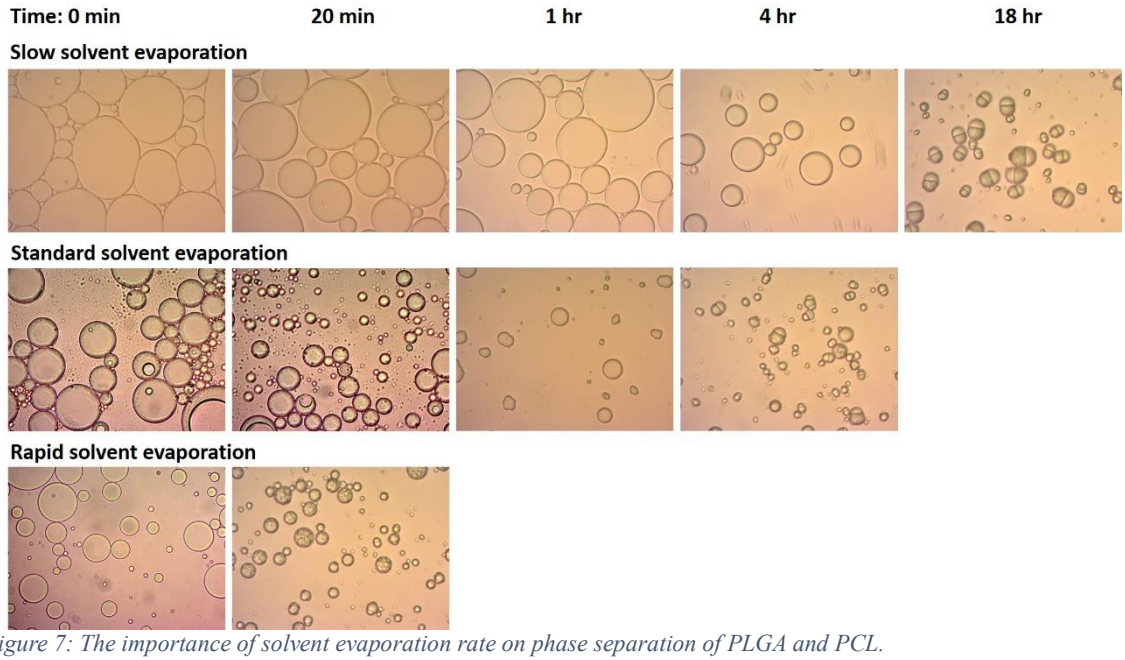

Figure 7: The importance of solvent evaporation rate on phase separation of PLGA and PCL.

Rapid evaporation (40 °C, 400 mL beaker) does not allow enough time for the polymers to phase separate and the polymers are "stuck" in their initial arrangement, resulting in spherical particles with PLGA and PCL interspersed. Standard evaporation (room temperature, 100 mL beaker) yielded a combination of Janus and isotropic particles. Optimal results are obtained when the solvent evaporation process is retarded (room temperature, 20 mL vial). PLGA and PCL are homogeneously dispersed in the oil phase. As the solvent evaporates, the volume of the droplets decreases and PLGA and PCL phase separate. An interface becomes apparent in the center of the droplet as evaporation proceeds, indicative of phase separation. Sample aliquots were removed from the evaporation chamber and observed at various intervals to gain a better understanding of the formation process. Results are shown in Figure 8.

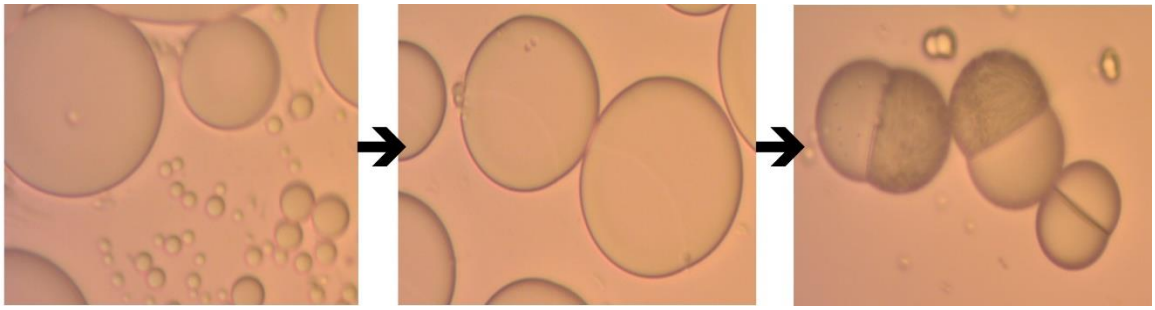

Figure 8: Transformation of spherical oil droplet to Janus particle via Janus-like droplets having an interface.

PLGA/Precirol® particles did not follow the same formation kinetics as PLGA/PCL particles. Instead, Precirol® precipitated much faster than PLGA. The lipid tail remained attached to the oil droplet until the polymer precipitated.

2.3.5 Effect of Solvent on Particle Morphology

Volatile organic solvents are used in the formation of micro- and nanoparticles from O/W emulsions. Water-immiscible solvents such as DCM and chloroform are generally used for the emulsion-solvent evaporation technique, but partially water-miscible solvents such as ethyl acetate can also be used. In our work, DCM was found to be the optimal solvent. When ethyl acetate was used in place of DCM, holes were observed on the surface of the particles resulting from a longer residence time of the solvent during evaporation as shown in Figure 9. When toluene or chloroform was used as the solvent, there was no effect on particle surface or characteristics.

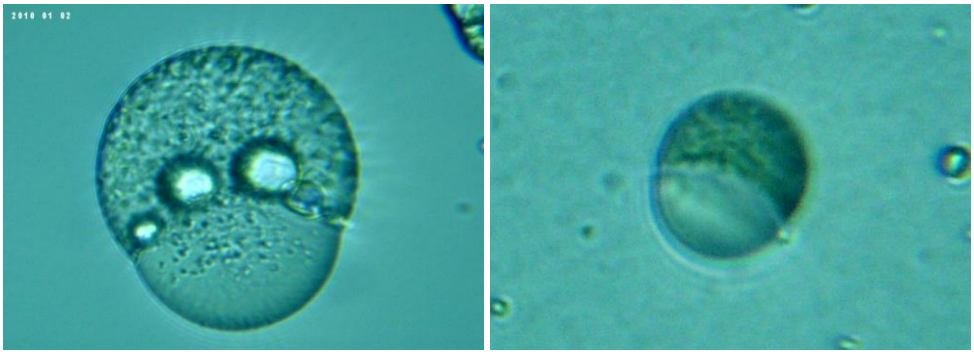

Figure 9: Janus particles prepared using a) ethyl acetate and b) DCM as solvent.

2.3.6 Effect of Surfactant Type and Concentration on Particle Morphology

Particle shape is a function of the interfacial tensions between the two polymers, as well as the interfacial tensions between each of the polymers and the aqueous phase. The interfacial tension of the system can be adjusted by changing the type of surfactant and its concentration. When PVA was replaced by an equal mass fraction of SDS, the Janus particles adopted a crescent moon morphology as opposed to the usual biphasic structure. Figure 10 shows SEM and optical images of the PLGA/PCL Janus particles prepared using SDS as the surfactant.

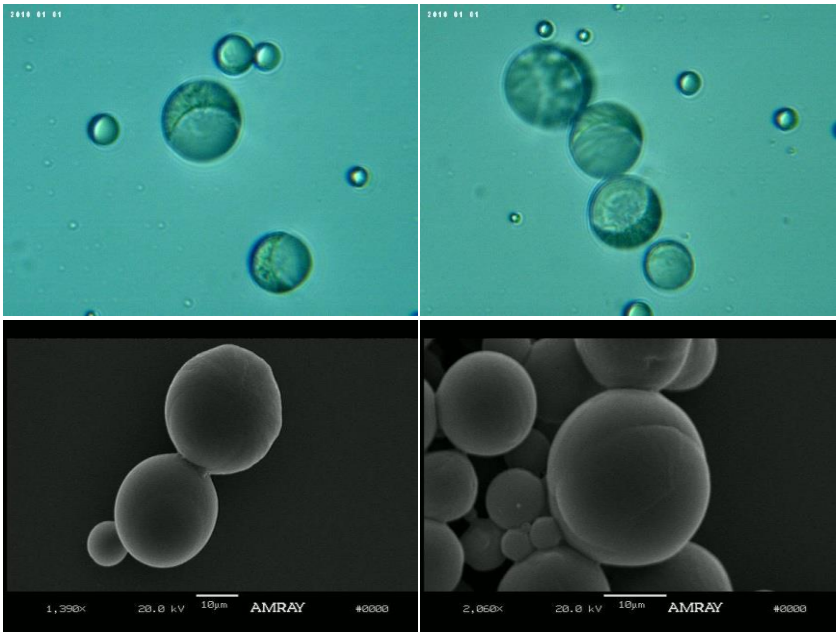

Figure 10: Optical (top) and SEM (bottom) images of PLGA/PCL crescent moon-like particles produced using 04% w/v SDS as surfactant.

Other ionic surfactants such as SDBS and CTAB also had a profound effect on the morphology of the PLGA/PCL Janus particles. Figure 11 shows the Janus particle morphology for different concentrations of SDS, SDBS, CTAB, and PVA from 0.1% to 10%.

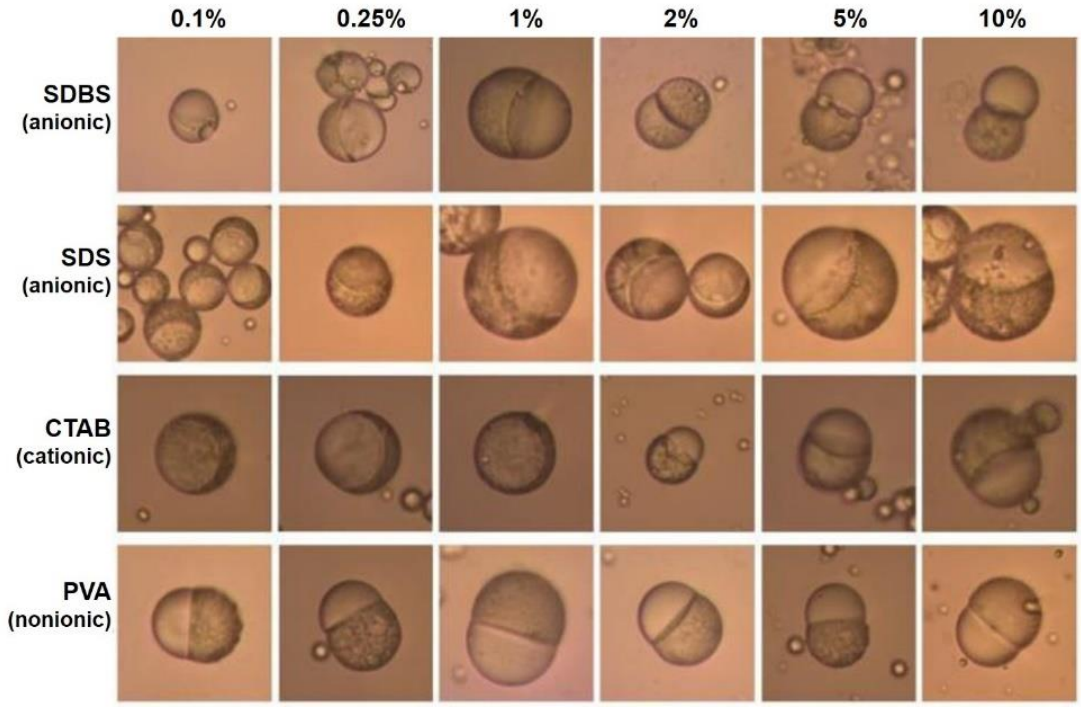

Figure 11: PLGA/PCL Janus particle morphology at different SDBS, SDS, CTAB, and PVA concentrations.

Previous studies involving PS/PMMA composite particles show that increasing the concentration of SDS drastically reduces the polymer-water interfacial tensions, leading to spherical particles [49, 72]. The crescent moon shape observed at low concentrations of ionic surfactant suggests preferential adsorption of surfactant molecules to PCL, resulting in low PCL-water interfacial tension but high PLGA-water interfacial tension. Heterogeneous SDS adsorption has been observed in the formation of PS/PMMA composite particles [72]. The PLGA phase is nearly surrounded by the PCL phase to minimize PLGA contact with water. As more surfactant is added, the interfacial tension of PLGA-water decreases to a degree comparable to that of PCL-water, and hemispherical Janus particles are obtained. At high concentrations of SDBS, PLGA-water and PCL-water interfacial tensions are decreased to the point that polymer contact with water becomes as energetically favorable as or more favorable than that of the polymers with each other, and the two polymer phases begin to pull apart. Nonionic surfactants resulted in biphasic Janus

particles regardless of the type or concentration of surfactant used. This is in agreement with previous studies, where the morphology of PS/PMMA composite particles changed when SDS was used as a surfactant, but not PVA [71, 117]. Other nonionic surfactants such as Span 20, Tween 80, Poloxamer 188, and soy lecithin also did not result in a deviation from the biphasic Janus morphology.

2.3.7 Effect of Drug Loading on Particle Morphology

Because the intended application of these biodegradable Janus particles is drug delivery, many different drugs were loaded into the particles to determine their suitability as drug carriers. The following hydrophobic compounds were studied: ibuprofen, griseofulvin, fenofibrate, indomethacin, omeprazole, curcumin, and quercetin. The drugs were loaded at concentrations ranging from 2.5 wt.% to 20 wt.% of the total polymer content. Interestingly, PLGA/PCL Janus particles loaded with griseofulvin displayed a spherical morphology with surface pox marks. None of the other drugs tested had an effect on particle morphology. SEM images of griseofulvin pox mark particles are shown in Figure 12.

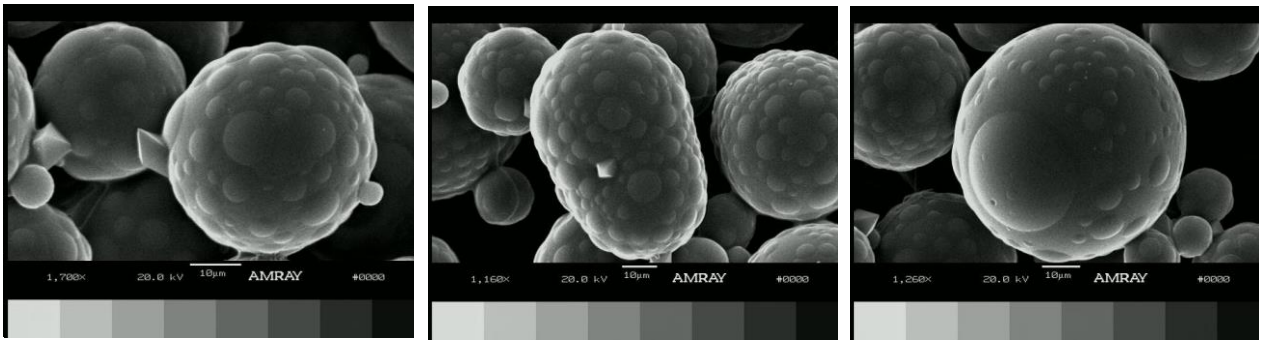

Figure 12: PLGA/PCL Janus particles containing griseofulvin.

It is clear from the SEM images that small blisters of PLGA formed on the surface of the outer PCL matrix. Similar microphase structures have been reported in polystyrene (PSt)/polyisoprene (PI) particles when block-copolymers containing PSt and PI segments

were introduced into the oil phase [118]. It is hypothesized that griseofulvin acts as a compatibilizer and lowers the interfacial tension between the two polymers, thus preventing phase separation from occurring and instead promoting the formation of PLGA islands.

2.3.8 Zeta Potential Studies

Zeta potentials of Janus particles prepared using four different surfactants, namely PVA, CTAB, SDS, and SDBS, were measured. PCL particles prepared under identical conditions were used as the control. Results are shown in Table 3.

Surfactant	Janus particles ζ (mV)	PCL particles ζ (mV)
1% PVA (nonionic)	-32.20 ± 0.78	-30.13 ± 1.26
1% CTAB (cationic)	26.27 ± 2.59	14.97 ± 3.49
1% SDS (anionic)	-52.67 ± 0.64	-60.73 ± 0.91
1% SDBS (anionic)	-51.2 ± 1.99	-47.7 ± 0.44

Table 3: Zeta potential of Janus particles and pure PCL particles prepared using the indicated surfactant.

Zeta potential values of at least |30| mV and |20| mV are required to obtain a physically stable suspension for electrostatic and sterically stabilized systems, respectively [119]. All Janus particle samples exceeded the criteria for colloidal stability. Although PVA is uncharged, PVA and other nonionic surfactants have been found to impart surface charges to nanoparticles as result of hydrophobic interactions [120, 121]. The anionic surfactants SDS and SDBS resulted in the largest absolute value negative zeta potentials for both the Janus particles and the PCL particles. Conversely, the cationic surfactant CTAB resulted in positive zeta potential values. These results indicate that surfactant molecules adsorb onto the particle surface and remain there after formation.

2.3.9 Anisotropic Features of Janus Particles

XRD was performed on empty PLGA/PCL Janus particles and PLGA/PCL Janus

particles containing 5% w/w griseofulvin. PLGA particles, PCL particles, and griseofulvin powder were used as reference samples. Diffraction patterns are shown in Figure 13.

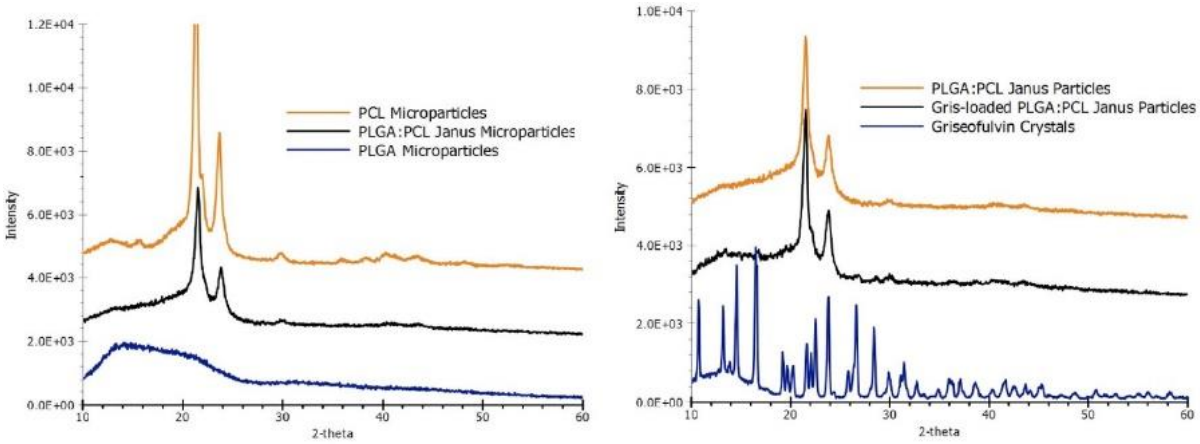

Figure 13: (a) XRD pattern of PLGA/PCL Janus microparticles, (b) XRD pattern of PLGA/PCL Janus microparticles containing 5% w/w griseofulvin.

PCL particles and griseofulvin powder exhibited crystalline diffraction patterns consistent with the literature. PLGA is amorphous, therefore its diffraction pattern does not contain peaks. The diffraction pattern of PLGA/PCL Janus particles is a sum of the diffraction patterns of the reference PLGA particles and PCL particles, indicating the presence of two distinct PLGA and PCL compartments. The two large peaks between 20 and 25 degrees are the contribution from the PCL phase. The diffraction pattern for PLGA/PCL Janus microparticles with 5% w/w griseofulvin did not differ significantly from that of empty PLGA/PCL Janus particles. This suggests that the drug is encapsulated inside the particle rather than dispersed within the polymer matrix. PLGA/Precirol® particles were excluded from this study due to the low crystallinity of both materials; XRD does not provide reliable analysis of crystallinity in systems containing less than 10% crystalline material [122].

Raman spectroscopy was also used to probe the chemical composition of the two separate compartments of the Janus particles. The spectrum is shown in Figure 14. The signal of the smaller compartment exhibits the characteristic peaks corresponding to PLGA

(2945 cm^{-1} and 3002 cm^{-1}), while that of the larger compartment exhibits the characteristic peaks belonging to PCL (2872 cm^{-1} and 2919 cm^{-1}) [123].

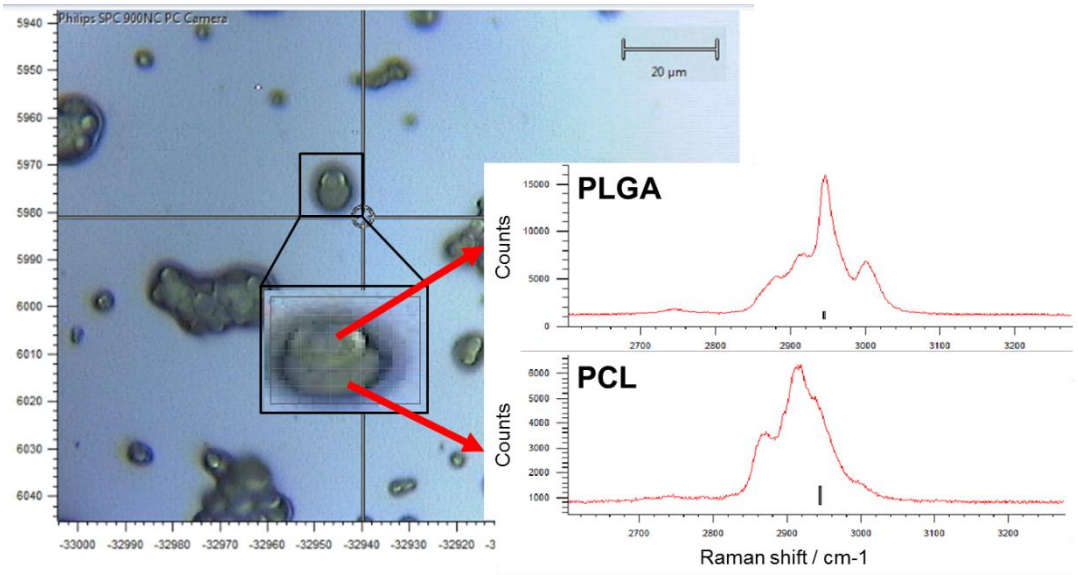

Figure 14: Raman spectrum of a 50:50 PLGA/PCL Janus particle.

To further study anisotropy, the hydrophobic azo dye Sudan Red III was introduced into the oil phase with the polymers prior to emulsification in order to determine localization within the particle. Initially, the red dye was evenly dispersed within both compartments. After some time, the dye migrated to the more hydrophobic PCL compartment and remained there for 10 days. Figure 15 shows PLGA/PCL Janus particles containing 50 mg Sudan Red III four hours after formation, two days after formation, and 10 days after formation.

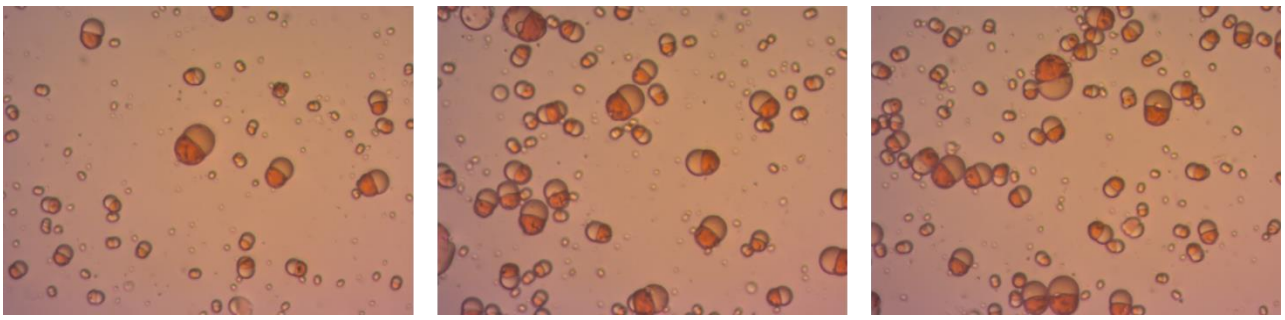

Figure 15: PLGA/PCL Janus particles containing Sudan Red III hydrophobic dye (from left to right: four hours, two days, and 10 days after formation).

The anisotropic nature of the particles was further corroborated by observing their behavior under an electric field. Upon application of a 1.5-volt potential, PLGA/PCL Janus particles rapidly oriented with their more hydrophobic compartment, PCL, facing the positive anode. Similarly, the Precirol® tails of PLGA/Precirol® Janus particles migrated towards the positive anode under an electric field. In both studies, particles reverted back to their original orientation after removal of the electric field. Figure 16 shows PLGA/PCL Janus particles before and after application of an electric field.

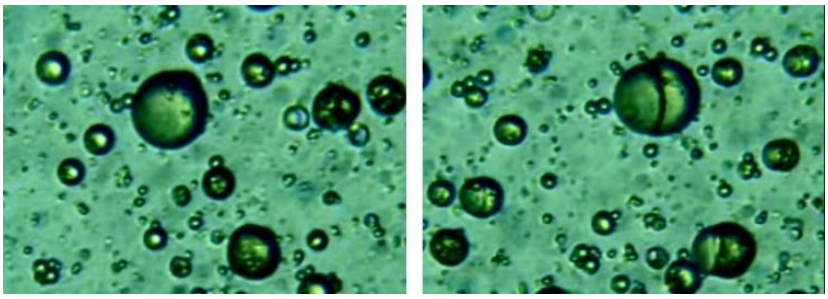

Figure 16: (a) PLGA/PCL Janus particles before application of electrical field, (b) PLGA/PCL Janus particles under a 1.5-volt potential.

2.4 Conclusions

A novel technique for synthesizing compartmentalized Janus particles based on the phase separation of biodegradable materials is presented. In this method, preformed polymers or lipids are mixed together and allowed to phase separate within emulsion droplets during solvent evaporation. The final particle morphology is determined by both kinetic and thermodynamic factors, such as evaporation rate and interfacial tensions,

respectively. Slow evaporation is crucial to allow enough time for phase separation to occur and to achieve the desired biphasic Janus morphology. Otherwise, the polymers will remain in mixed state and the resulting spherical particles will have pockets of each polymer on the surface. Solvent evaporation rate can be modulated by temperature, pressure, and vessel surface area. From a thermodynamic perspective, the equilibrium morphology is the one with the lowest free energy. The extent of surface tension reduction depends on the chemical properties of the surfactant; therefore, the type and concentration of surfactant greatly affects particle morphology. However, it was found that nonionic surfactants have no effect on particle morphology. This will be explored in greater detail in Chapter 5.

The compartmentalization and anisotropy of the Janus particles was confirmed via optical and scanning electron microscopy, XRD, Raman spectroscopy, and observation under an electric field. Results from zeta potential studies show that Janus particles have zeta potential values greater than 20 mV in absolute value, rendering them colloidally stable. As with traditional spherical particles, the mean particle diameter of Janus particles is largely dependent on surfactant concentration as well as the level of shear applied during the emulsification and homogenization steps. Manual shaking results in Janus particles with diameters in the tens of microns, rotor stator homogenization gives particles between 500-1000 nm in diameter, and high pressure homogenization yields sub-500 nm particles.

CHAPTER 3: DUAL DRUG-LOADED JANUS PARTICLES FOR CO-DELIVERY OF HYDROPHOBIC AND HYDROPHILIC COMPOUNDS

This chapter will be reproduced for the following publication:

Winkler, J.S., Tomassone, M.S. Dual Drug Delivery and Controlled Release from Biodegradable Janus Particles. To be submitted to Langmuir.

3.1 Introduction

The desire for drug delivery systems with tunable properties and multiple functionalities has spawned a new generation of particulate carriers, including Janus particles. Biocompatible Janus particles with internal compartmentalization are attractive as drug delivery vehicles because they offer a platform for co-delivery of two drugs with decoupled release kinetics. The onset and rate of drug release from each of the two compartments is determined by the properties of the polymer matrix. Particles could be designed to release both drugs simultaneously or sequentially. Staggered release profiles are especially desirable in treating certain diseases that require exposure to one active agent at a specific rate, followed by exposure to another active agent at a different rate. For instance, in cancer treatment, it would be greatly beneficial to release chemosensitizers followed by chemotherapy in order to mitigate multidrug resistance (MDR).

Curcumin (CUR) and quercetin (QCT) were chosen as the model hydrophobic compounds, while acetaminophen (APAP) and naproxen (NPX) were chosen as the model hydrophilic-hydrophobic drug pair. Curcumin and quercetin are bioflavonoids with anti-inflammatory, anti-proliferative, and immunosuppressive properties used to treat a host of diseases, including multi-drug resistant cancer and arthritis [124, 125]. Acetaminophen and naproxen are often used in combination due to their additive effects in pain management and treatment of rheumatoid arthritis [126, 127]. The goal of this work is to obtain dual-

loaded Janus particles with a different drug in each compartment, and to determine their encapsulation efficiency and drug content.

Hydrophobic drugs were encapsulated into Janus particles by including them in the oil phase prior to emulsification. The O/W single emulsion method is not suitable for microencapsulation of water soluble compounds due to rapid partitioning into the outer aqueous phase. Incorporation of a hydrophilic compound is achieved by the following strategies: single oil-in-water (O/W) emulsion containing a partially water-miscible solvent, O/W emulsion using a co-solvent (O/W-S), and double water-in-oil-in-water (W/O/W) emulsion. Double emulsions are widely used in preparing polymer nanoparticles for the delivery of hydrophilic compounds [128-132]. The double emulsion method requires two surfactants: one for the inner aqueous phase and one for the outer aqueous phase. The drug is dissolved in the inner aqueous phase, which is emulsified into a polymer solution in organic solvent to form the primary emulsion. The primary emulsion is then added to the outer aqueous phase containing surfactant and homogenized to produce the double emulsion. The solvent is allowed to evaporate, leaving an aqueous suspension of particles. The same factors that influence particle formation from single emulsions discussed in the previous chapter also apply to double emulsions. In addition, there are more variables related to the internal W/O emulsion to take into consideration, such as W/O emulsifier type and concentration and internal water phase volume and composition.

3.2 Materials and Methods

3.2.1 Materials

Poly(lactide-co-glycolide) (PLGA, lactide:glycolide=65:35, M.W.=40,000-75,000), polycaprolactone (PCL, M.W.=42,500-65,000), poly(ethylene glycol) (PEG, M.N.=400),

sodium dodecyl benzylsulfate (SDBS), curcumin (CUR), quercetin (QCT), naproxen (NPX), acetaminophen (APAP), dichloromethane (DCM), methanol, acetone, and tetrahydrofuran (THF) were purchased from Sigma Aldrich (St. Louis, MO, USA). Span 80 was obtained from Fisher Scientific (Waltham, MA, USA). Polyvinyl alcohol (PVA, 98 mol% hydrolyzed, M.W.=9,000-10,000) was obtained from Polysciences (Warrington, PA, USA). All materials used in this study are of analytical grade.

3.2.2 Preparation of PLGA/PCL Janus Particles by the Single Emulsion Method

PLGA/PCL Janus particles containing CUR and QCT were synthesized using the O/W emulsion-solvent evaporation method as described in Section 2.2.2. Janus particles containing APAP and NPX were also synthesized using an O/W emulsion-solvent evaporation method, but with some modifications to accommodate the loading of APAP. Due to the fact that APAP is poorly soluble in the chlorinated hydrocarbon solvents that are typically used for O/W emulsions (i.e., DCM and chloroform), two different strategies were employed: 1) single oil-in-water (O/W) emulsion containing a partially water-miscible solvent, and 2) O/W emulsion using a co-solvent (O/W-S). Ethyl acetate was used as the solvent for the single O/W emulsion method, and a mixture of DCM and methanol was used as the solvent for the O/W-S method. The solubility of APAP in each of these solvents is provided in Table 4.

Solvent	APAP Solubility (g/kg)
Water	17.39
Ethyl Acetate	10.73
Acetone	111.65
Methanol	371.61
Dichloromethane (DCM)	0.32

Table 4: Solubility of APAP in selected solvents. Data adapted from [133].

The oil phase was comprised of 5% w/v 50:50 PLGA/PCL, 10% w/w APAP, and 10% w/w NPX. For the O/W-S method, methanol was added at various methanol-to-DCM ratios

from 1:1 to 1:4. The water phase was comprised of 1% w/w PVA solution. Typically, 4 mL of oil was added to 10 mL water and emulsified using an Ultra Turrax T-25 rotor-stator for 5 minutes at 12k rpm. The resultant O/W emulsion was magnetically stirred until complete solvent evaporation.

3.2.3 Preparation of PLGA/PCL Janus Particles by the Double Emulsion Method

The inner aqueous phase consisted of 20% w/v APAP dissolved in 75:25 PEG400/water. First, we obtain the primary W1/O emulsion by adding 500 μL of the PEG400/water solution to the oil phase, which consisted of 0.25 g PLGA, 0.25 g PCL, 0.025 g NPX, and 0.2 g Span 80/Tween 80 (HLB 5) dissolved in 5 mL DCM. The W/O emulsion was homogenized using an Ultra Turrax T-25 rotor-stator for 5 minutes at 16k rpm. Finally, the W/O emulsion was added to the outer aqueous phase (12.5 mL 1% PVA w/v solution with 10% w/v NaCl) and emulsified at 6k rpm for 2 minutes. The resultant W1/O/W2 emulsion was magnetically stirred in an open beaker to allow solvent evaporation to proceed. Several formulation variables such as the volume of the W1 phase, the W/O-to-W phase ratio, concentration of W/O emulsifier, total polymer concentration, and NaCl content of the outer aqueous phase were optimized in the design of the Janus particles.

3.2.4 Measuring Encapsulation Efficiency Using UV/Vis

Ultraviolet–visible spectroscopy (UV/Vis) is a technique used to detect the concentration of an absorbed species in solution, in this case, drug compounds. The concentration of an unknown amount of drug can be calculated from standard curves of known concentrations of drug on the basis of Beer-Lambert Law, which states that there is the linear relationship between absorbance and concentration. The following six

wavelengths were chosen for analysis by UV/Vis spectroscopy based on large ΔA: 243, 273, 291, 429, 475, and 500 nm. QCT has peaks at 243 and 273 nm, while CUR has a sharp peak at 429 nm. CUR has a minimum at 291 nm, and QCT has close to zero absorbance at 475 and 500 nm. Standard curves of CUR and QCT containing absorbance values at the six selected wavelengths were constructed from 50:50 methanol/water solutions of known concentration prior to analysis. Methanol was chosen for inclusion in the buffer solution due to its solvation power for CUR, QCT, and NPX. Calibration curves for CUR, QCT, APAP, and NPX are contained in the Appendix.

Following centrifugation, the supernatant was analyzed for drug content. The amount of each drug present in the samples was calculated by deconvoluting the CUR and QCT spectra using the Excel solver function. The same procedure was followed for determining NPX and APAP content, except different wavelengths were selected for analysis (230, 243, 252, 272, 318, and 331 nm). Encapsulation efficiency was calculated using the following equation:

$$\text{E.E. (\%)} = \frac{Initial\ drug\ loaded - Free\ drug}{Initial\ drug\ loaded} * 100$$

The drug loading was calculated using the following equation:

$$\text{D.L. (\%)} = \frac{Actual\ drug\ content\ of\ particles}{Amount\ of\ drug + polymer} * 100$$

The EE of Janus particles containing CUR and QCT was also measured by dissolving an accurately weighed amount of particles in THF (calibration curves are contained in the Appendix). The equation used to directly measure EE is given below:

$$\text{E.E. (\%)} = \frac{Drug\ in\ Particles}{Initial\ Drug\ Loaded} * 100$$

This approach can be used for CUR and QCT because these two compounds are in the visible range and their signals are not affected by the presence of the polymers, unlike NPX

and APAP.

3.3 Results and Discussion

3.3.1 Preparation of PLGA/PCL Janus Particles Containing CUR and QCT

The inclusion of CUR and QCT, two poorly-water soluble compounds, did not affect the Janus particle morphology. SEM and optical microscope images of Janus particles containing CUR and QCT are shown in Figure 17.

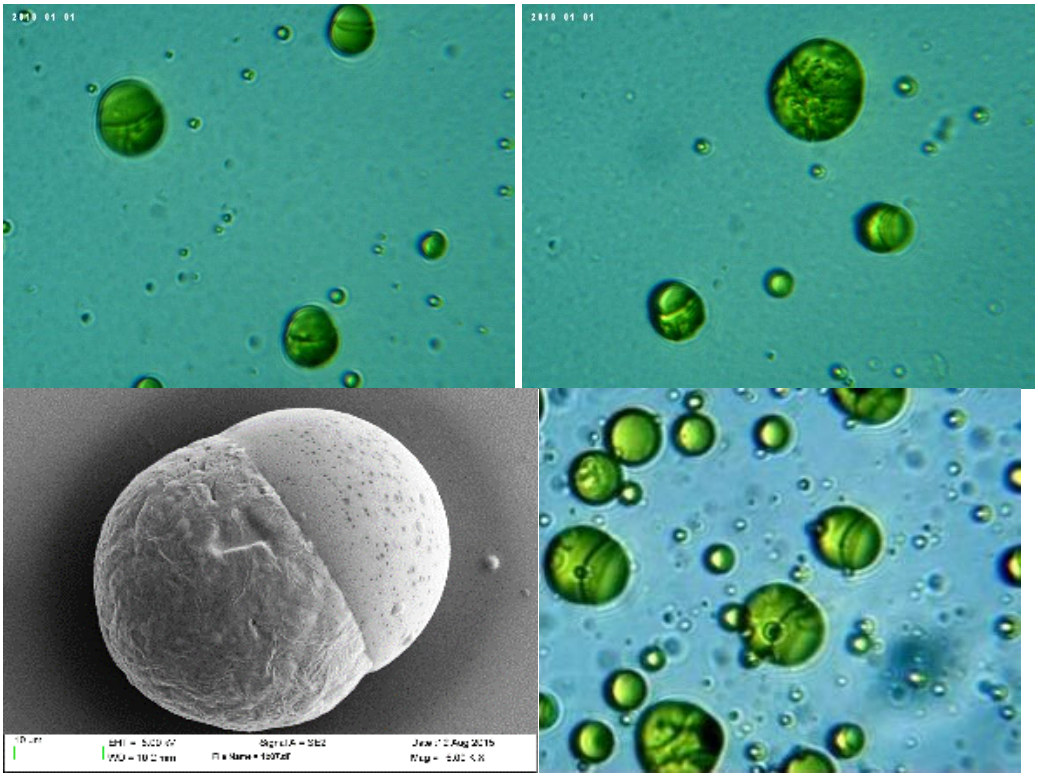

Figure 17: SEM and optical microscope images of PLGA/PCL Janus particles containing CUR and QCT.

CUR and QCT were loaded at concentrations of 2.5% w/w and 5% w/w, respectively, to facilitate simultaneous UV/Vis spectroscopy measurement of both compounds. The UV/Vis spectra of CUR is much stronger than that of QCT, which would result in a mismatch of absorbance values at equal concentrations and make it impossible to measure both simultaneously. An example of this is shown in Figure 18 below. Clearly, the curcumin signal is so strong that the quercetin would not be able to be measured at all

in a mix of the two.

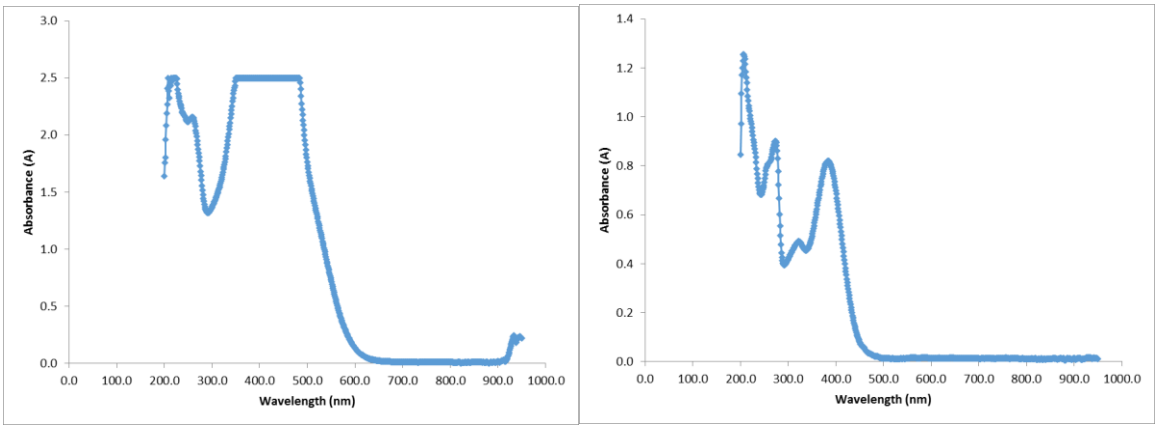

Figure 18: UV spectra of CUR and QCT in 50:50 methanol/water at a concentration of 0.00625 mg/mL.

3.3.2 Preparation of PLGA/PCL Janus Particles Containing APAP and NPX using the O/W Emulsion Method with a Partially Water-Miscible Co-solvent

Ethyl acetate was used as the partially water-miscible solvent for co-encapsulation of APAP and NPX. Although the solubility of APAP in ethyl acetate is quite low, it is higher than that in DCM (10.73 g/kg vs. 0.32 g/kg). Optical images of PLGA/PCL Janus particles containing APAP and NPX are shown in Figure 19. These Janus particles appear to have holes on the surface as result of the slow evaporation rate and long residence time of ethyl acetate.

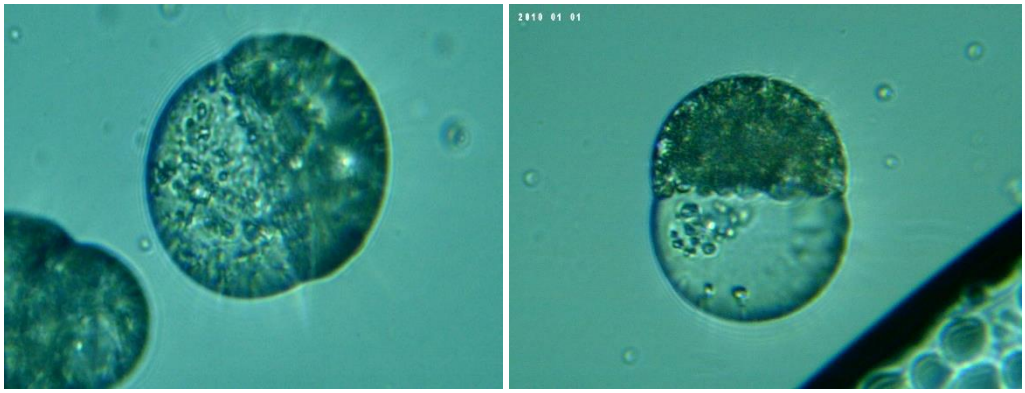

Figure 19: PLGA/PCL Janus particles containing APAP and NPX prepared by the O/W method using ethyl acetate.

3.3.3 Preparation of PLGA/PCL Janus Particles Containing APAP and NPX using the O/W Emulsion Method with a Partially Water-Miscible Co-solvent

Janus particles containing APAP and NPX were prepared using the co-solvent method using methanol as the co-solvent. The resulting Janus particles are shown in Figure 20.

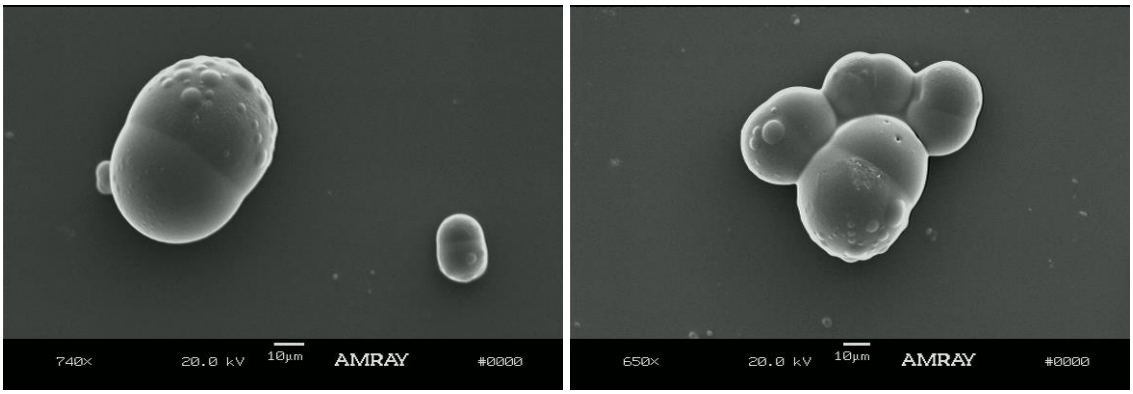

Figure 20: PLGA/PCL Janus particles containing APAP and NPX prepared by the O/W-S method using methanol.

Various co-solvent-to-solvent ratios were tested in the development of the formulation. It was found that using too much co-solvent disrupts phase separation, leading to triphasic particles. Conversely, not having enough co-solvent results in the formation of free drug needles due to the partitioning of the drugs to the aqueous phase. The importance of the co-solvent volume ratio is demonstrated in Figure 21.

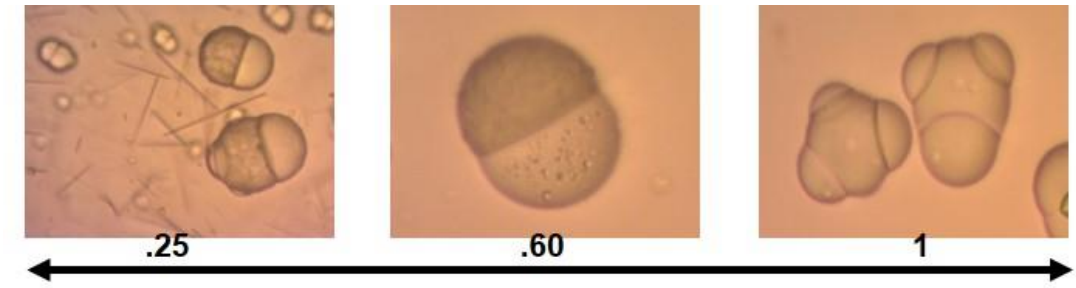

Figure 21: PLGA/PCL Janus particles containing APAP and NPX prepared by the O/W-S method at the indicated methanol-to-DCM ratios.

Acetone was also tested as a co-solvent. These particles had noticeably more surface protrusions than when methanol was used as a co-solvent. Examples are shown in Figure 22.

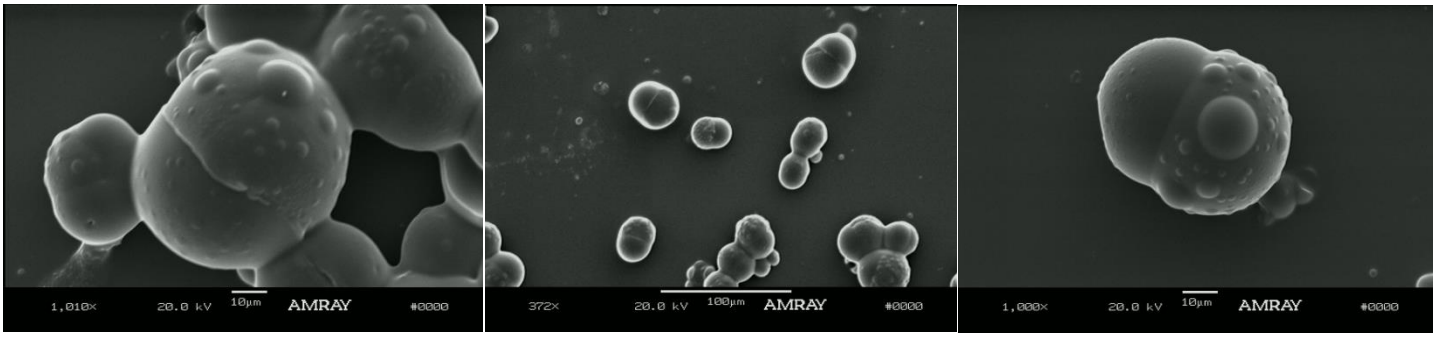

Figure 22: PLGA/PCL Janus particles containing APAP and NPX prepared by the O/W-S method using acetone.

3.3.4 Preparation of PLGA/PCL Janus Particles Containing APAP and NPX using the W/O/W Emulsion Method

The double emulsion method was used to encapsulate APAP in inner water droplets within Janus particles containing NPX. Using a 75:25 v/v mixture of PEG 400/water as the inner aqueous phase instead of water greatly increased the amount of APAP that could be incorporated into the particles. The solubility of APAP in a 75:25 blend of PEG 400/water is ~220 mg/mL, compared to only approximately 12 mg/mL in water. It is important to minimize the volume of W1 because smaller internal water phase volume has been shown to reduce porosity and burst release [68, 134]. Thus, a W1/O/W2 ratio of 1/10/30 was used. PLGA/PCL Janus particles containing APAP and NPX prepared by the double emulsion method are shown in Figure 23. These particles exhibit an oblong shape compared to the standard PLGA/PCL biphasic Janus particles normally obtained with single emulsions.

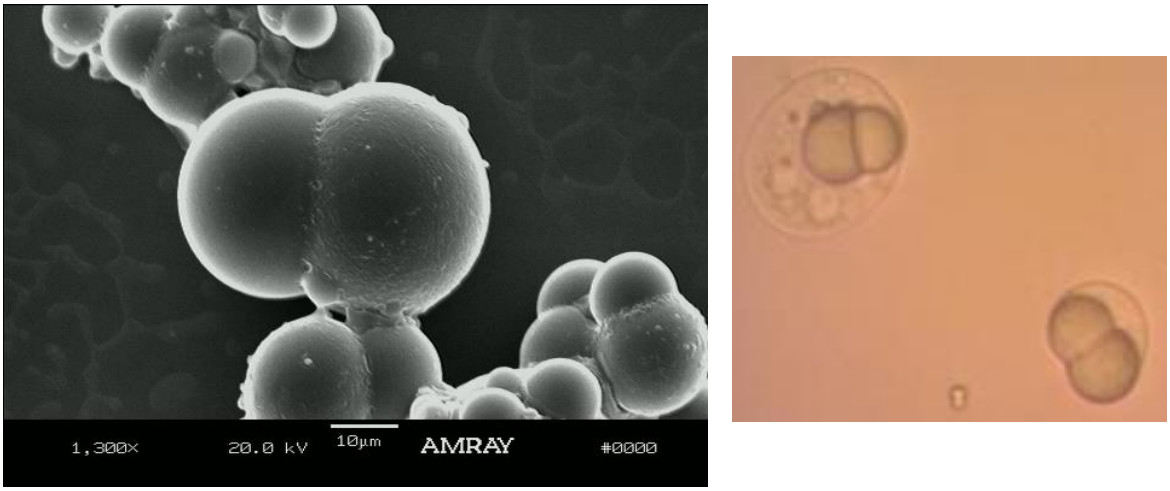

Figure 23: PLGA/PCL Janus particles containing APAP and NPX prepared by the double emulsion method.

The complexity of W/O/W emulsions renders the formulation and process variables much more important and less flexible than a standard O/W emulsion process. For example, it was found that the primary W/O droplets should be significantly smaller in diameter than the outer O/W emulsion droplets to prevent coalescence and rupture of inner droplets. Surface protrusions due to large W/O emulsion droplets are shown in Figure 24. Additionally, NaCl was added to the external aqueous phase in order to balance the osmotic pressure gradient, leading to greater emulsion stability [68, 135]. This allows the W/O emulsion droplets to remain small and prevents destabilization of the W/O/W emulsion.

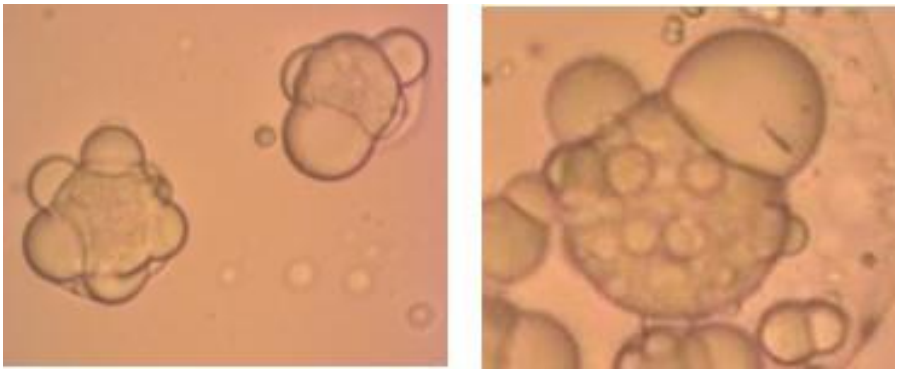

Figure 24: Disruped phase separation and protrusion of inner water droplets.

3.3.5 Encapsulation Efficiency of Janus Particles

The encapsulation of CUR and QCT, two hydrophobic compounds, by the single

emulsion technique is relatively straightforward. The EE of Janus particles loaded with 2.5% w/w CUR and 5% w/w QCT was calculated both directly (particles dissolved in THF) and indirectly (subtracting free drug in supernatant) with similar results (Table 5). As expected, both CUR and QCT were loaded into Janus particles and pure PCL particles with high encapsulation efficiency. The EE of CUR and QCT in Janus particles was approximately 93.11% and 92.03%, respectively, which is comparable to that of CUR and QCT in pure PCL particles (93.38% and 86.90%). EE is partly determined by the strength of drug-polymer interactions; therefore, Janus particles can be designed to provide a higher EE by using polymers with which each drug is known to interact. The EE values measured by analyzing the supernatant were very close to those measured by dissolving the particles, which validates this method of analysis.

	Particles Dissolved in THF		**Supernatant**	
	CUR EE (%)	**QCT EE (%)**	**CUR EE (%)**	**QCT EE (%)**
Janus Particles	93.11 ± 0.86	92.03 ± 4.19	93.10 ± 1.95	89.55 ± 5.69
PCL Particles	93.38 ± 0.55	86.90 ± 1.05	92.99 ± 0.21	83.97 ± 0.87

Table 5: Encapsulation efficiencies of CUR and QCT in Janus and PCL particles prepared by the O/W emulsion technique.

As mentioned previously, the encapsulation efficiency of APAP and NPX can only be measured from the supernatant and not dissolved particles due to interference from the polymers' spectra. The EE and DL of Janus particles containing APAP and NPX synthesized via the ethyl acetate-in-water single emulsion method, the O/W emulsion method using DCM as the solvent and methanol as a co-solvent, and the W/O/W emulsion method are contained in Table 6.

Synthesis Method	**APAP EE (%)**	**APAP DL (%)**	**NPX EE (%)**	**NPX DL (%)**
O/W with Ethyl Acetate	54.90 ± 16.01	4.26 ± 0.49	93.98 ± 0.45	7.22 ± 0.83
O/W with DCM + Methanol	21.04 ± 0.72	1.69 ± 0.28	91.88 ± 1.00	7.36 ± 0.86
Double Emulsion	68.29 ± 3.04	15.93 ± 4.39	85.49 ± 0.20	9.14 ± 2.50

Table 6: Encapsulation efficiencies of APAP and NPX in Janus particles synthesized via single and double emulsions.

The initial drug loading for APAP and NPX was approximately 10% w/w total for all formulations, with the exception of APAP in the double emulsion batch. The theoretical loading for APAP in Janus particles prepared by the double emulsion was approximately 21.8% w/w. The actual drug loading was determined based on the EE and the total mass of the particles (polymers + drugs). As expected, the double emulsion method resulted in the highest EE for APAP due to its high solubility in water and insolubility in oil. Double emulsions are frequently used for the entrapment of hydrophilic compounds. A very high concentration of APAP is possible using the W/O/W emulsion technique with PEG400/water as the inner water phase despite the small volume of W1. For example, even with an inner water phase only $1/10^{th}$ of the volume of the oil phase that contains NPX, there is a higher content of APAP than NPX (15.93% w/w total formulation vs. 9.14%). The O/W-S method using methanol resulted in the lowest EE despite APAP's high solubility in methanol. This is due to the fact that methanol is completely miscible with water, causing most of the APAP dissolved in methanol to escape to the water phase during evaporation since APAP is soluble in water and practically insoluble in DCM. Using ethyl acetate as the solvent resulted in a moderate EE of APAP. All three methods resulted in relatively high EE of NPX, which is expected for the encapsulation of hydrophobic compounds using O/W emulsion-based techniques.

3.4 Conclusions

PLGA/PCL Janus particles were loaded with two hydrophobic compounds, CUR and QCT, via the standard single O/W emulsion technique. The EE of Janus particles was comparable to that of pure PCL particles. Three different strategies were employed to achieve encapsulation of a hydrophobic drug: 1) O/W emulsion containing a partially

water-miscible solvent (ethyl acetate), 2) O/W emulsion consisting of a DCM-methanol mixture, and 3) W/O/W double emulsion with PEG400/water as the inner aqueous phase. Of these, the W/O/W double emulsion showed the highest EE and overall DL of APAP. NPX was encapsulated into the particles at a reasonably high EE regardless of the synthesis method. These results demonstrate the feasibility of using Janus particles for drug delivery applications.

CHAPTER 4: EVALUATION OF PLGA/PRECIROL® JANUS PARTICLES AS DRUG DELIVERY VEHICLES

This chapter has been adapted with minor modifications from the following publication:

Garbuzenko, O.G.*, **Winkler, J.S.***, Tomassone, M.S., Minko, T. Biodegradable Janus Nanoparticles for Local Pulmonary Delivery of Hydrophilic and Hydrophobic Molecules to the Lungs. Langmuir 2014 (30) 12941-9. (*co-author)
All *in vitro* and *in vivo* studies were performed by the Minko Lab (Ernest Mario School of Pharmacy).

4.1 Introduction

Lipids are frequently employed in drug delivery because they are physiologically well-tolerated and nontoxic. Lipid-based drug delivery systems offer increased serum stability, enhanced bioavailability, and greater drug retention [88-90]. Additionally, entrapping the drug in the lipid portion of the carrier has been shown to improve drug absorption [136]. The three main types of lipid carriers are solid lipid nanoparticles (SLNs), nanostructured lipid carriers (NLCs), and liposomes. SLNs are the lipid analogues to polymeric nanoparticles. Loading of hydrophilic drugs poses a major problem for SLNs due to their solid lipid cores. Liposomes can encapsulate both hydrophilic and hydrophobic compounds, but they suffer from high cost, low drug loading capacity, drug leakage, fast release, and limited storage stability [137]. In an effort to combine the positive attributes of polymeric nanoparticles and lipid carriers while circumventing some of their drawbacks, polymer-lipid hybrid particles were developed [88, 138, 139]. The lipid layer confers bioavailability, while the polymeric core enables higher drug loading of hydrophobic compounds and gives the particles greater physical stability. The lipid shell also promotes drug retention within the core and acts as a physical barrier to slow drug release. However, hydrophilic drugs can only be encapsulated at very low concentrations. The novel polymer-lipid Janus particles presented here offer a platform for encapsulation of hydrophobic and

hydrophilic drugs and sequential or simultaneous release. Polymer-lipid Janus particles are the first hybrid carriers the offer compartmentalization.

In order to demonstrate their therapeutic benefit, Janus particles were loaded with two synergistic drugs for the treatment of lung cancer. Doxorubicin (DOX) is an anthracycline antibiotic commonly used as a first-line treatment for a broad spectrum of cancers. DOX binds to DNA through intercalation and poisons topoisomerase II, which halts DNA replication. However, the clinical efficacy of DOX is limited by its cardiotoxicity as well as the development of multi-drug resistance (MDR). Curcumin (CUR) is a polyphenol derived from turmeric spice with antioxidant, anti-inflammatory, anti-angiogenic, and anti-tumoral activities. CUR is known to downregulate three major drug transporters implicated in MDR [140]. It has been shown that CUR enhances nuclear uptake of DOX, inhibits expression of drug transporters, and induces apoptosis of cancer cells [141].

4.2 Materials and Methods

4.2.1 Materials

Polymers and lipids are good candidates for phase separation due to their intrinsic immiscibility. PLGA or PCL was used as the polymer, while Precirol® or Compritol® was used as the lipid. Precirol® ATO 5 and Compritol® 888 ATO are FDA-approved lipids that are frequently used in the production of solid lipid nanoparticles for drug delivery. Precirol® and Compritol® are mixtures of mono, di, and triglycerides [142].

4.2.1 Preparation of PLGA/Precirol Janus Particles by the Double Emulsion Method

Double W/O/W emulsions were used in order to facilitate co-encapsulation of a hydrophilic and a hydrophobic compound. An overview of the process is shown in Figure

25. The inner water phase was created by dissolving 25 mg DOX in 2 mL DI water. The oil phase was created by dissolving 0.5% w/v Span 80, 25 mg CUR, and 2.5% w/v of a 3:1 mixture of PLGA/Precirol® in 4 mL of DCM. The water phase was added to the oil phase and emulsified using a Misonix Sonicator 3000 probe-tip sonicator (QSonica, Newton, CT) to form the primary W/O emulsion. The W/O emulsion was immediately added to a 15 mL surfactant solution consisting of 0.3% w/v PVA and 0.1% w/v SDBS and emulsified. The resulting W/O/W emulsion was magnetically stirred and kept at 40 °C in an open beaker to allow for solvent evaporation. Upon complete solvent removal, particles were harvested by centrifugation at 20,000 rpm for 30 minutes. The supernatant was discarded and the remaining powder bed was washed with deionized water. Particles were stored in a vacuum desiccator for further analysis.

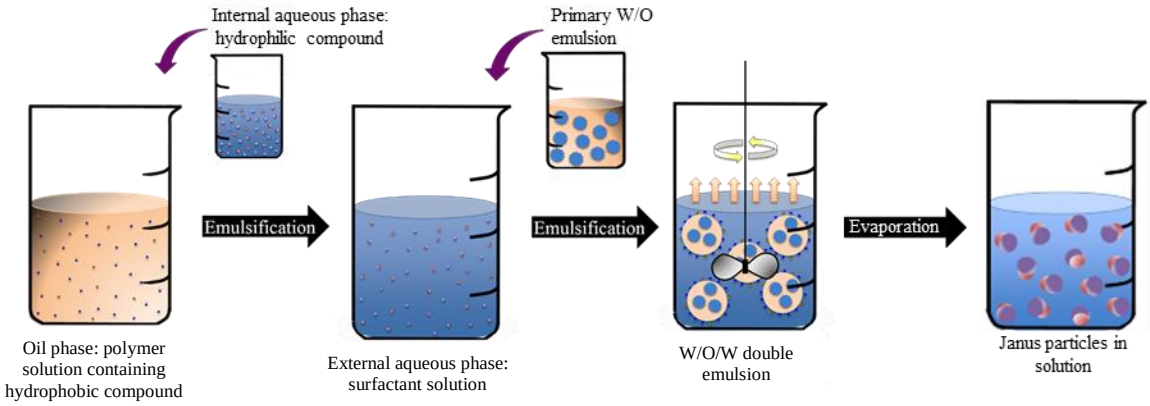

Figure 25: Overview of the double emulsion solvent evaporation method used to encapsulate hydrophilic compounds inside Janus particles.

Empty PLGA/Precirol® Janus particles and CUR-only Janus particles were formed using the single O/W emulsion method. Briefly, 75 mg PLGA and 25 mg Precirol® were dissolved in 4 mL DCM. For CUR-loaded particles, 25 mg CUR was also dissolved in the oil phase. The oil phase was added to a 10 mL water phase consisting of 0.3% w/v PVA and 0.1% w/v SDBS. The solution was emulsified, homogenized, and set in a beaker for

complete solvent evaporation under light agitation by magnetic stirring.

4.2.3 Synthesis of Fluorescently-Labeled PLGA and Precirol®

FITC-labeled PLGA was synthesized via the carbodiimide method [143]. Briefly, 0.5 g PLGA was dissolved in 0.75 mL DCM. The carboxylate groups of PLGA were activated by the addition of 0.1 g NHS and 0.15 g *N*-(3-(Dimethylamino)propyl)-*N*′-ethylcarbodiimide to form PLGA-NHS. The reaction was stirred for 2 hours. Separately, 0.6 g FITC was dissolved in 0.25 mL DCM and 0.25 mL pyridine. The FITC solution was added to the PLGA-NHS solution and stirred for 24 hours, then quenched with 0.1 N HCl. The organic layer was extracted by DCM and washed with water. Following complete solvent evaporation, the solution was centrifuged for 20 minutes. The supernatant was discarded and the precipitate was washed with diethyl ether to obtain PLGA-FITC. The dyed polymer was dried in a desiccator overnight and refrigerated until use.

A 2.5 mg/mL stock solution of lipophilic tracer DiR in DCM was prepared. Precirol® was labeled with DiR by first dissolving 0.5 g Precirol in 25 mL DCM. Next, 0.2 mL DiR solution was added to the lipid solution. The mixture was stirred overnight in a closed container. The DCM was then evaporated, leaving Precirol®-DiR. The stained lipid was dried in a desiccator overnight and refrigerated until use.

4.2.4 Cellular Internalization

The cell uptake of Janus nanoparticles by A549 human lung cancer cells was visualized by fluorescent microscopy (LSM 500, Carl Zeiss, Germany) following a standard method [144, 145]. Cells were incubated with PLGA-FITC/Precirol®-DiR Janus particles for 24 hours at 37 °C. Images were taken using the green and red channels to

detect PLGA and FITC, respectively. Superimposition of the images allowed for visualization of the polymer and lipid phases within the A549 cells.

4.2.5 Cytotoxicity and Genotoxicity of Janus Particles

The cytotoxicity of 450 nm Janus particles was measured using a modified 3-(4,5-dimethylthiazol-2-*yl*)-(2,5-diphenyltetrazolium bromide) (MTT) assay with 24, 48, and 72 hour time points as previously described [146]. Briefly, 10,000 A549 human lung cancer cells were incubated in separate wells of a 96-well plate. Different concentrations of empty Janus nanoparticles (2–20 mg/mL), free DOX (0.0003–0.65 mg/mL), Janus nanoparticles with CUR (0.00004–0.35 mg/mL), Janus nanoparticles with DOX (0.0002–1.75 mg/mL), Janus nanoparticles with CUR (0.00004–0.35 mg/mL), and DOX (0.0002–1.75 mg/mL) was added to each well. The noncytotoxic dose of Janus nanoparticles that provided for 100% cell survival was the concentration chosen for future experiments.

Genotoxicity was measured using an in vitro micronucleus assay as previously described [146]. Approximately 3,000 cells were cultured with media in 25 cm^2 flasks for 24 hours prior to treatment. Cells were then incubated with particles for 24, 48, and 72 hours. Negative control cells were incubated with fresh media, whereas positive control cells were treated with 400 g/mL ethylmethanesulfonate. After incubation, the cells were fixed in a cold solution of 100% methanol. The methanol was removed and the cells were washed with phosphate buffer. Cell nuclei were stained using 600 nM DAPI for 8 minutes. This solution was removed and flasks were washed using PBS containing 0.05% w/v Tween 20. After staining, the formation of micronuclei was detected by fluorescent microscopy. The number of micronuclei per 1000 cells was counted.

4.2.6 Biodistribution of Janus Particles

Athymic nude mice 6–8 weeks old were obtained from Taconic (Hudson, NY). All mice were maintained in microisolated cages under pathogen free conditions in the animal maintenance facilities of Rutgers, The State University of New Jersey. Veterinary care followed the guidelines described in the guide for the care and use of laboratory animals (AAALAC) as well as the requirements established by the animal protocol approved by the Rutgers Institutional Animal Care and Use Committee (IACUC).

Fluorescently labeled Janus particles (150 nm and 450 nm) were aerosolized by a single jet Collison nebulizer (BGI Inc., Waltham, MA) at a flow rate of 2 L/min using dry and purified air (Airgas East, Salem, NH). An additional air flow of 2–3 L/min was introduced to dilute and desiccate the resulting aerosol according to the previously described procedure [147]. The total 4-5 L/min aerosol flow was directed into the mixing box of a five port exposure chamber (CH Technologies, Westwood, NJ) and transported to each animal containment tube by round pipes. During the inhalation experiments, each animal was positioned in the containment tube so that the animal's nose was at the spout. The air exhaled by the animals escaped through openings in the backside of the cone and was exhausted.

Experimental groups consisted of 6-10 mice. The volume of suspension was 100 μL for both intravenous and inhaled treatments. Janus particle distribution was measured as previously described [147]. Animals were anesthetized with isoflurane and euthanized either 1 hour or 24 hours post treatment. The lungs, liver, spleen, heart, and kidneys were excised, rinsed in saline, and fluorescent intensity was measured by the IVIS imaging system (Xenogen Corporation, Alameda, CA). Images of each organ were scanned and total fluorescence intensity was calculated using the manufacturer software. This method

allows a quantitative comparison of the concentration of the same fluorescent dye between different series of the experiments. The mass of all organs was measured and the fluorescence intensity was normalized by organ mass.

4.2.6 In Vivo Efficacy of Janus Particles

An orthopic mouse model of lung cancer was used to determine in vivo therapeutic efficacy [147]. A549 human lung cancer cells (5-8 x 10^6) transfected with luciferase were resuspended in 0.1 mL of RPMI medium containing 20% fetal bovine serum, mixed with 5 μL of EDTA, and administered intratracheally to the lungs of athymic nude mice through a catheter. Once tumors reached approximately 50 mm^3 in size, treatment was administered biweekly over a period of one month.

Control groups included no treatment, empty Janus particles, free DOX administered intravenously, Janus particles containing CUR only, and Janus particles containing DOX only. The treatment group received Janus particles loaded with both DOX and CUR. The dose of both drugs in all drug-containing formulations was 2.5 mg/kg for each administration. This dose corresponds to the maximum tolerated dose (MTD) estimated in separate experiments based on animal weight change after the instillation of increasing doses of drug formulation. The dose that led to the decrease of mouse body weight by 15% was considered as the MTD. The animals were treated twice per week over a period of one month. Body weight of each mouse was measured using the electronic balances every other day.

Tumor growth was monitored, and tumor volume was calculated using imaging systems as previously described [147]. Imaging was performed under inhalation anesthesia with isoflurane at a concentration of 4% for induction of anesthesia and 1–2% for

maintenance. After the image data acquisition, the recovery time of the animals from anesthesia was usually less than 5 minutes. Optical imaging was performed using in vivo bioluminescent IVIS (Xenogen, Alameda, CA) and magnetic resonance imaging (MRI) was carried by 1TM2 whole body scanner (Aspect Imaging Shoham, Israel) systems as previously described [145]. In order to visualize cancer cells transfected with luciferase, luciferin was injected intraperitoneally in dose of 150 mg luciferin/kg of body weight approximately 15 minutes prior to imaging.

All results are presented as mean values ± the standard deviation (SD) from six to ten independent measurements. Data was analyzed using descriptive statistics, single-factor analysis of variance (ANOVA). The comparison among groups was performed by the independent sample Student's test. The difference between variants is considered significant if $P < 0.05$.

4.3 Results and Discussion

4.3.1 Particle Synthesis and Characterization

By replacing PLGA/PCL with a 3:1 mixture of PLGA/Precirol®, we observed the formation of novel ice cream cone shaped polymer-lipid Janus particles. Figure 26 shows PLGA/Precirol® Janus particles prepared using either 0.3% PVA and 0.1% SDBS or 0.3% SDS and 0.1% SDBS. When SDS was used in place of PVA, the particles exhibited a longer lipid tail. Similar structures were obtained when PCL was used in place of PLGA or Compritol® was used in place Precirol®.

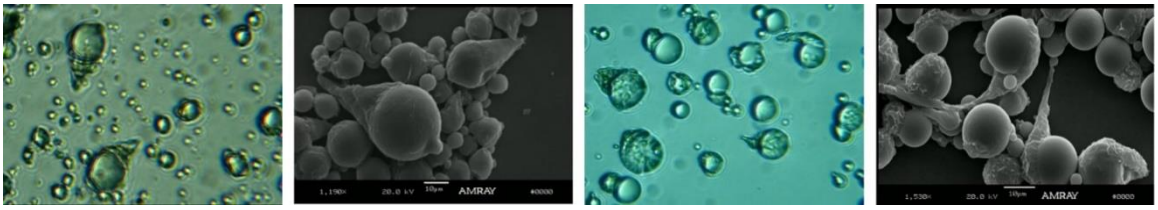

Figure 26: Optical and scanning electron microscope images of PLGA/Precirol Janus particles prepared using (a,b) 0.3% PVA and 0.1% SDBS, (c,d) 0.3% SDS and 0.1% SDBS.

Double W/O/W emulsions were used to encapsulate the hydrophilic and hydrophobic compounds DOX and CUR in PLGA/Precirol® Janus particles. During phase separation in the later stages of solvent evaporation, CUR and DOX segregate into the PLGA and Precirol® compartments, respectively. DOX is contained inside inner W/O emulsion droplets, which localize into the Precirol® phase. Figure 27 shows the transformation of W/O/W emulsion droplets into biphasic PLGA/Precirol® particles via solvent evaporation.

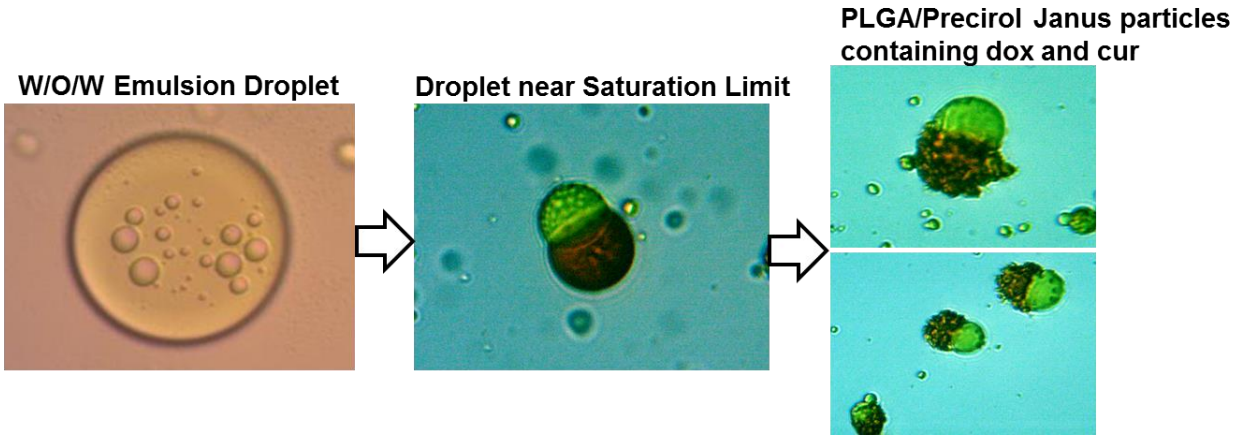

Figure 27: Janus particle formation from W/O/W emulsions.

Resulting PLGA/Precirol® Janus particles exhibited a unique morphology resembling an ice cream cone, with a Precirol® tail hanging from a spherical PLGA head. The particles are compartmentalized, as evidenced by the containment of a different dye in each compartment. The PLGA phase was labeled with FITC, and the Precirol® phase was labeled with DiR. Fluorescently labeled PLGA/Precirol® particles are shown in Figure 28.

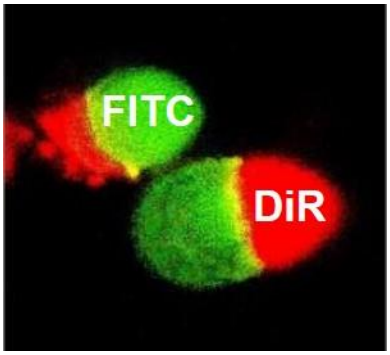

Figure 28: Fluorescently labeled PLGA/Precirol Janus particles.

Experimental groups for in vitro and in vivo studies included empty Janus particles, Janus particles containing DOX only, Janus particles containing CUR only, and Janus particles containing both DOX and CUR. As mentioned previously, the DOX and CUR separated into the Precirol® and PLGA compartments, respectively. PLGA/Precirol® Janus particles containing DOX and CUR, CUR only, and no drug are shown in Figure 29.

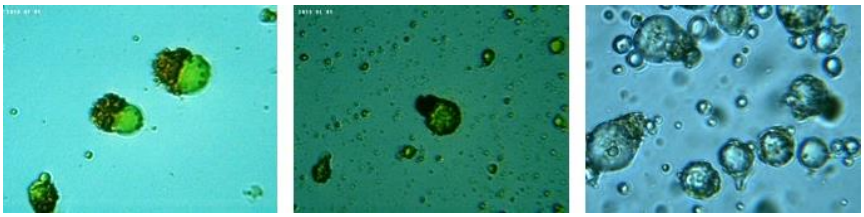

Figure 29: (a) PLGA/Precirol Janus particles loaded with both DOX and CUR, (b) PLGA/Precirol Janus particle with CUR only, and (c) PLGA/Precirol Janus particles without drug.

4.3.2 Cellular Internalization of Janus Particles

To study the effects of size on cellular internalization, Janus particles with a mean diameter of 155 ± 10 nm were synthesized. The polydispersity index (PDI) of these particles was 0.29 ± 0.08, and the zeta potential was -15.22 ± 1.78 mV. Complete cell uptake of fluorescently labeled PLGA/Precirol® Janus particles was achieved by the 150 nm group after 24 hours. Figure 30 shows the uptake of Janus particles by A549 cells. Particles reached both the cytoplasm and the nucleus. Several z-sections were taken to ensure that the particles were internalized as opposed to adhered to the cell surface.

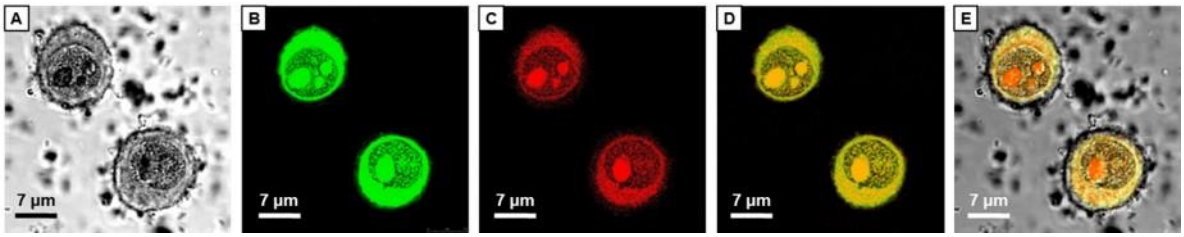

Figure 30: (a) Optical image of A549 human lung cancer cells, (b) fluorescent image showing PLGA-FITC component, (c) fluorescent image showing Precirol-DiR component, (d) superimposition showing co-localization of the PLGA and Precirol components, and (e) superimposition overlaid on optical image.

4.3.3 In vitro Efficacy Studies

In order to determine cytotoxicity of the particles, A549 cells were incubated with Janus particles for 24 hours. Cell viability was determined using the MTT assay. Results are shown in Figure 31.

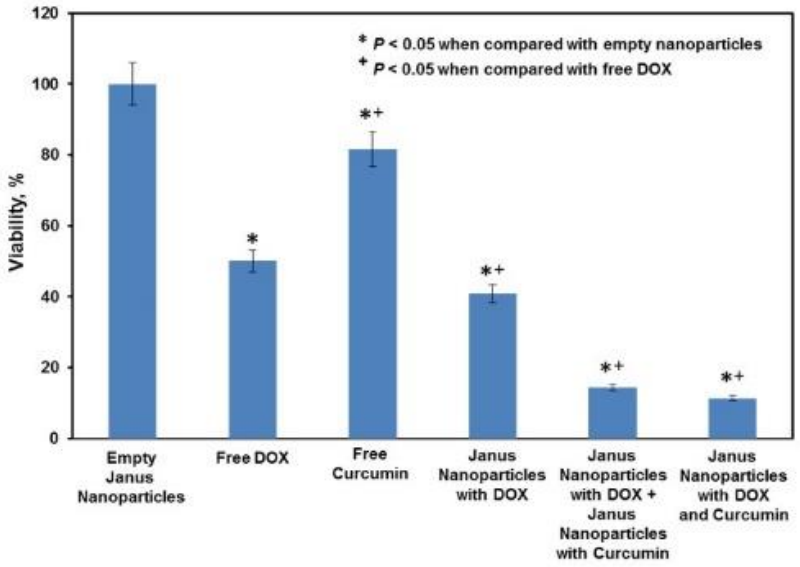

Figure 31: Viability of A549 human lung cancer cells after 24 hour incubation with the indicated treatment.

Empty Janus particles did not affect the viability of A549 cells regardless of concentration. Janus particles containing DOX only elicited a statistically significant therapeutic effect. The therapeutic benefit was even greater when Janus particles containing both DOX and CUR were used. In fact, the viability of lung cancer cells decreased approximately in 5 times after their incubation with nanoparticles containing both drugs. This decrease in cell viability was statistically significant ($P < 0.05$) compared to free DOX and nanoparticles

containing just one drug. A nearly equivalent efficacy was achieved by using a mixture of Janus particles with DOX only and Janus particles with CUR only. These results are expected for a 2D *in vitro* model, where the treatments are applied directly to cells and drugs in nanoparticles are easily internalized due to their small size. Further studies showed that Janus particles do not induce genotoxic effects in A549 cells after 72 hours. As shown in Figure 32, Janus particles did not induce the formation of micronuclei, as did the positive control.

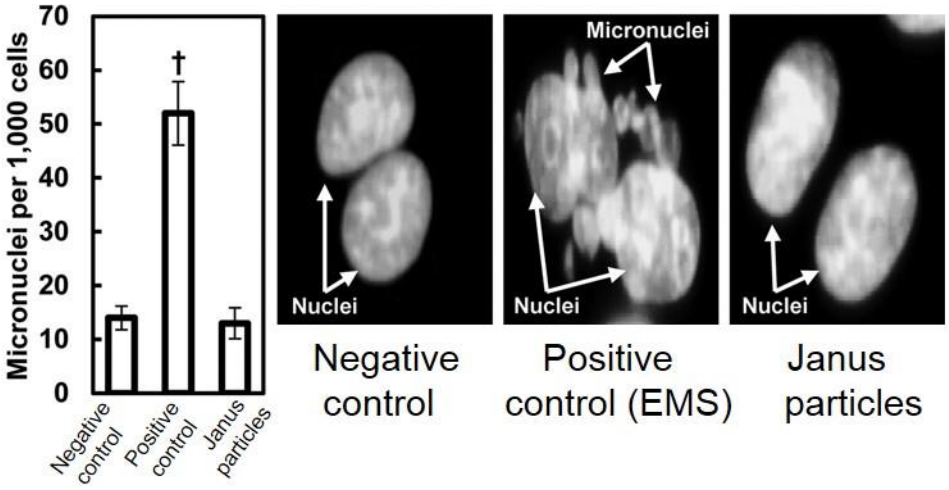

Figure 32: Genotoxicity of Janus particles and controls.

4.3.4 Biodistribution Studies

The biodistribution of 155 nm and 450 nm fluorescently labeled Janus particles was studied in nude mice following either intravenous or aerosol administration. Nebulizing particles prior to inhalation did not alter their mean diameter, as shown in Figure 33.

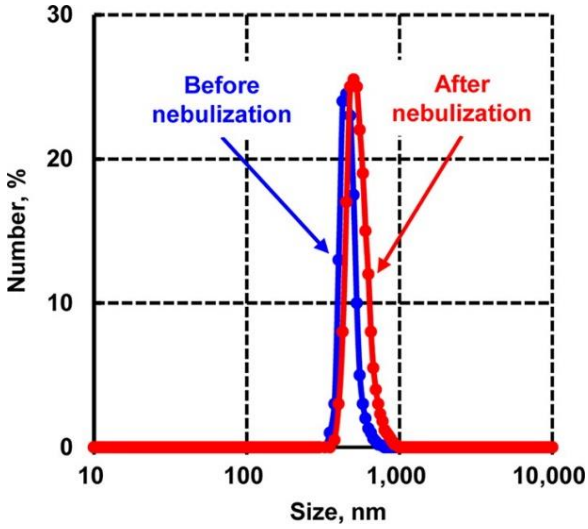

Figure 33: Particle size distribution of PLGA-FITC/Precirol-DiR Janus nanoparticles before and after nebulization.

The lungs were the intended target for this study. Histological analyses 1 hour and 24 hours post administration revealed that 450 nm Janus particles delivered via inhalation gives significantly greater lung deposition than injection. In fact, more than 60% of 450 nm Janus particles reached the lungs after inhalation. These results are in line with the literature, which indicates that if inhaled particles are too small they will be exhaled, and if particles are too large they will deposit in the mouth and throat [148]. There was negligible lung accumulation when particles were injected. Representative histology slices and organ distribution results are shown in Figure 34.

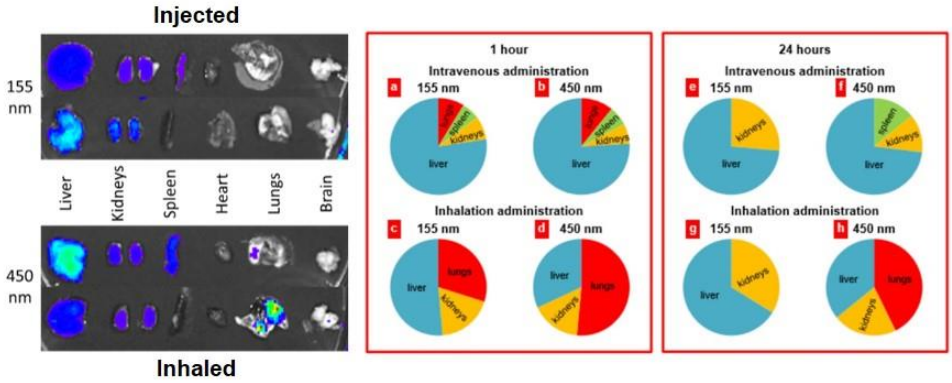

Figure 34: Distribution PLGA-FITC/Precirol-DiR Janus nanoparticles in different organs after intravenous or inhalation administration. The intensity of fluorescence is expressed by different colors ranging from violet (lowest intensity) to red (highest intensity).

4.3.5 In vivo Efficacy Studies

Lung tumor volume was measured over a four-week treatment period using live imaging software. Representative MRI and optical images showing bioluminescence of the lung tumor are provided in Figure 35. Janus particles containing DOX and CUR almost completely suppressed lung tumor growth over a one-month treatment period. Janus particles containing DOX only hindered tumor growth somewhat, and those containing CUR only did so to a lesser extent. This exemplifies the synergistic effects achievable using Janus particles. Intravenous administration of free DOX was not successful in inhibiting tumor progression.

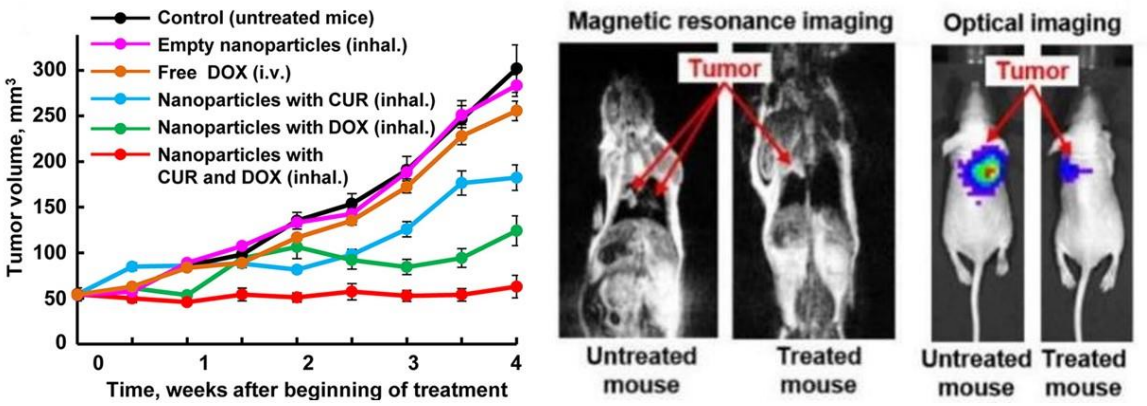

Figure 35: (a) Changes in lung tumor volume after beginning of treatment and (b) representative MRI and optical image four weeks after tumor instillation.

4.4 Conclusions

To date, the majority of Janus particle research focuses on synthesis and self-assembly[149]. One of the major goals of this work was to demonstrate the advantages of Janus particles over isotropic particles in drug delivery. The emulsion solvent evaporation methodology was extended to a lipid-containing formulation in order to demonstrate the robustness of the process and to further increase the applicability of Janus particles in drug delivery. When a 3:1 mixture of PLGA and Precirol® was used in place of a binary

combination of PLGA and PCL, the resulting Janus particles exhibited an ice cream cone morphology. PLGA/Precirol® Janus particles displayed many interesting properties, such as electrical anisotropy and compartmentalization. Hydrophilic compounds were successfully loaded into PLGA/Precirol® Janus particles using a double emulsion.

PLGA/Precirol® Janus particles loaded with doxorubicin and curcumin completely inhibited lung tumor growth in mice over a treatment period of one month. Janus particles containing only doxorubicin hindered tumor growth somewhat, and those containing only curcumin did so to a lesser extent. This exemplifies the synergistic effects achievable using Janus particles. When Janus particles were applied directly to A549 human lung cancer cells in vitro, dual-loaded Janus nanoparticles did not show superior performance over a mixture of Janus nanoparticles containing doxorubicin only and Janus nanoparticles containing curcumin only because both drugs were internalized by the cells regardless of whether they were contained in the same particle. These results combined with the in vivo results attest to the clinical importance of unified delivery and release.

CHAPTER 5: THERMODYNAMIC PREDICTION OF JANUS PARTICLE MORPHOLOGY

This chapter will be reproduced for the following publication:

Winkler, J.S., Clark M.D., Tomassone, M.S. Thermodynamic Prediction of Janus Particle Morphology. To be submitted to Langmuir.

5.1 Introduction

The morphology of PS/PMMA composite particles prepared by the emulsion solvent evaporation method has been well-studied [49, 50, 71, 72, 117, 150, 151]. When PVA was used as a surfactant, PS/PMMA particles with a dimple were produced [71]. PS/PMMA particles retained the same dimple shape when Emulgen 911, another nonionic surfactant, was used at low concentrations but displayed a snowman-like morphology at high concentrations [50]. On the other hand, when SDS was used in place of PVA, the shape of the PS/PMMA particles transformed from dimple to acorn to spherical with increasing SDS content [72].

The effect of surfactant on composite particle morphology can be explained by thermodynamics. Phase separation is driven by the minimization of free energy. Therefore, it is possible to derive a thermodynamic model to predict Janus particle morphology based on Gibbs free energy. It is assumed that no polymer dissolves in the water or vice versa, and that the total volume of each polymer remains constant. As result, the enthalpy and entropy of both polymers will not change with Janus particle morphology. This allows the Gibbs free energy to be calculated only in terms of total interfacial free energy. Biphasic Janus particles have three competing interfacial areas that need to be minimized, namely those between each polymer and the water phase, and that of the two polymers.

Interfacial tensions between the polymer and water phases are controlled by the amount and chemical composition of surfactant. Surfactants in the water phase have little

to no effect on the interfacial tension between two polymers, as the interfacial tension would not be affected by the surfactant unless it adsorbs at the interface of the polymer phases. The interfacial tension between two polymers is generally low in comparison to those between the polymer phases and water phase anyway [50, 72, 152]. Therefore, the interfacial tension between any two polymers is "fixed" and morphology can only be changed by adjusting the interfacial tension between each of the polymer phases and the water phase. When the interfacial tension between one polymer and the water phase is significantly higher than that of the other polymer and the water phase and between the two polymers, core-shell particles result. If the interfacial tension between the two polymers is very high, then two separate particles would form. Otherwise, Janus particles would be produced. The general configurations of Janus particles based on relative interfacial tensions between the three phases (polymer 1, polymer 2, and water) are provided in Table 7.

Polymer 1-Polymer 2	**Polymer 1-Water**	**Polymer 2-Water**	**Morphology**
Low	High	High	Spherical Janus particle with flat interface
High	Low	Low	Janus particle with two nearly separated droplets
Medium	Medium	Medium	Snowman-like Janus particle with two equal halves
High	Medium	Low	Crescent moon shaped Janus particle with polymer 2 nearly surrounding polymer 1

Table 7: Janus particle morphologies resulting from the indicated relative interfacial tensions.

An exact morphology prediction can be obtained by modeling the Janus particle as two overlapping spheres and solving for the minimum Gibbs free energy. The result is a system of equations in which the surface tensions of two of the three the interfaces and the volume ratio, a polymer property, allows for explicit calculation of Janus particle geometry

as defined by the following distances: the heights of Polymer 1 and Polymer 2, the height of the Polymer 1-Polymer 2 interface, and the width of the Polymer 1-Polymer 2 interface.

There have been several attempts to quantitatively describe Janus particle morphology using theoretical calculations with relative success [49, 50, 152, 153]. Unlike previous models, our model does not assume a sphere and is solved in terms of measurable distances instead of radii of curvature. To the best of our knowledge, this is the first model that enables explicit calculation of polymer properties such as interfacial tension and volume ratio from standard microscope images. The thermodynamic analysis is carried out for multiple surfactants at different concentrations in order to compare predicted and experimental morphologies.

5.2 Materials and Methods

5.2.1 Materials

For contact angle measurements, a system comprising a light source, a magnifying lens, and a camera was constructed using the following parts from ThorLabs: 8”x8”x1/2” aluminum breadboard (MB8), four 1”x3”x3/8” mounting bases (BA1), 3” post holder (PH3), two 2” post holders (PH2), 0.25” mounting adaptor (AD2), retaining ring for lens tubes and mounts (SM1RR), 10 1/4" locking thumbscrew for post holders (TS25H), three 1/2” optical posts (TR1.5), cap screw kit ((HW-KIT2/M), and one AR-coated plano-convex lens (LA1131-A). LAMP Images were obtained using a Sony Cybershot MODEL and analyzed using ImageJ, an open source software.

Poly(lactide-co-glycolide) (PLGA, lactide:glycolide=65:35, M.W.=40,000-75,000), polycaprolactone (PCL, M.W.=42,500-65,000), sodium dodecyl sulfate (SDS), sodium dodecyl benzylsulfate (SDBS), cetyltrimethylammonium bromide (CTAB),

acetaminophen, naproxen, griseofulvin, curcumin, quercetin, naproxen, acetaminophen, and dichloromethane (DCM) were purchased from Sigma Aldrich (St. Louis, MO, USA). Polyvinyl alcohol (PVA, 80 mol% hydrolyzed, M.W.~6,000) was obtained from Polysciences (Warrington, PA, USA). All materials used in this study are of analytical grade.

5.2.2 Contact angle measurements

The contact angles of water droplets containing various types and concentrations of surfactant were measured following an experimental setup described elsewhere [154]. Briefly, glass slides were immersed in a 5% w/v polymer solution in DCM in a petri dish. The DCM was allowed to evaporate, leaving a polymer film coating on the glass slide. The slide was mounted and a 5 μL drop of water containing surfactant was pipetted onto the film. Images were obtained using a Sony PowerShot camera after adjusting the lens as necessary. Drop shape analysis was carried out by ImageJ. The experimental setup is shown in Figure 36.

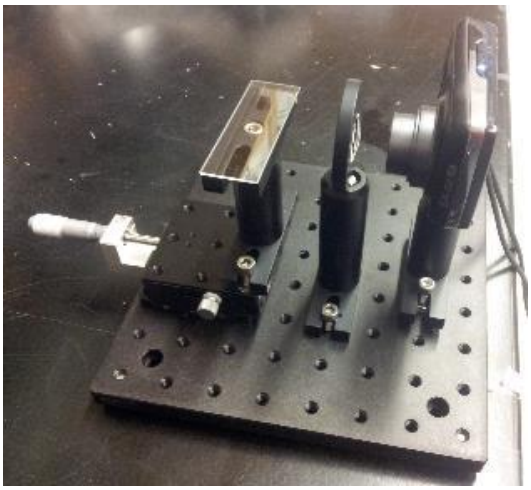

Figure 36: Setup used to measure contact angles.

5.2.3 Theory

Model derivation

The Janus particle is modeled as two overlapping spheres comprised of a Polymer 1 and Polymer 2. The geometric representation of a Janus particle is given in Figure 37.

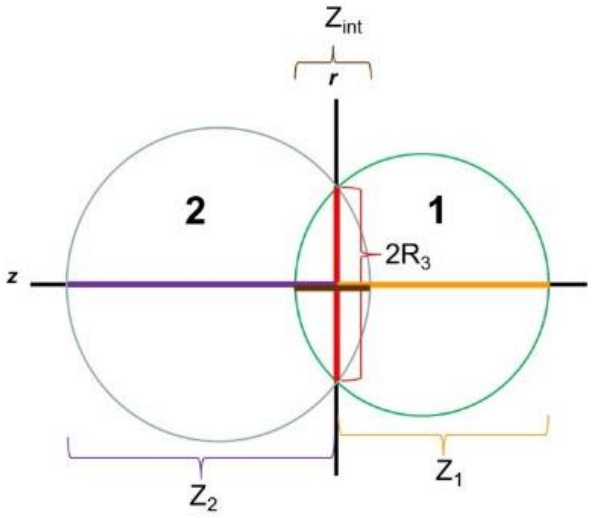

Figure 37: Geometry diagram of Janus particle.

Each surface is defined by the function for a semi-circle, $r^2 = R^2 - (z - z_c)^2$, where R is the semicircle's radius and z_c is its center. As shown in Figure 37, there are four measurable quantities of interest: Z_1, which is the "top" of Polymer 1; Z_2, which is the "bottom" of Polymer 2; R_3, which is the point where all three components (Polymer 1, Polymer 2, and water) join together; and Z_{int}, which is the point where the Polymer 1-Polymer 2 interface intersects the z-axis. The three-component interface lies at z=0. We define Z_2 such that it is always negative, and Z_{int} such that it is positive when it protrudes into Polymer 1 and negative when it protrudes into Polymer 2. The three surface functions are as follows:

$$r_1(z) = \sqrt{\left(\frac{{Z_1}^2 + {R_3}^2}{2Z_1}\right)^2 - \left[z - \frac{{Z_1}^2 - {R_3}^2}{2Z_1}\right]^2}$$
$$r_2(z) = \sqrt{\left(\frac{{Z_2}^2 + {R_3}^2}{2Z_2}\right)^2 - \left[z - \frac{{Z_2}^2 - {R_3}^2}{2Z_2}\right]^2} \quad (1)$$
$$r_{\text{int}}(z) = \sqrt{\left(\frac{{Z_{\text{int}}}^2 + {R_3}^2}{2Z_{\text{int}}}\right)^2 - \left[z - \frac{{Z_{\text{int}}}^2 - {R_3}^2}{2Z_{\text{int}}}\right]^2}$$

The surface area of *r(z)* and the volume enclosed by *r(z)* are expressed as the following integrals:

$$V = \pi \int r^2(z) dz$$
$$A = 2\pi \int r(z) \sqrt{1 + \left(\tfrac{dr}{dz}\right)^2} dz \quad (2)$$

The volume of Polymer 1 ($V_{1,calc}$) and the volume of Polymer 2 ($V_{2,calc}$), as well as the surfaces areas of the Polymer 1-water interface (A_1), the Polymer 2-water interface (A_2), and the Polymer 1-Polymer 2 interface (A_{int}) from $r_1(z)$, $r_2(z)$, and $r_{\text{int}}(z)$ are given by the following equations:

$$V_{1,calc} = \pi \int_0^{Z_1} r_1(z)^2 dz - \pi \int_0^{Z_{\text{int}}} r_{\text{int}}(z)^2 dz = \frac{\pi}{6} Z_1 \left({Z_1}^2 + 3{R_3}^2\right) - \frac{\pi}{6} Z_{\text{int}} \left({Z_{\text{int}}}^2 + 3{R_3}^2\right)$$
$$V_{2,calc} = \pi \int_{Z_2}^{0} r_2(z)^2 dz + \pi \int_0^{Z_{\text{int}}} r_{\text{int}}(z)^2 dz = -\frac{\pi}{6} Z_2 \left({Z_2}^2 + 3{R_3}^2\right) + \frac{\pi}{6} Z_{\text{int}} \left({Z_{\text{int}}}^2 + 3{R_3}^2\right)$$
$$A_1 = 2\pi \int_0^{Z_1} r_1 \sqrt{1 + \left(\frac{dr_1}{dz}\right)^2} dz = 2\pi \left({Z_1}^2 + {R_3}^2\right) \quad (3)$$
$$A_2 = 2\pi \int_{Z_2}^{0} r_2 \sqrt{1 + \left(\frac{dr_2}{dz}\right)^2} dz = 2\pi \left({Z_2}^2 + {R_3}^2\right)$$
$$A_{\text{int}} = 2\pi \int_0^{Z_{\text{int}}} r_{\text{int}} \sqrt{1 + \left(\frac{dr_{\text{int}}}{dz}\right)^2} dz = 2\pi \left({Z_{\text{int}}}^2 + {R_3}^2\right)$$

For a Janus particle comprised of volume V_1 of Polymer 1 and volume V_2 of Polymer 2,

the structural variables Z_1, Z_2, Z_{int}, and R_3 will adjust themselves such that the total (unfavorable) interfacial energy is minimized. A free energy function is built of all the interfacial tensions plus volume constraints (V_1 and V_2 must remain constant). The free energy function can be minimized with respect to Z_1, Z_2, Z_{int}, R_3, using Lagrange multipliers (volume constraints for P1 and P2 during minimization of the free energy function) λ_1 and λ_2. Lagrange multipliers are used to find the maxima or minima of a function F(x,y) subject to the constraint g(x,y)=0.

$$\sum G = \gamma_{1W} A_1 + \gamma_{2W} A_2 + \gamma_{12} A_{int} + \lambda_1 (V_1 - V_{1-calc}) + \lambda_2 (V_2 - V_{2-calc}) \tag{4}$$

$$\frac{\partial G}{\partial Z_1} = 0 \qquad \frac{\partial G}{\partial Z_2} = 0 \qquad \frac{\partial G}{\partial Z_{int}} = 0 \qquad \frac{\partial G}{\partial R_3} = 0 \qquad \frac{\partial G}{\partial \lambda_1} = 0 \qquad \frac{\partial G}{\partial \lambda_2} = 0,$$

where G is the Gibbs free energy function, λ_1 and λ_2 are the Lagrange multipliers, V_1 and V_2 are fixed, $V_1=V_{1calc}$ and $V_2=V_{2calc}$

The full free energy function (normalized by 2π for convenience) is shown below:

$$\begin{aligned}\frac{\sum G}{2\pi} &= \gamma_{1W}(Z_1^2 + R_3^2) + \gamma_{2W}(Z_2^2 + R_3^2) + \gamma_{12}(Z_{int}^2 + R_3^2) \\ &+ \frac{\lambda_1}{3}\left(Z_1(Z_1^2 + 3R_3^2) - Z_{int}(Z_{int}^2 + 3R_3^2) - \frac{6V_1}{\pi} \right) \\ &+ \frac{\lambda_2}{3}\left(-Z_2(Z_2^2 + 3R_3^2) + Z_{int}(Z_{int}^2 + 3R_3^2) - \frac{6V_2}{\pi} \right)\end{aligned} \tag{5}$$

The free energy function is minimized with respect to Z_1, Z_2, Z_{int}, R_3, λ_1, and λ_2:

$$\frac{\partial F}{\partial Z_1} = 0 = 2Z_1\gamma_{1W} + \lambda_1\left(Z_1^{\,2} + R_3^{\,2}\right) \tag{6}$$

$$\frac{\partial F}{\partial Z_2} = 0 = 2Z_2\gamma_{2W} - \lambda_2\left(Z_2^{\,2} + R_3^{\,2}\right) \tag{7}$$

$$\frac{\partial F}{\partial Z_{int}} = 0 = 2Z_{int}\gamma_{12} + (\lambda_2 - \lambda_1)\left(Z_{int}^{\,2} + R_3^{\,2}\right) \tag{8}$$

$$\frac{\partial F}{\partial {R_3}^2} = 0 = \gamma_{1W} + \gamma_{2W} + \gamma_{12} + \lambda_1 Z_1 - \lambda_2 Z_2 + (\lambda_2 - \lambda_1) Z_{\text{int}} \tag{9}$$

$$\frac{\partial F}{\partial \lambda_1} = 0 = Z_1 \left({Z_1}^2 + 3{R_3}^2 \right) - Z_{\text{int}} \left({Z_{\text{int}}}^2 + 3{R_3}^2 \right) - \frac{6V_1}{\pi} \tag{10}$$

$$\frac{\partial F}{\partial \lambda_2} = 0 = -Z_2 \left({Z_2}^2 + 3{R_3}^2 \right) + Z_{\text{int}} \left({Z_{\text{int}}}^2 + 3{R_3}^2 \right) - \frac{6V_2}{\pi} \tag{11}$$

Solving for l_1 and l_2 from Eqns. (6) and (7) yields

$$\lambda_1 = -\frac{2Z_1 \gamma_{1W}}{{Z_1}^2 + {R_3}^2} \tag{12}$$

$$\lambda_2 = \frac{2Z_2 \gamma_{1W}}{{Z_2}^2 + {R_3}^2} \tag{13}$$

Solving for the difference ($\lambda_2 - \lambda_1$) from (8):

$$\lambda_2 - \lambda_1 = -\frac{2Z_{\text{int}}}{{Z_{\text{int}}}^2 + {R_3}^2} \tag{14}$$

The first governing equation is derived by plugging (12) and (13) into (14):

$$0 = \left(\frac{2Z_1}{{Z_1}^2 + {R_3}^2} \right) \gamma_{1W} + \left(\frac{2Z_2}{{Z_2}^2 + {R_3}^2} \right) \gamma_{2W} + \left(\frac{2Z_{\text{int}}}{{Z_{\text{int}}}^2 + {R_3}^2} \right) \gamma_{12} \tag{15}$$

The quantity $(Z_1^2+R_3^2)/2Z_1$ is actually the radius of curvature of the semicircle $r_1(z)$, i.e. the radius R_1 of the Polymer 1-particle. Similarly, $(Z_2^2+R_3^2)/2Z_2$ and $(Z_{\text{int}}^2+R_3^2)/2Z_{\text{int}}$ are the radii of curvature R_2 and R_{int}, respectively. The second governing equation is derived by plugging (12), (13), and (14) into (9):

$$0 = \gamma_{1W} + \gamma_{2W} + \gamma_{12} - \frac{2{Z_1}^2}{{Z_1}^2 + {R_3}^2} \gamma_{1W} - \frac{2{Z_2}^2}{{Z_2}^2 + {R_3}^2} \gamma_{2W} - \frac{2{Z_{\text{int}}}^2}{{Z_{\text{int}}}^2 + {R_3}^2} \tag{16}$$

which simplifies to the following:

$$0 = \left(\frac{Z_1^{\,2} - R_3^{\,2}}{Z_1^{\,2} + R_3^{\,2}}\right)\gamma_{1W} + \left(\frac{Z_2^{\,2} - R_3^{\,2}}{Z_2^{\,2} + R_3^{\,2}}\right)\gamma_{2W} + \left(\frac{Z_{\text{int}}^{\,2} - R_3^{\,2}}{Z_{\text{int}}^{\,2} + R_3^{\,2}}\right)\gamma_{12} \tag{17}$$

We now have a system of 4 equations containing our 4 variables of interest (Z_1, Z_2, Z_{int}, R_3):

$$0 = \left(\frac{2Z_1}{Z_1^{\,2} + R_3^{\,2}}\right)\gamma_{1W} + \left(\frac{2Z_2}{Z_2^{\,2} + R_3^{\,2}}\right)\gamma_{2W} + \left(\frac{2Z_{\text{int}}}{Z_{\text{int}}^{\,2} + R_3^{\,2}}\right)\gamma_{12} \tag{15}$$

$$0 = \left(\frac{Z_1^{\,2} - R_3^{\,2}}{Z_1^{\,2} + R_3^{\,2}}\right)\gamma_{1W} + \left(\frac{Z_2^{\,2} - R_3^{\,2}}{Z_2^{\,2} + R_3^{\,2}}\right)\gamma_{2W} + \left(\frac{Z_{\text{int}}^{\,2} - R_3^{\,2}}{Z_{\text{int}}^{\,2} + R_3^{\,2}}\right)\gamma_{12} \tag{17}$$

$$0 = Z_1\left(Z_1^{\,2} + 3R_3^{\,2}\right) - Z_{\text{int}}\left(Z_{\text{int}}^{\,2} + 3R_3^{\,2}\right) - \frac{6V_1}{\pi} \tag{10}$$

$$0 = -Z_2\left(Z_2^{\,2} + 3R_3^{\,2}\right) + Z_{\text{int}}\left(Z_{\text{int}}^{\,2} + 3R_3^{\,2}\right) - \frac{6V_2}{\pi} \tag{11}$$

For simplification, absolute lengths, volumes, and surface tensions are converted into a relative scale (relative volume $v = V_1/V_2$, the 3 relative length scales $z_2 = Z_2/Z_1$, $z_{\text{int}} = Z_{\text{int}}/Z_1$, and $r = R_3/Z_1$, and the relative surface tensions $y_1 = \gamma_{1W}/\gamma_{12}$ and $y_2 = \gamma_{2W}/\gamma_{12}$). We also set Z_1 to be the characteristic length scale and define all other lengths as dimensionless lengths by dividing by Z_1:

$$z_2 = \frac{Z_2}{Z_1} \qquad \therefore Z_2 = Z_1 z_2$$
$$z_{\text{int}} = \frac{Z_{\text{int}}}{Z_1} \qquad \therefore Z_{\text{int}} = Z_1 z_{\text{int}}$$
$$r = \frac{R_3}{Z_1} \qquad \therefore R_3 = Z_1 r$$

Inserting these identities into Eqns. 15, 17, 10, and 11 and factoring out all the Z_1's yields the following system of equations:

$$0 = \left(\frac{1}{1 + r^2}\right)\gamma_{1W} + \left(\frac{z_2}{z_2^{\,2} + r^2}\right)\gamma_{2W} + \left(\frac{z_{\text{int}}}{z_{\text{int}}^{\,2} + r^2}\right)\gamma_{12} \tag{18}$$

$$0 = \left(\frac{1-r^2}{1+r^2}\right)\gamma_{1W} + \left(\frac{z_2{}^2 - r^2}{z_2{}^2 + r^2}\right)\gamma_{2W} + \left(\frac{z_{\text{int}}{}^2 - r^2}{z_{\text{int}}{}^2 + r^2}\right)\gamma_{12} \tag{19}$$

$$\frac{6V_1}{\pi Z_1{}^3} = \left(1+3r^2\right) - z_{\text{int}}\left(z_{\text{int}}{}^2 + 3r^2\right) \tag{20}$$

$$\frac{6V_2}{\pi Z_1{}^3} = -z_2\left(z_2{}^2 + 3r^2\right) + z_{\text{int}}\left(z_{\text{int}}{}^2 + 3r^2\right) \tag{21}$$

By reducing volumes V_1 and V_2 into a dimensionless volume ratio $v = V_1/V_2$ and combining Eqns. 20 and 21, we obtain the following equation:

$$\left(1+3r^2\right) - z_{\text{int}}\left(z_{\text{int}}{}^2 + 3r^2\right) = -vz_2\left(z_2{}^2 + 3r^2\right) + vz_{\text{int}}\left(z_{\text{int}}{}^2 + 3r^2\right)$$

which reduces to

$$0 = v\left(1+3r^2\right) - (1+v)z_{\text{int}}\left(z_{\text{int}}{}^2 + 3r^2\right) + z_2\left(z_2{}^2 + 3r^2\right) \tag{22}$$

Further, Eqns. 18 and 19 can both be divided by γ_{12} (the interfacial tension between Polymer 1 and Polymer 2, which is always positive otherwise no Janus particle can form). Using the two dimensionless surface tension ratios, y_1 and y_2, gives the following equations:

$$0 = \left(\frac{1}{1+r^2}\right)y_1 + \left(\frac{z_2}{z_2{}^2 + r^2}\right)y_2 + \left(\frac{z_{\text{int}}}{z_{\text{int}}{}^2 + r^2}\right) \tag{23}$$

$$0 = \left(\frac{1-r^2}{1+r^2}\right)y_1 + \left(\frac{z_2{}^2 - r^2}{z_2{}^2 + r^2}\right)y_2 + \left(\frac{z_{\text{int}}{}^2 - r^2}{z_{\text{int}}{}^2 + r^2}\right) \tag{24}$$

Eqns. 22, 23, and 24 are the 3 equations for our 3 unknowns (z_2, z_{int}, and r). This enables direct calculation of particle geometry given the properties y_1, y_2, and v. However, if a particle's geometry is obtained from microscopy (i.e. if z_2, z_{int}, and r can be measured), then its properties y_1, y_2, and v may be determined numerically. If z_2, z_{int}, and r are known, then v can be solved by rearranging Eqn. 22:

$$v = \frac{\left(1+3r^2\right) - z_{\text{int}}\left(z_{\text{int}}{}^2 + 3r\right)}{-z_2\left(z_2{}^2 + 3r^2\right) + z_{\text{int}}\left(z_{\text{int}}{}^2 + 3r\right)} \tag{25}$$

Furthermore, it is possible to solve for y_1 and y_2 using a system of two equations, Eqns. 23 and 24. To solve for y_2, Eqn. 24 is subtracted from Eqn. 23 multiplied by $(1-r^2)$. To solve for y_1, Eqn. 24 is subtracted from Eqn. 23 multiplied by $\left(\frac{z_2{}^2 - r^2}{z_2}\right)$, yielding the following equations:

$$y_1 = \left(\frac{1+r^2}{z_{\text{int}}{}^2 + r^2}\right)\left(\frac{z_2\left(z_{\text{int}}{}^2 - r^2\right) - z_{\text{int}}\left(z_2{}^2 - r^2\right)}{-z_2\left(1-r^2\right) + \left(z_2{}^2 - r^2\right)}\right) \tag{26}$$

$$y_2 = \left(\frac{z_2{}^2 + r^2}{z_{\text{int}}{}^2 + r^2}\right)\left(\frac{z_{\text{int}}\left(1-r^2\right) - \left(z_{\text{int}}{}^2 - r^2\right)}{-z_2\left(1-r^2\right) + \left(z_2{}^2 - r^2\right)}\right) \tag{27}$$

Finally, it is possible to solve for y_1, y_2, and z_{int} when the variables z_2, r, and v are given. First, we rearrange Eqn. 22 to put all the z_{int} terms on one side, yielding the following cubic equation:

$$z_{\text{int}}\left(z_{\text{int}}{}^2 + 3r\right) = \frac{v\left(1+3r\right) + z_2\left(z_2{}^2 + 3r\right)}{1+v} \tag{28}$$

All cubic equations *f(z)* have 3 solutions, one always real and the other two solutions either real or complex. For any $r > 0$, the structure of equation Eqn. 2 indicates that z_{int} starts positive for small z_2 and goes negative for large z_2, and the behavior is otherwise monotonically decreasing. This monotonic behavior indicates that z_{int} always has exactly one real solution. The general equation for the root of a cubic equation which is always real is easily found and the result for z_{int} is given here:

$$z_{\text{int}} = \left(\frac{\sqrt{F^2 + [2(1+\nu)]^2 r^6} + F}{2(1+\nu)} \right)^{1/3} - r \left(\frac{2(1+\nu)}{\sqrt{F^2 + [2(1+\nu)] r^6} + F} \right)^{1/3} \tag{29}$$

$$where \;\; F = z_2 \left(z_2^{\,2} + 3r^2 \right) + \nu \left(1 + 3r^2 \right)$$

Once the solution to z_{int} is determined, Eqns. 26 and 27 can be used to find y_1 and y_2.

In special cases, the two polymers will separate to form two separate droplets. Mathematically, this corresponds to the state $R_3 = 0$ and $Z_{\text{int}} = 0$ (or $r = 0$ and $z_{\text{int}} = 0$). We will use Eqns. 26 and 27 for this analysis by plugging in r=0 and z_{int}=0:

$$y_1 = \left(\frac{1}{z_2^{\,2} - 1} \right) \lim_{z_{\text{int}}, r \to 0} \left(\frac{z_{\text{int}} \left(z_2^{\,2} - r^2 \right) - \left(z_{\text{int}}^{\,2} - r^2 \right)}{z_{\text{int}}^{\,2} + r^2} \right)$$

$$y_2 = \left(\frac{z_2^{\,2}}{1 - z_2^{\,2}} \right) \lim_{z_{\text{int}}, r \to 0} \left(\frac{z_{\text{int}} \left(1 - r^2 \right) - \left(z_{\text{int}}^{\,2} - r^2 \right)}{z_{\text{int}}^{\,2} + r^2} \right)$$

We are interested in the limit where both r and z_{int} go to zero, but it turns out that the answer changes depending on whether r or z_{int} is set to zero first. To solve this problem, we employ the volume-constraint Eqn. 22 and solve for r^2:

$$r^2 = -\frac{1}{3} \frac{\nu - (1+\nu) z_{\text{int}}^{\,3} + z_2^{\,3}}{\nu - (1+\nu) z_{\text{int}} + z_2}$$

and then insert it into the limit-quantities:

$$\lim_{z_{\text{int}} \to 0} \frac{z_{\text{int}} \left(z_2^{\,2} - r^2 \right) - z_{\text{int}}^{\,2} + r^2}{z_{\text{int}}^{\,2} + r^2} = -1$$

$$\lim_{z_2 \to 0} \frac{z_{\text{int}} \left(1 - r^2 \right) - \left(z_{\text{int}}^{\,2} - r^2 \right)}{z_{\text{int}}^{\,2} + r^2} = -1$$

When these limits are plugged back into the equations for y_1 and y_2, the result reproduces the classical spreading coefficient relationship:

$$\gamma_{P1\text{–}W} + \gamma_{P2\text{–}W} - \gamma_{P1\text{–}P2} < 0 \quad \text{(separated)} \tag{30}$$

The same analysis can be conducted for a core-shell scenario, in which $r = 0$ and $z_2 = 0$, yielding the other classical spreading coefficient relationship:

$$\gamma_{P1-W} - \gamma_{P2-W} + \gamma_{P1-P2} < 0 \quad \text{(core-shell)} \tag{31}$$

Eqns. 30 and 31 reveal whether a Janus particle will form, while Eqns. 22, 23, and 24 indicate the exact shape of a Janus particle based on v as well as surface tensions.

Instructions for determining the geometrical quantities

The steps for obtaining polymer properties y_1, y_2, and v from microscope images and its reverse are outlined below for PLGA/PCL particles prepared using 2% PVA as the surfactant.

1) Draw a line connecting the two "divots" (i.e. the triple interface between Polymer 1, Polymer 2, and Water). This line's length is $2R_3$. Note: if there is no visible interface or feature in the microscopy image that exactly matches this line that the particle may be tilted toward the screen and the z-measurements may be incorrect.

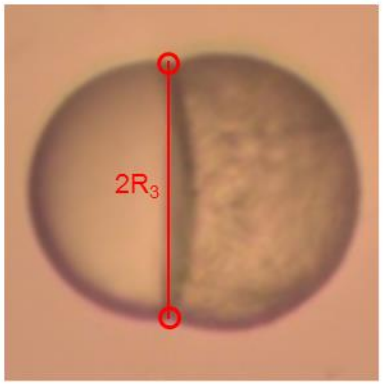

2) Draw a line (the z-axis) connecting the extreme edges of the Janus particle. This line must be perpendicular to the $2R_3$ line and the Janus particle must be completely symmetric

around it.

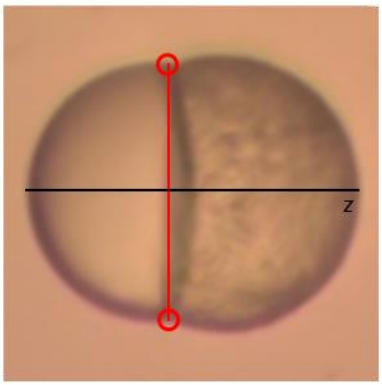

3) Define the point C as the intersection between the $2R_3$ line and the z-axis. The distances Z_1, Z_2, and Z_{int} are measured from C to the respective points where each interface intersects the z-axis.

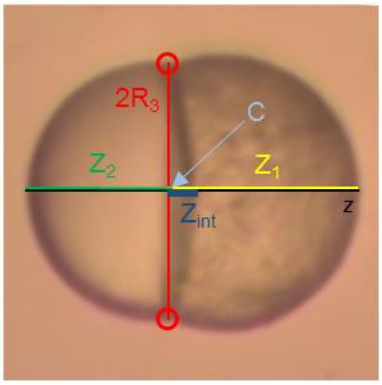

4) This step can be used to double check the results. Draw a perfect circle which exactly fits the Polymer 1-Water interface; record its radius as R'_1 and its center as C'_1. Draw a perfect circle which exactly fits the Polymer 2-Water interface and records its radius as R'_2 and its center as C'_2. Draw a perfect circle that exactly fits the Polymer 1-Polymer 2 interface and record its radius as R'_{int} and its center as C'_{int}. The following identities should be true:

$$R_1' = \frac{Z_1^{\,2} + R_3^{\,2}}{2Z_1} \qquad R_2' = \frac{Z_2^{\,2} + R_3^{\,2}}{2|Z_2|} \qquad R_{\text{int}}' = \frac{Z_{\text{int}}^{\,2} + R_3^{\,2}}{2Z_{\text{int}}}$$

$$C_1' = \frac{Z_1^{\,2} - R_3^{\,2}}{2Z_1} \qquad C_2' = \frac{Z_2^{\,2} - R_3^{\,2}}{2|Z_2|} \qquad C_{\text{int}}' = \frac{Z_{\text{int}}^{\,2} - R_3^{\,2}}{2Z_{\text{int}}}$$

An example of a Janus particle with the circles drawn around the interfaces to check the results is shown in Figure 38.

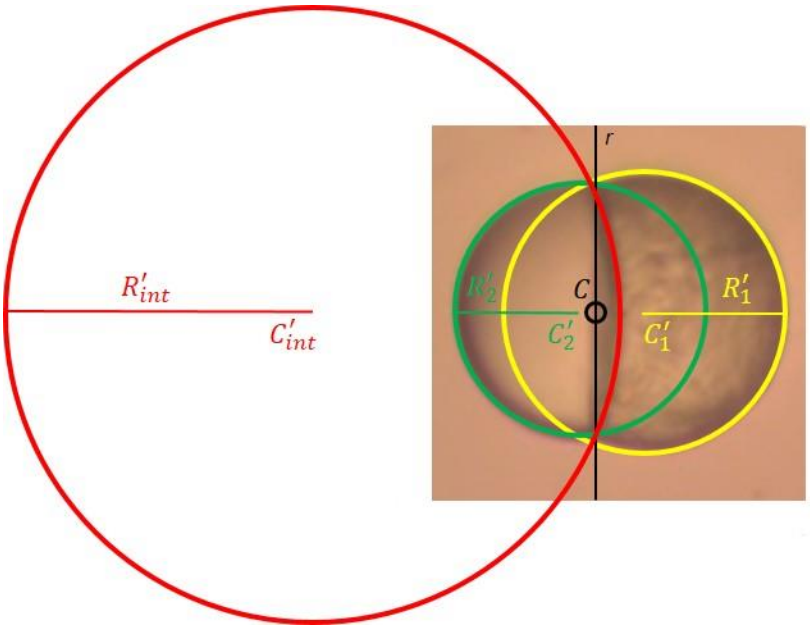

Figure 38: Checking results using the centers and radii of circles drawn around the three interfaces.

In this example, $2R_3$ = 1.34, Z_1 = 1.00, Z_2 = -0.77, and Z_{int} = 0.16 inches. Measured and calculated values for the new radii and center of the circles drawn around each of the three interfaces are given in Table 8.

	Measured (in.)	**Calculated (in.)**	**Percent Error (%)**
R_1'	0.724	0.735	1.456
R_2'	0.676	0.655	3.177
R_{int}'	1.483	1.540	3.856
C_1'	0.276	0.265	3.828
C_2'	0.094	0.090	3.750
C_{int}'	1.323	1.375	3.945

Table 8: Measured and calculated values to check the results.

The measured R'_1, R'_2, R'_{int}, C'_1, C'_2, and C'_{int} closely match the calculated values, indicating

that the measured values of R_3, Z_1, Z_2, and Z_{int} are suitable for use in calculations to find y_1, y_2, and v. Using Eqns. 25-27, we find $y_1 = 1.627381$, $y_2 = 1.975877$, and $v = 0.805338$. Recall that y_1 is the normalized interfacial tension γ_{1w}/γ_{12}, y_2 is the normalized interfacial tension γ_{2w}/γ_{12}, and v is the volume ratio V_1/V_2 of the two compartments. The expected volume ratio can be calculated using the following equation:

$v = \frac{V_1}{V_2} = \frac{m_1}{m_2} \cdot \frac{\rho_2}{\rho_1}$, where m_1 and m_2 are the mass fractions of Polymer 1 and Polymer 2, respectively. Plugging in the density values for PCL and PLGA, $\rho_{PCL} = 1.145$ g/cm^3 and $\rho_{PLGA} = 1.35$ g/cm^3, the expected value of v is 0.848148[155, 156]. This compares well to our calculated value of $v = 0.805338$.

Predicting Janus particle morphology based on polymer properties

Now that we have v, y_1, and y_2, we can reconstruct the particle geometry by solving Eqns. 22-24 for z_2, z_{int}, and r. A 3x3 Jacobian matrix containing the partial derivatives of the three equations with respect to z_2, z_{int}, and r was constructed. The matrix is shown below.

$$\begin{pmatrix} \frac{-2z_2^2}{(z_2^2+r^2)^2}y_2 - \frac{2}{(r^2+1)^2}y_1 - \frac{2z_{int}}{z_{int}^2+r^2} & \frac{2z_2^2}{z_2^2+r^2}y_2 - \frac{2z_2(z_2^2-r^2)}{(z_2^2+r^2)^2} & \frac{2z_{int}}{z_{int}^2+r^2} - \frac{2z_{int}(z_{int}^2-r^2)}{(z_{int}^2+r^2)^2} \\ \frac{-z_2}{(z_2^2+r^2)^2}y_2 - \frac{2}{(r^2+1)^2}y_1 - \frac{z_{int}}{(z_{int}^2+r^2)^2} & \frac{1}{z_2^2+r^2}y_2 - \frac{2z_2^2}{(z_2^2+r^2)^2}y_2 & \frac{1}{z_{int}^2+r^2} - \frac{2z_{int}^2}{(z_{int}^2+r^2)^2} \\ 3z_{int}(v+1)+3v+3z_2 & 3z_2^2+3r^2 & -(z_{int}^2+3r^2)(v+1) - 2z_{int}^2(v+1) \end{pmatrix}$$

Using Newton's method, the "new" z_2, z_{int}, and r values are obtained by subtracting the inverse Jacobian matrix multiplied by the three functions (Eqns. 22-24) from the "old" z_2, z_{int}, and r values until all F=0. For graphing, Janus particles are modelled as three distinct curves representing Polymer 1, Polymer 2, and the Polymer 1-Polymer 2 interface. Polymer 1 and Polymer 2 are defined by the functions for a circle, generally $x = h + R*\cos\Theta$ and $y = k + R*\sin\Theta$, while the Polymer 1-Polymer 2 interface is defined by the function for a semi-circle, $r^2 = R^2 - (z - z_c)^2$. The distance from the origin (h,k), the radii R and Θ are

calculated from z_2, z_{int}, and r. The functions are plotted as 100 discrete (x,y) points. Figure 39 shows the output of the Excel worksheet programmed to calculate the exact Janus particle morphology from the input parameters y_1, y_2, and v. The y_1, y_2, and v values were calculated from the geometric measurements of the example particle (y_1 = 1.627381, y_2 = 1.975877, and v = 0.805338), so the model should accurately depict the actual morphology.

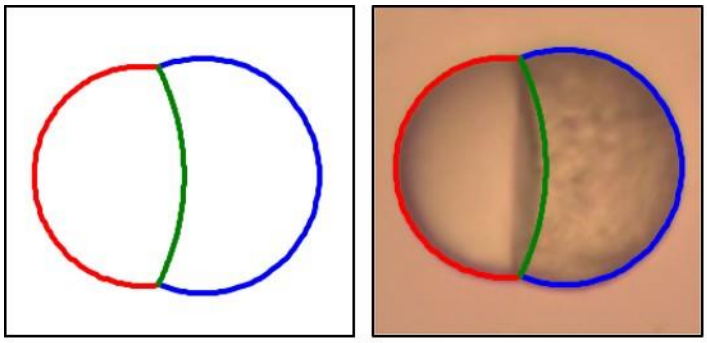

Figure 39: Output of the functions describing Janus particle shape, and the model superimposed over the microscope image.

5.3 Results

The thermodynamic model was validated for multiple Janus particle morphologies obtained by varying the type and concentration of surfactant used in synthesis (Figure 11). The lengths of Polymer 1, Polymer 2, the Polymer 1-Polymer 2 interface, and the distance between the two triple interfaces (P1-P2-W) were extracted from microscope images. The model accurately reconstructed the observed morphologies based on the microscopy measurements as shown in Figure 40.

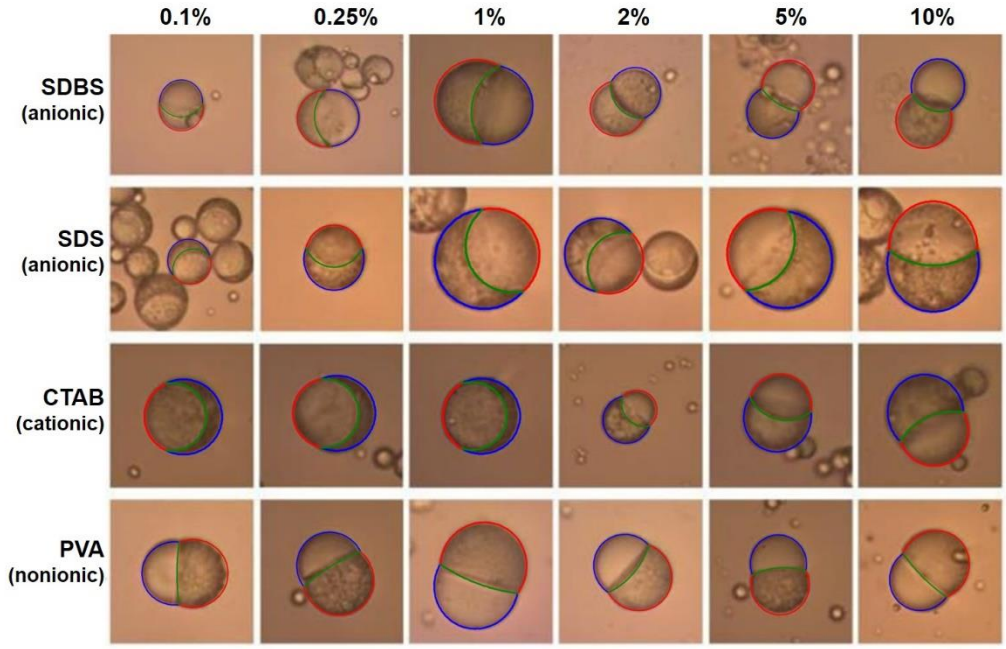

Figure 40: Predicted morphology superimposed over actual morphology of Janus particles at different SDBS, SDS, CTAB, and PVA concentrations.

Although the percent composition by mass is 50:50 PLGA/PCL, the Janus particle shape adjusts itself to minimize the interfacial free energy. This can result in an apparent deviation from the 50:50 configuration, where one polymer appears to make up a greater percent of the particle than the other polymer depending on the frame of reference. The relative percent of PLGA and PCL was determined by drawing circles around the three interfaces as previously described and shown in Figure 38. The area between two overlapping circles (lune) is given by the following equation:

$$A = r^2 \cos^{-1}\left(\frac{d^2+r^2-R^2}{2dr}\right) + R^2 \cos^{-1}\left(\frac{d^2+R^2-r^2}{2dR}\right) -$$

$\frac{1}{2}\sqrt{(-d+r+R)(d+r-R)(d-r+R)(d+r+R)}$, where d = distance between the two centers, r = radius of the smaller circle, and R = radius of the larger circle.

Depending on the direction of the curvature of the Polymer 1-Polymer 2 interface, the area of the lune between the circles drawn around the polymer and the interface was subtracted

from the area of the polymer circle to find the area of the polymer phase. Apparent volume percentages for each of the polymers and the radius of curvature of the PLGA/PCL interface are displayed in Table 9 for the Janus particle configurations shown in Figure 40.

		0.1%	0.25%	1%	2%	5%	10%
SDBS	**PCL %**	35.46	31.11	44.00	43.47	52.46	49.14
	PLGA %	64.54	68.89	56.00	56.53	47.54	50.86
	Radius of Curvature (°/ft)	60.31	34.72	26.96	21.82	17.79	14.72
SDS	**PCL %**	28.78	43.92	42.44	42.52	49.83	51.48
	PLGA %	71.23	56.08	57.56	57.48	50.17	48.52
	Radius of Curvature (°/ft)	61.94	44.07	27.81	27.94	27.95	17.36
CTAB	**PCL %**	29.78	27.72	27.36	54.72	49.36	51.84
	PLGA %	70.22	72.28	72.64	45.28	50.64	48.16
	Radius of Curvature (°/ft)	60.64	59.79	52.44	37.30	23.51	20.65
PVA	**PCL %**	60.53	67.07	56.88	52.85	57.89	62.01
	PLGA %	39.47	32.93	43.12	47.14	42.11	37.99
	Radius of Curvature (°/ft)	16.82	17.59	17.30	17.00	17.10	17.49

Table 9: Composition and interfacial radius of curvature for each given Janus particle configuration.

In the case of PVA, the volume of each polymer remains constant with the exception of 0.1% and 0.25% PVA concentration. PCL comprises a slightly larger percentage due to its greater swelling behavior in DCM. For the ionic surfactants (SDBS, SDS, and CTAB), the relative percentage of PCL was initially much lower than that of PLGA. As the surfactant concentration increased to 5-10%, the PCL compartment became nearly as large as the PLGA compartment. Although the 2D size of the PCL compartment is smaller at lower

surfactant concentrations, it almost completely surrounds the particle as can be seen in Figure 40. The crescent moon shape observed at low concentrations of ionic surfactant suggests preferential adsorption of surfactant molecules to PCL, resulting in low PCL-water interfacial tension but high PLGA-water interfacial tension. Heterogeneous SDS adsorption has also been observed in the formation of PS/PMMA composite particles [72]. The PLGA phase is nearly surrounded by the PCL phase to minimize PLGA contact with water. As more surfactant is added, the interfacial tension of PLGA-water decreases to a degree comparable to that of PCL-water, and hemispherical Janus particles are obtained. At high concentrations of SDBS, PLGA-water and PCL-water interfacial tensions are decreased to the point that polymer contact with water becomes as energetically favorable as or more favorable than that of the polymers with each other, and the two polymer phases begin to pull apart. Although the interfacial tension between PLGA and PCL is not expected to be affected by the presence of surfactant, its interfacial area adjusts in response to changes in the interfacial tensions between each of the polymers and the water phase with the addition of surfactant in order to minimize unfavorable interactions. For example, in the case of SDS, the PLGA-PCL interfacial area increases at the energetic expense of decreasing the PLGA-water and PCL-water interfacial areas relative to the reference PVA case. Therefore, we expect the polymer-water interfacial tensions to be higher for SDS case than PVA. At the other end of the spectrum, when SDBS is used as surfactant we see that the PLGA-water and PCL-water interfacial areas increase to accommodate a decrease in PLGA-PCL area. Thus we expect PLGA-water and PCL-water to be lowest for SDBS.

Calculating interfacial tension from microscope images

Our thermodynamic model allows us to calculate the interfacial tension between

PLGA and PCL. This is an important result, as there are no methods currently available to directly measure the interfacial tension between two solids. If any one of the three interfacial tensions of the system are known, then the other two can be calculated explicitly from the ratios y_1 and y_2. The interfacial tension between each of the polymers and the water phase can be determined by measuring the contact angle and applying the Young-Dupré equation:

$\sigma_{SV} = \sigma_{SL} + \sigma_{LV}\cos\Theta$, where S = solid, V = vapor, L = liquid, and Θ = contact angle

The surface tension values used in the interfacial tension calculations are shown in Table 10 below.

Material	Surface Tension (mN/m)	Source
PLGA	37.28	[104]
PCL	44.76	[104]
5% PVA	37	[157]
5% SDS	35	[158]
5% SDBS	33.75	[159]

Table 10: Surface tensions of materials used in this study.

Using the thermodynamic model combined with microscope measurements, we can calculate the PLGA-PCL interfacial tension two ways: from either 1) the PLGA-water interfacial tension and y_1, or 2) the PCL-water interfacial tension and y_2. Recall that $y_1 = \gamma_{1w}/\gamma_{12}$ and $y_2 = \gamma_{2w}/\gamma_{12}$, where the subscripts '1' and '2' denote Polymer 1 (PLGA) and Polymer 2 (PCL), respectively. The ratios y_1 and y_2 can be determined directly from microscope measurements, and the interfacial tensions between each of the polymers and the water phase (γ_{1w} and γ_{2w}) can be determined by contact angles. Therefore, each microscope experiment generates two PLGA-PCL interfacial tensions. In principle, these PLGA-PCL interfacial tensions should be identical, as surfactants are only expected to alter the polymer-water interfacial tensions and not the polymer-polymer interfacial tension.

The calculations were performed for three different experiments: 5% PVA, 5% SDS, and 5% SDBS. Representative microscope images of PLGA/PCL Janus particles produced using the indicated surfactants are shown in Figure 41, and the ratios calculated from the images are given in Table 11.

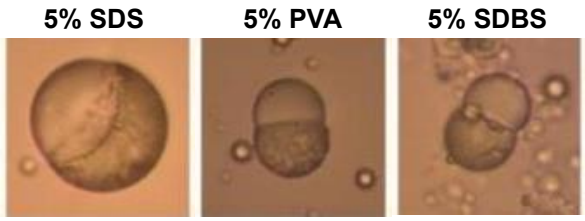

Figure 41: Microscope images used for interfacial tension calculations.

Ratio	5% SDS	5% PVA	5% SDBS
y_1=γ(PLGA-W)/γ(PLGA-PCL)	2.76 ± 0.23	1.77 ± 0.31	0.83 ± 0.10
y_2=γ(PCL-W)/γ(PLGA-PCL)	3.45 ± 0.21	1.93 ± 0.25	1.22 ± 0.18

Table 11: Interfacial tension ratios calculated from microscope images.

Now that we have the ratios y_1 and y_2, we need the interfacial tensions between each of the polymers and the water phase ($\gamma_{PLGA\text{-}W}$ and $\gamma_{PCL\text{-}W}$) to solve for the interfacial tension between the two polymers ($\gamma_{PLGA\text{-}PCL}$). The polymer-water interfacial tensions were determined using contact angles and the Young- Dupré equation. Results are contained in Table 12. PLGA-water and PCL-water interfacial tensions both decrease in the order of SDS > PVA > SDBS. The surface tension values can be explained on the basis of the interfacial areas observed in the corresponding particle morphologies shown in Figure 41. The Janus particles created using PVA as a surfactant are biphasic with approximately equal halves and a flat interface. In contrast, when SDS is used as the surfactant, the particles are more spherical with a larger PLGA-PCL interfacial area. The PLGA-PCL interfacial area increases relative to the PVA configuration in order to reduce the PLGA-water and PCL-water interfacial areas. Therefore, as mentioned previously, we expect the

PLGA-water and PCL water interfacial tensions to be higher for SDS than PVA. When SDBS is used in place of PVA, the PLGA-water and PCL-water interfacial areas are much larger and the PLGA-PCL interface is smaller. This means that PLGA-water and PCL-water should be lower for SDBS than PVA. All surface tension measurements show excellent agreement with the expected predictions based on particle morphology.

System	Contact Angle Θ (°)	Uncertainty (°)	Surface Tension γ (mN/m)
PLGA-water 5% PVA	51.6	1.0	10.08 ± 0.65
PCL-water 5% PVA	45.3	1.2	12.08 ± 0.37
PLGA-water 5% SDS	39.0	0.8	15.35 ± 0.92
PCL-water 5% SDS	21.0	0.8	19.93 ± 1.01
PLGA-water 5% SDBS	25.2	1.7	6.74 ± 0.85
PCL-water 5% SDBS	9.1	1.0	11.43 ± 0.20

Table 12: Contact angles and surface tensions for polymer films with surfactant solutions.

We now have the ratios y_1 and y_2 from microscope measurements and the interfacial tensions $\gamma_{PLGA\text{-}W}$ and $\gamma_{PCL\text{-}W}$ from contact angle measurements for all three polymer-water combinations. Solving for $\gamma_{PLGA\text{-}PCL}$ from the three case studies should yield six identical interfacial tensions. Instead, we have six different values for $\gamma_{PLGA\text{-}PCL}$ (Table 13).

Calculated from	$\gamma_{PLGA\text{-}PCL}$ (mN/m)	Average $\gamma_{PLGA\text{-}PCL}$ (mN/m)
y_1 (SDS)	3.65	7.89 ± 3.21
y_2 (SDS)	3.49	
y_1 (SDBS)	11.85	
y_2 (SDBS)	9.40	
y_1 (PVA)	8.63	
y_2 (PVA)	10.31	

Table 13: PLGA-PCL interfacial tensions calculated by the indicated ratio and surfactant.

We expect six identical calculations of $\gamma_{PLGA\text{-}PCL}$ because the interfacial tension between the two polymers would not be affected by the surfactant unless it adsorbs at the

interface between the polymer phases. However, there is some error in both the y_1 and y_2 ratio calculations and the contact angle measurements (reported in Table 11 and Table 12, respectively). For example, solvent evaporation from a 2D film undoubtedly differs from that from a 3D particle even though DCM was used as the solvent for the fabrication of thin films in order to best replicate Janus particle synthesis conditions. This leads to a difference in surface properties between the film and the particle which the film is meant to approximate. Thin film surface roughness has been shown to have a strong effect on the measurement of contact angles [160, 161, 162]. Furthermore, the y_1 and y_2 ratios are calculated based on microscope measurements taken by hand. The software used to measure the relevant lengths (polymer 1 length, polymer 2 length, polymer 1-polymer 2 interface, and the triple interface between polymer 1, polymer 2, and water) only provides readings with three significant figures. The error from both the ratio measurements and the contact angle measurements propagates through the calculations and ultimately affects the final result. Since the standard deviations of the inputs are known, the standard deviation of the interfacial tension calculation can be determined. The propagation of error for each case was calculated using the following equation:

$$\frac{\sigma_z}{z} = \sqrt{\left(\frac{\sigma_x}{x}\right)^2 + \left(\frac{\sigma_y}{y}\right)^2}, \text{ where z=xy}$$

Results are contained in Table 14. The $\gamma_{PLGA\text{-}PCL}$ values calculated from SDBS and PVA surface tensions are close to each other within the uncertainty of measurements. The $\gamma_{PLGA\text{-}PCL}$ calculated using SDS, however, is significantly different from those calculated using SDBS and PVA. This suggests that some amount of SDS is getting inside the polymers and reducing $\gamma_{PLGA\text{-}PCL}$.

Calculated from	$\gamma_{PLGA-PCL}$ (mN/m)	Uncertainty (%)
y_1 (SDS)	3.65	10.26
y_2 (SDS)	3.49	7.92
y_1 (SDBS)	11.85	17.44
y_2 (SDBS)	9.40	14.86
y_1 (PVA)	8.63	18.66
y_2 (PVA)	10.31	13.31

Table 14: Propagation of error in interfacial tension calculation.

In addition to measurement errors, there are also confounding experimental considerations to take into account. For example, it has been shown that some of each polymer mixes with the other polymer in the formation of composite PS/PMMA particles [49]. The presence of even a small amount of PMMA in PS resulted in a decrease of γ_{PS-W} from 34.4 mN/m to 20.0 mN/m [163]. It is also possible that there is some surfactant mixing with the polymers during Janus particle formation, which would change γ_{PLGA-W} and γ_{PCL-W}, and/or surfactant adsorbing on the PLGA-PCL interface, which would change $\gamma_{PLGA-PCL}$. Another potential issue is the effect of kinetics on final particle morphology, which is not accounted for in the thermodynamic model. It is well known that kinetic factors such as the rate of evaporation and the molecular weight of the polymers affect Janus particle morphology [150, 164]. The calculated y_1 and y_2 ratios are entirely dependent upon particle geometry measurements, so it is easy to see that a deviation from the expected thermodynamic morphology would result in erroneous calculations of $\gamma_{PLGA-PCL}$.

There are no experimentally measured values reported in the literature for the interfacial tension between PLGA and PCL with which we can directly compare our calculated values due to the inherent difficulty in experimentally measuring the interfacial tension between two polymers. It is not feasible to directly measure the interfacial tension between two solid polymers. The interfacial tension reported for PS and PMMA dissolved

in toluene at a concentration of 20 wt.% as measured by the spinning drop method is 0.025 ± 0.005 mN/m [72]. However, this is not a suitable benchmark to use for comparison with the interfacial tension between two solid polymers. We would expect the interfacial tension between two dissolved polymers in solution to be very small or even zero depending upon the molecular weight of the polymers and their concentration. Another group calculated the interfacial tension between PLGA and PCL in a dimethyl carbonate-in-water emulsion stabilized by 2 wt.% PVA based on the surface energy of PLGA and PCL. Our overall average $\gamma_{PLGA\text{-}PCL}$ value of 7.89 ± 3.21 compares well with their calculated value of 7.48 mN/m [104].

Predicting Particle Morphology from Interfacial Tensions

The main objective of our thermodynamic model is to quantitatively predict the morphology of Janus particles given the three interfacial tensions of the system ($\gamma_{PLGA\text{-}PCL}$, $\gamma_{PLGA\text{-}W}$, and $\gamma_{PCL\text{-}W}$). In order to assess the accuracy of the model, the $\gamma_{PLGA\text{-}W}$ and $\gamma_{PCL\text{-}W}$ values obtained by contact angle measurements and $\gamma_{PLGA\text{-}PCL}$ obtained from microscope measurements were used as inputs to generate the expected Janus particle morphology. The numbers used in this simulation are contained in Table 15. Note that the average of the two calculated $\gamma_{PLGA\text{-}PCL}$ values were used for this case study, as $\gamma_{PLGA\text{-}PCL}$ is theoretically the same within each individual particle despite the slight variations within the same surfactant.

	5 wt.% SDS	**5 wt.% PVA**	**5 wt.% SDBS**
$\gamma_{PLGA\text{-}PCL}$ **(mN/m)***	3.57	9.47	10.625
$\gamma_{PLGA\text{-}W}$ **(mN/m)**	15.35	10.08	6.74
$\gamma_{PCL\text{-}W}$ **(mN/m)**	19.93	12.08	11.43
$y_1=\gamma_{PLGA\text{-}W}/\gamma_{PLGA\text{-}PCL}$	4.30	1.06	0.63
$y_1=\gamma_{PCL\text{-}W}/\gamma_{PLGA\text{-}PCL}$	5.58	1.28	1.08

*Table 15: Interfacial tensions used to predict the morphology of Janus particles. * indicates the average value from the data in Table 14 was used.*

The Janus particle morphology was generated for each surfactant. The three inputs for the model are y_1, y_2, and v. The volume ratio v can be calculated using the following equation: $v = \frac{V_1}{V_2} = \frac{m_1}{m_2} \cdot \frac{\rho_2}{\rho_1}$, where m_1 and m_2 are the mass fractions of Polymer 1 and Polymer 2, respectively, and ρ_1 and ρ_2 are their densities. The mass term cancels out because equal mass amounts of PLGA and PCL were used in all experiments. Plugging in the density values for PCL and PLGA, ρ_{PCL} = 1.145 g/cm^3 and ρ_{PLGA} = 1.35 g/cm^3, the expected value of v is 0.848148. This is the value used for all theoretical predictions. Predicted morphologies are shown overlaid on top of representative images of the observed morphologies for 5 wt.% SDS, PVA, and SDBS in Figure 42. The model was able to accurately predict the morphologies of the Janus particles given $\gamma_{PLGA\text{-}PCL}$, $\gamma_{PLGA\text{-}W}$, and $\gamma_{PCL\text{-}W}$. Recall that $\gamma_{PLGA\text{-}W}$ and $\gamma_{PCL\text{-}W}$ were measured using contact angles (Table 12), and $\gamma_{PLGA\text{-}PCL}$ was calculated using microscopy measurements and either $\gamma_{PLGA\text{-}W}$ or $\gamma_{PCL\text{-}W}$ (Table 13). The model shows excellent agreement with the observed morphologies for both PVA and SDBS, and good agreement for SDS.

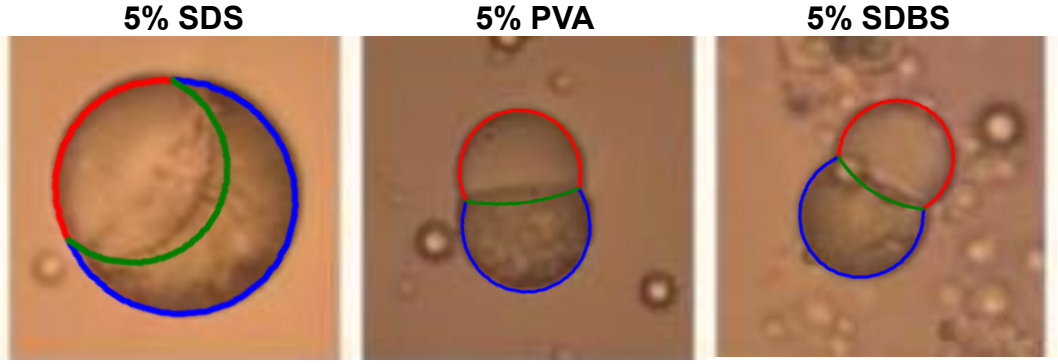

Figure 42: Expected morphologies based on measured interfacial tensions compared to observed morphologies.

In order to remove the effect of uncertainty arising from the discrepancies in our $\gamma_{PLGA\text{-}PCL}$ values across the different surfactants, the analysis was repeated using the literature value

of 7.48 mN/m [104]. The inputs are shown in Table 16.

	5 wt.% SDS	5 wt.% PVA	5 wt.% SDBS
$y_1=\gamma_{PLGA\text{-}W}/\gamma_{PLGA\text{-}PCL}$	2.08	1.35	0.90
$y_1=\gamma_{PCL\text{-}W}/\gamma_{PLGA\text{-}PCL}$	2.66	1.61	1.53

Table 16: Inputs for the thermodynamic model using $\gamma_{PLGA\text{-}PCL}=7.48$ mN/m.

Figure 43 shows the model predictions with the observed morphologies. In this instance, the model shows excellent agreement with the observed morphology for SDS and PVA and good agreement for SDBS.

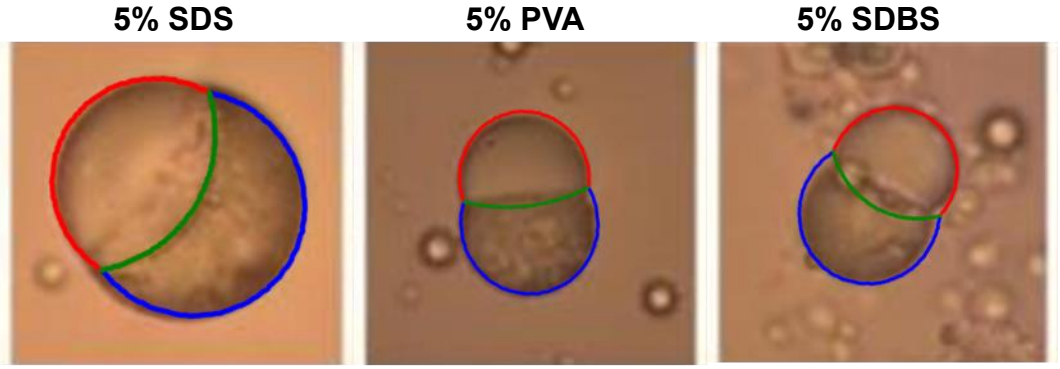

Figure 43: Expected morphologies based on measured interfacial tensions compared to observed morphologies using 7.48 mN/m as γPLGA-PCL.

The fact that the model could accurately predict Janus particle morphology whether our calculated $\gamma_{PLGA\text{-}PCL}$ values were used or the one that was reported in the literature (7.48 mN/m) indicates that the interfacial tensions between each of the polymers and the water phase play a much larger role in determining particle shape than that of the two polymers. This is in line with previous work focused on PS/PMMA composite particles, where it was found that surfactants have little to no effect on the interfacial tension between two polymers. It is also known that the interfacial tension between two polymers is low compared to that between the polymer phases and water phase [50, 72, 152]. While this result is promising for our intended application of predicting Janus particle morphology since it allows for a margin of error with regard to $\gamma_{PLGA\text{-}PCL}$, more work needs to be done

before the model can accurately and reliably calculate the interfacial tension between two solid polymers.

5.4 Conclusions

Particle shape is a function of the interfacial tensions between the two polymers, as well as the interfacial tensions between each of the polymers and the aqueous phase. The interfacial tension of the system can be adjusted by changing the type of *ionic* surfactant and its concentration. Nonionic surfactants do not affect particle morphology. PLGA/PCL Janus particles prepared using PVA, Poloxamer 188, Tween 80, or soy lecithin as the surfactant have two phases of approximately equal areas joined at an interface. The PCL compartment is slightly larger than the PLGA compartment. These results are consistent with previous studies on composite PS/PMMA particles, where the morphology changed when different concentrations of SDS were used, but not PVA [71, 117].

The morphology of the PLGA/PCL Janus particles changed from a crescent moon with a small PCL phase to acorn-like with approximately equal PCL and PLGA phases with increasing SDS content. Particles prepared using CTAB followed a similar trend. When SDBS was used as surfactant, the particle morphology transformed from crescent moon to acorn-like to nearly separated droplets as the concentration of surfactant was increased.

The final particle morphology is determined by a delicate interplay between kinetic and thermodynamic factors. The thermodynamic equilibrium morphology is the one with the lowest total free energy amongst the three interfaces: polymer 1-polymer 2, polymer 1-water, and polymer 2-water. Experimentally, the morphology can be thermodynamically controlled by adjusting the type and concentration of ionic surfactant, which changes the

interfacial tensions between each of the polymer-water interfaces. Kinetic factors such as rate of solvent evaporation and viscosity inside oil droplets determine the ease with which the thermodynamic equilibrium morphology can be reached. For example, viscosity of polymer-rich oil droplets increases as solvent evaporation proceeds, acting as a kinetic barrier to phase separation [165]. When the volume of the oil droplet decreases to the point where the internal viscosity is so high that the polymers have limited mobility, the particle morphology is essentially frozen at that point regardless of whether the thermodynamically favored morphology has been reached. In this study, kinetic barriers were minimized by performing experiments at a slow evaporation rate to allow the particle morphology to reach the equilibrium structure. Even within the same batch, several different morphologies can be observed if kinetic conditions are not controlled. This was discussed in an earlier section (Figure 7).

We have developed thermodynamic model to quantitatively describe Janus particle morphology based on interfacial tensions. Our model is derived from first-principles, in which the exact shape of a Janus particle is found and the total free energy is minimized given constant volume constraints for each polymer. The result is a system of equations in which the surface tensions of two of the three the interfaces and the volume ratio allows for explicit calculation of Janus particle geometry. Surface tensions for the polymer-water interfaces are calculated using the Young-Dupré equation, where contact angles between polymer films and various surfactant solutions are measured using a simple experimental setup comprised of a light source, a stage, a lens, and a camera. The model has good agreement between predicted morphology and experimental morphology so long as kinetic effects are minimized. The model was able to accurately predict the morphologies of the

Janus particles given $\gamma_{PLGA\text{-}PCL}$, $\gamma_{PLGA\text{-}W}$, and $\gamma_{PCL\text{-}W}$ for the case studies with 5 wt.% PVA, SDS, and SDBS. Conversely, interfacial tensions can be calculated given Janus particle geometry measurements obtained from standard microscope images. This result has significance across many fields, as no other methods allow for the explicit determination of interfacial tensions between two solid polymer phases. Our model can be applied to any two polymers capable of forming particles with two compartments.

CHAPTER 6: EFFECT OF SURFACTANT AND SOLVENT PROPERTIES ON THE FORMATION OF PHARMACUETICAL NANOSUSPENSIONS BY EMULSION DIFFUSION

Data from this chapter has been submitted for the following publication:

Winkler, J.S., Romanski, F.S., Gerzsberg, J.D., Tomassone, M.S. Effect of Surfactant and Solvent Properties on the Formation of Pharmaceutical Nanosuspensions by Emulsion Diffusion. Submitted to Chemical Engineering Science.

6.1 Introduction

Emulsion-based synthesis methods can also be applied to the formation of pharmaceutical nanosuspensions. Nanosuspensions are defined as submicron colloidal dispersions of drug particles stabilized by surfactants [166]. The high surface area-to-volume ratio and increased saturation solubility of nanosized drugs leads to an increase in dissolution rate, and, consequently, drug exposure levels [167, 168]. Nanosuspensions offer many advantages over other nanotechnology-based drug delivery systems, including increased chemical stability, drug loading, and reduced toxicity and side effects [169, 170]. Moreover, these suspensions can be further processed into conventional dosage forms for oral, parenteral, pulmonary, dermal, or ocular administration.

Nanosuspension manufacturing processes are classified as “top-down” if large particles are broken down into the nano-regime or “bottom-up” if dissolved compounds are grown into nanoscale crystals from solution [171, 172]. Top-down technologies such as high pressure homogenization and media milling utilize shear forces, comminution, and cavitation to achieve particle size reduction [173]. Although these methods produce nanosuspensions with narrow size distributions and little batch-to-batch variation, they are time-consuming and require the use of expensive equipment. Alternatively, nanosuspensions can be created using a bottom-up approach by emulsion-diffusion. In this

method, the drug is dissolved in a pharmaceutically favorable partially water-miscible solvent with low toxicity such as ethyl acetate, methyl ethyl ketone (MEK), triacetin, or n-butyl lactate and an emulsion is formed. The solvent is extracted from the O/W emulsion droplets by simply adding water. Upon the addition of an excess volume of water, the partially water-miscible solvent readily diffuses to the external phase, resulting in instantaneous precipitation of the drug particles and the formation of a nanosuspension. Emulsion-based precipitation is an excellent option for drugs whose crystal structures resist comminution by shear forces and impact [174, 175]. A schematic of the emulsion-diffusion process is shown in Figure 44.

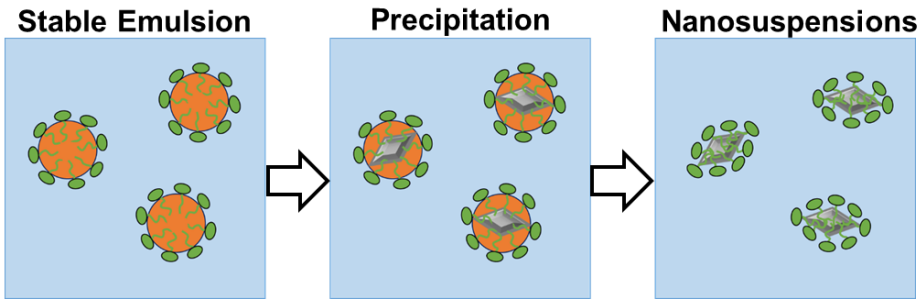

Figure 44: Overview of nanosuspension preparation by the emulsion-diffusion method.

Regardless of the preparation method, surfactants are needed to prevent aggregation during synthesis, storage, and administration [176]. Despite the critical role of surfactants in the creation and stabilization of nanosuspensions, surfactant selection remains a largely empirical process guided by trial-and-error experimentation [177]. The hydrophile-lipophile balance (HLB) was designed in 1949 by William C. Griffin as a tool to assist in the selection of surfactants. In the HLB system, the emulsifying tendency of a nonionic surfactant is quantified based on the size and strength of its hydrophilic and lipophilic moieties [178]. The HLB is an arbitrary scale that ranges from 0 to 20, but extends up to 50 for ionic surfactants. The more dominant the hydrophilic portion, the

higher the HLB value. Generally, surfactants with an HLB value in the 10-18 range are used to form O/W emulsions [179].

The aim of this study is to evaluate the effect of surfactant synergism, HLB value, and solvent properties on the characteristics of nanosuspensions of poorly soluble drugs prepared by the emulsion-diffusion method. It is well known that particle size decreases with increased surfactant concentration and shear rate, therefore these variables were not studied in this paper [66, 180]. Several screening studies of stabilizers for the preparation of nanosuspensions have been conducted elsewhere [180-182]. However, this study is the first of its kind to systematically investigate synergistic surfactant blends and the relevance of bidirectional solvent diffusivity in the diffusion step of nanosuspension formation. Surfactant synergism is studied by comparing the performance of blends to that of chemically similar surfactants with low, medium, and high HLB for each of the surfactant pairs studied.

Nonionic surfactants are preferred for pharmaceutical applications due to their low toxicity profiles. The nonionic surfactants studied here represent two major chemical classes: sorbitan esters (Spans and Tweens) and linear block copolymers (Poloxamers). Spans are fatty acid esters of sorbitol and Tweens are ethoxylated derivatives of Spans. Poloxamers comprise a central chain of either the hydrophobic polypropylene oxide (PPO) or polyethylene oxide (EPO) units, followed by side chains of the opposite [91]. Poloxamers with a wide range of molecular weights, HLB values, and structures are attainable by adjusting the number and ratio of constituent PPO and PEO blocks. Spans, Tweens, and Poloxamers were chosen because they are commonly used as inactive ingredients in suspensions and a multitude of other pharmaceutical products [92, 95]. Ionic

surfactants such as SDS and SLS were excluded from this study due to their propensity to cause irritation.

Three compounds with varying physicochemical properties, ibuprofen, indomethacin, and fenofibrate, were used as model drugs in order to demonstrate the robustness of the emulsion-diffusion method and to establish general guidelines applicable to other BCS Class II compounds. The equilibrium water solubility of the model drugs ranged from 0.000937 mg/mL to 0.25 mg/mL. The low solubility and high permeability of BCS Class II drugs make them ideal candidates for solubility enhancement techniques. Fenofibrate is especially problematic, as absorption varies from 30-50% when taken under fasting conditions to 60-90% under fed conditions [183]. Solvents were selected based on their low toxicity, water miscibility, and solvency power for the model drugs. Fenofibrate and ibuprofen are highly soluble in ethyl acetate, while indomethacin is highly soluble in MEK. Ibuprofen is also soluble in n-butyl lactate, allowing for direct examination of the effect of solvent properties on particle size.

6.2 Materials and Methods

6.2.1 Materials

Ibuprofen was obtained from VWR International (USA), fenofibrate was from Sigma-Aldrich (USA), and indomethacin was from Fisher Scientific (USA). Ethyl acetate, n-butyl lactate, and methyl ethyl ketone (MEK) were purchased from Fisher Scientific (USA). Tween 80, Tween 61, and Span 80 were obtained from Fisher Scientific (USA) and produced by Croda (Edison, NJ). Poloxamer 124, Poloxamer 181, and Poloxamer 188 were obtained from VWR International (USA) and produced by BASF Corporation (Florham Park, NJ). All materials were used as received.

6.2.2 Rationale for the Selection of Drugs

Three poorly water soluble compounds (ibuprofen, fenofibrate, and indomethacin) were used as model drugs for this study; the basic chemical and physical properties of the drugs are presented in Table 17. The molecular weights of the compounds ranged from 206 g/mol for ibuprofen to around 360 g/mol for both fenofibrate and indomethacin. The logP values varied between 3.97 for ibuprofen and 5.3 for fenofibrate, while water solubility ranged from 0.000937 for indomethacin mg/mL to 0.25 mg/mL for fenofibrate. These compounds differ widely in their properties, making them ideal for screening studies.

Property	Ibuprofen	Fenofibrate	Indomethacin
Molecular formula	$C_{13}H_{18}O_2$	$C_{20}H_{21}O_4Cl$	$C_{19}H_{16}ClNO_4$
Molar mass (g/mol)	206.29	360.83	357.79
Melting point (°C)	76	80.5	158.96
Water solubility (mg/mL)	0.021	0.25	0.000937
LogP	3.97	5.3	4.27
Refractive Index	1.436	1.546	1.74

Table 17: Properties of ibuprofen, fenofibrate, and indomethacin.

6.2.3 Rationale for the Selection of Stabilizers

We have chosen a set of poloxamers and a set of sorbitan esters commonly used in pharmaceutical applications to study the formation of nanosuspensions. These surfactants were selected to cover a wide range of hydrophilicity and hydrophobicity. Surfactants with chemically similar structure were also selected to provide optimal interfacial packing.

Poloxamer 181 and Poloxamer 188 were used in combination because they are similar in chemical structure and their mixtures offer HLB values ranging from 3.5 to 29. Poloxamer 181 and Poloxamer 188 are both PEO-PPO-PEO triblock copolymers.

Poloxamer 188 is much more hydrophilic than Poloxamer 181 (and thus has a higher HLB value) Span 80 and Tween 80 were also selected because they are similar in chemical structure but dissimilar in hydrophobicity. Span 80 and Tween 80 both contain an 18-carbon long fatty acid chain. However, Tweens are more hydrophilic than Spans due to ethoxylation of the sorbitol portion of the molecule. The Span 80/Tween 80 surfactant series gives HLB values ranging from 4.3 to 15. Additionally, chemically similar surfactants with midrange HLB values were chosen for each surfactant pair in order to separate the effect of surfactant synergism from that of HLB value. Poloxamer 124 (HLB 16) was used in order to evaluate the performance of Poloxamer 181/Poloxamer 188 blend (HLB 16.25), and Tween 65 (HLB 10) was used to evaluate the performance of Span 80/Tween 80 blend (HLB 9.65). All of the surfactants studied here are FDA approved for use in pharmaceutical products [184]. Properties of the surfactants used in this study are shown in Table 18.

Poloxamers	HLB	Average Molecular Weight	Chemical Formula
Poloxamer 124	16	2090–2360 g/mol	$HO(C_2H_4O)_a(C_3H_6O)_b(C_2H_4O)_aH$ (a=12, b=20)
Poloxamer 181	3.5	2000 g/mol	$HO(C_2H_4O)_a(C_3H_6O)_b(C_2H_4O)_aH$ (a=3, b=30)
Poloxamer 188	29	7680–9510 g/mol	$HO(C_2H_4O)_a(C_3H_6O)_b(C_2H_4O)_aH$ (a=80, b=27)
Sorbitan Esters			
Span® 80	4.3	428.62 g/mol	$C_{24}H_{44}O_6$
Tween® 65	10.5	1842 g/mol	$C_{100}H_{194}O_{26}$
Tween® 80	15	1310 g/mol	$C_{64}H_{124}O_{26}$

Table 18: Properties of the Poloxamers, Spans, and Tweens used in this study.

6.2.4 Rationale for the Selection of Solvents

Solvents were selected based on their low toxicity, water miscibility, and solvency power for the model drugs. Several partially water-miscible solvents with low toxicity were screened in order to optimize emulsion formation and nanosuspension production, including triacetin, n-butyl lactate, benzyl alcohol, ethyl acetate, and methyl ethyl ketone.

Of these five solvents, we chose to proceed with n-butyl lactate, ethyl acetate, and methyl ethyl ketone due to their ability to form the smallest ibuprofen nanosuspensions (data not shown). The properties of n-butyl lactate, ethyl acetate, and methyl ethyl ketone are displayed in Table 19.

Property	*n*-butyl lactate	Ethyl acetate	Methyl ethyl ketone
Molecular formula	$C_7H_{14}O_3$	$C_4H_8O_2$	C_4H_8O
Molar mass (g/mol)	146.19	88.11	72.11
Water solubility (g/100 mL)	7.7	8.3	27.5
Density (g/mL)	0.984	0.897	0.805
Viscosity (cP)	3.58	0.45	0.426
Boiling point (°C)	189.4	77.1	79.64

Table 19: Properties of n-butyl lactate, ethyl acetate, and MEK. Density, viscosity and water miscibility values are given for 20°C.

6.2.5 Preparation of Surfactant Solutions

Span 80/Tween 80 and Poloxamer 181/Poloxamer 188 mixtures with a range of HLB values were prepared. The amount of each surfactant A and B needed to reach the desired HLB value was determined using the following equation:

$HLB_{Mix}=(X_A*HLB_A + X_B*HLB_B)$, where X_A is the mole fraction of A and X_B is the mole fraction of B

6.2.6 Preparation of Nanosuspensions

A 100 mg/mL solution of ibuprofen or fenofibrate in ethyl acetate or n-butyl lactate (20 mL) was added to a 4% w/w aqueous surfactant solution (80 mL) and emulsified with the Ultra Turrax rotor-stator homogenizer for 5 minutes at 12,500 rpm. An excess volume of water (200 mL) was added to the O/W emulsion at a rate of 200 mL/min while still under homogenization, resulting in the precipitation of drug particles. Indomethacin nanosuspensions were prepared in the same way, except using MEK as the solvent. Solvent

selection was based on the solubility of the drug. A 25 mg/mL solution of indomethacin in MEK (40 mL) was added to a 4% w/w surfactant solution (60 mL), emulsified, and precipitated with only 50 mL of additional water due to the higher water solubility of MEK. The phase volume ratio and the volume of added water in the final step were chosen based on the miscibility of the solvent with water. Experiments were performed at 25º C because the HLB system does not take into account the effect of temperature, which may have an effect on the size of emulsion droplets [185]. Temperature increase during homogenization was determined to be negligible (< 2ºC). Each formulation was prepared and analyzed in triplicate.

6.2.7 Particle Size Analysis

Volume size distribution was determined by laser diffraction using a Beckman-Coulter LS-13320. Samples were run with a combined obscuration and polarization intensity differential scattering (PIDS) using 1.486 as the refractive index for ibuprofen, 1.546 for fenofibrate, 1.74 for indomethacin, and 1.333 for the dispersion medium [186]. All data are presented as the mean particle diameter and standard deviation of three independent samples produced under identical conditions.

6.2.8 Zeta Potential Measurement

The zeta potential of the optimized formulations was determined using a Malvern Zetasizer Nano ZS90. Prior to analysis samples were diluted 1:10 with ultra-purified water. Measurements were repeated three times and the mean and standard deviations are reported.

6.3 Results and Discussion

6.3.1 Effect of HLB and Surfactant Synergism on Particle Size

The particle size of indomethacin, fenofibrate, and ibuprofen suspensions prepared using Poloxamer 181/Poloxamer 188 blends is shown as a function of HLB value in Figure 45a, 1b, and 1c, respectively. The diameter of these suspensions range in size from approximately 300 nm to 1.4 μm. The smallest particle sizes (sub-500 nm) were obtained using Poloxamer 181/Poloxamer 188 blends with HLB values between 12 and 22 for both indomethacin and ibuprofen and 10-28 for fenofibrate. When the individual surfactants Poloxamer 181 (HLB 3.5) and Poloxamer 188 (HLB 29) were used alone, the particle size ranged from roughly 1.5 μm to 3 μm as seen in Figure 45. The Poloxamer 181/188 blends resulted in smaller suspensions than each of the two poloxamers alone in all cases, with the minima occurring around midrange HLB values.

(a)

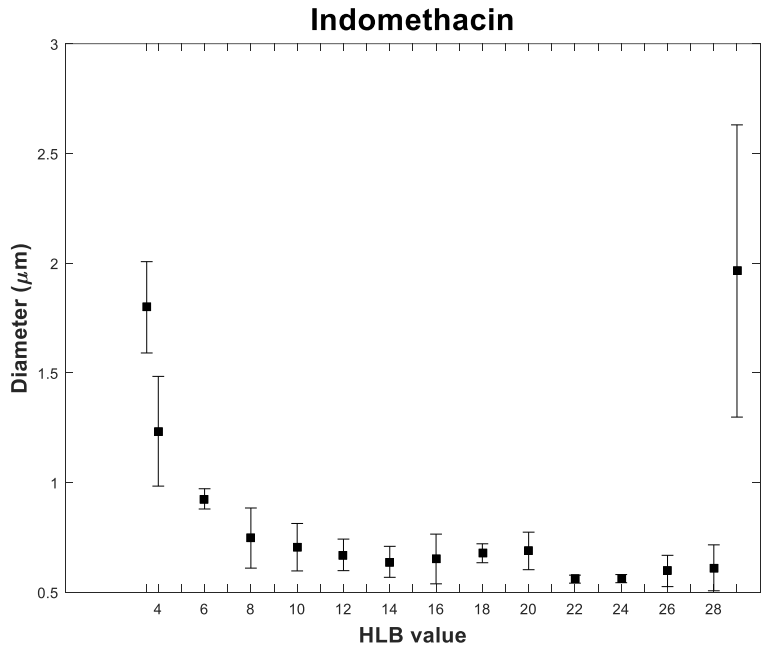

(b)

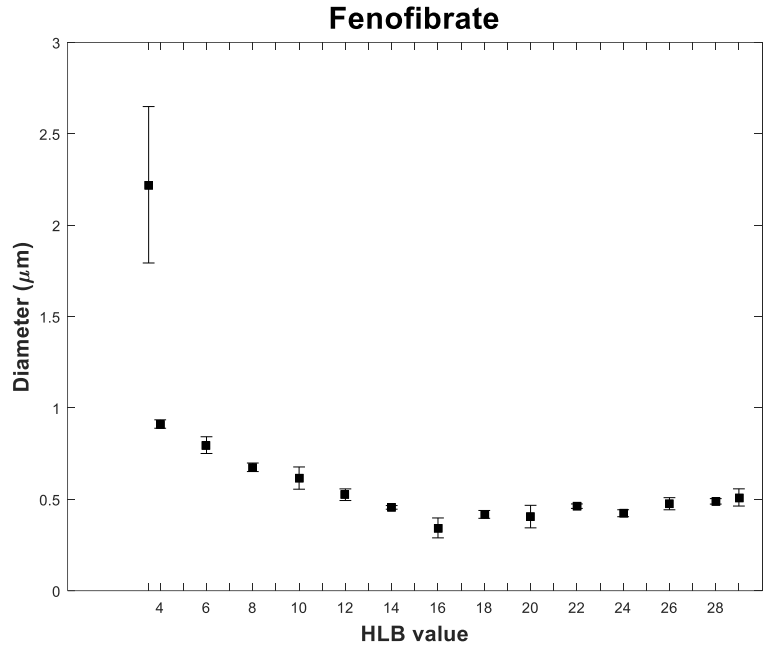

(c)

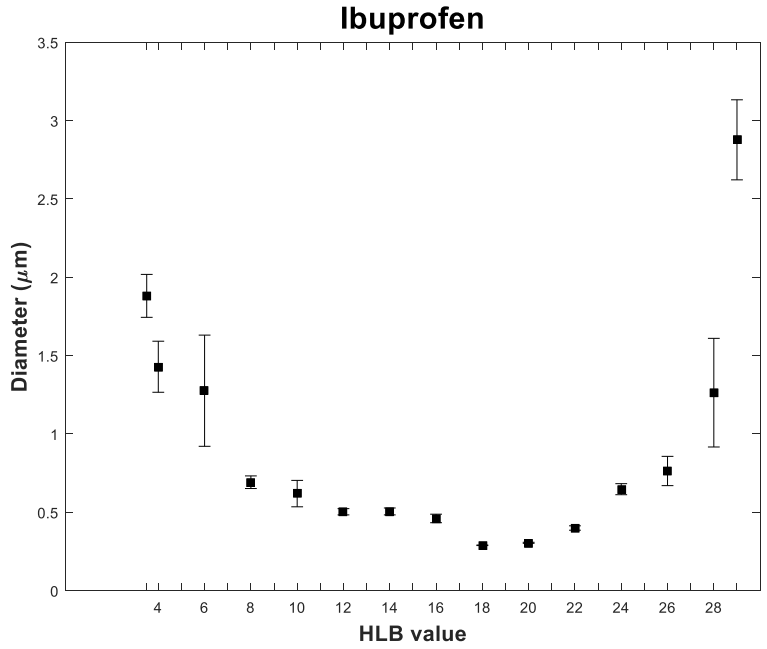

Figure 45: Mean particle diameter as a function of HLB value of (a) indomethacin suspensions prepared from MEK-in-water emulsions, (b) fenofibrate suspensions from EA-in-water emulsions, and (c) ibuprofen suspensions from EA-in-water emulsions using Poloxamer 181/188 blends.

Poloxamer 181/188 blends with HLB values between 4 and 28 yielded submicron suspensions of indomethacin and fenofibrate, while HLB values between 8 and 26 resulted in ibuprofen nanosuspensions. The fact that small nanosuspensions were created by surfactant blends with HLB values well outside of the recommended HLB range for the

formation of O/W emulsions (10-18) indicates that there is something beyond HLB value affecting final particle size, likely synergy between the two surfactants. In order to further study the effects of synergism, nanosuspensions were prepared using Poloxamer 124, which has an HLB value of 16. If the superior performance of Poloxamer 181/188 blends were due to HLB value alone, we would expect Poloxamer 124 to produce similarly-sized nanosuspensions as the blend. However, as shown in Figure 46, the Poloxamer 181/188 blend resulted in much smaller nanosuspensions than Poloxamer 124 despite having the same HLB value. Together these results indicate that the synergism provided by a blend of two chemically similar surfactants is more important than their HLB values.

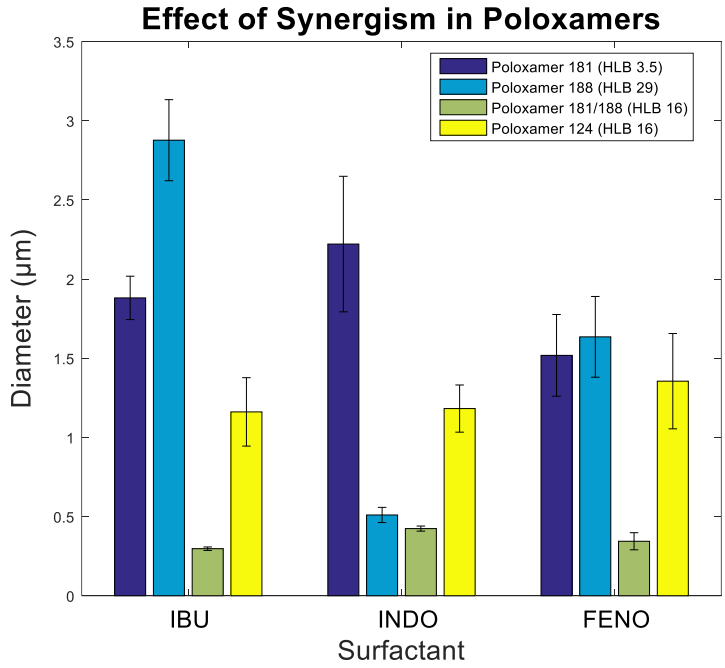

Figure 46: Comparison of mean particle diameter of suspensions prepared using Poloxamer 181 (HLB 3.5), Poloxamer 188 (HLB 29), Poloxamer 181/188 blend (HLB 16), or Poloxamer 124 (HLB 16).

The superior performance of all Poloxamer 181/188 blends compared to that of the three individual poloxamers (124, 181, 188) regardless of HLB value further corroborates the synergism between the surfactants when combined. Poloxamers interact with the surface of hydrophobic moieties via their hydrophobic PPO blocks [187]. Previous studies

have shown that surfactant mixtures benefit from the most synergism when the length of the hydrocarbon tails of the two surfactants is similar. The PPO blocks of Poloxamer 181 and Poloxamer 188 have chain lengths of 30 and 27, respectively [188]. There is a significant disparity in molecular weights between Poloxamer 181 and Poloxamer 188. Poloxamer 181 is approximately 2000 g/mol, whereas Poloxamer 188 is 7680-9510 g/mol. Generally speaking, high molecular weight stabilizers give thicker adsorption layers than low molecular weight stabilizers [189]. A thick layer of adsorbed surfactant is desirable to stabilize emulsions. However, if the layer is too thick or densely packed, it may hinder solvent diffusion from the emulsion droplets. A mix of a high molecular weight and low molecular weight surfactant seems to provide adequate surface coverage without hindering solvent diffusion.

Combinations of Span 80 and Tween 80 showed a similar synergistic effect. The Span 80/Tween 80 series with HLB values between 8 and 12 successfully produced nanosuspensions of all three drugs. For ibuprofen, all Span 80/Tween 80 combinations, including pure Span 80 and pure Tween 80, resulted in nanosuspensions when ethyl acetate was used as the solvent. Using n-butyl lactate instead of ethyl acetate resulted in slightly larger ibuprofen nanosuspensions. These results are shown in Figure 47a-d.

(a)

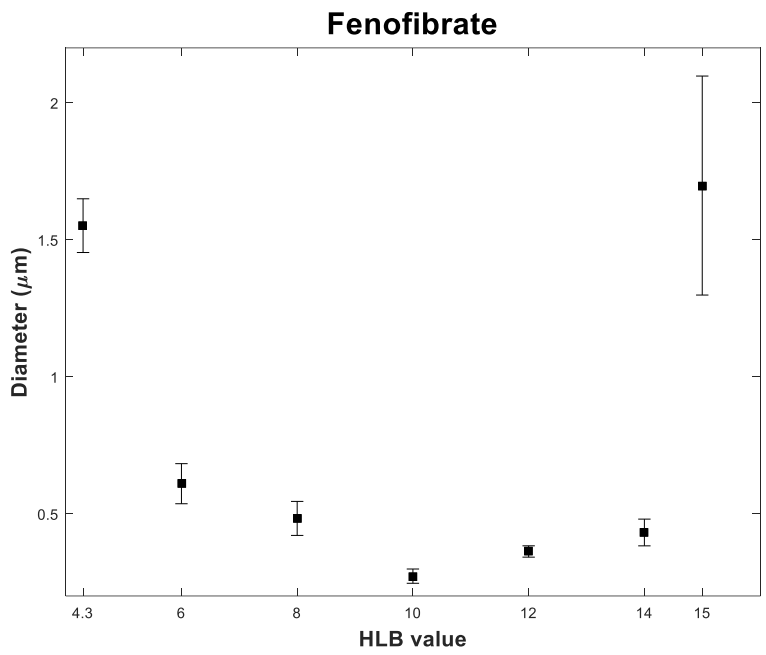
Fenofibrate
Diameter (μm)
2
1.5
1
0.5
4.3
6
8
10
12
14
15
HLB value

(b)

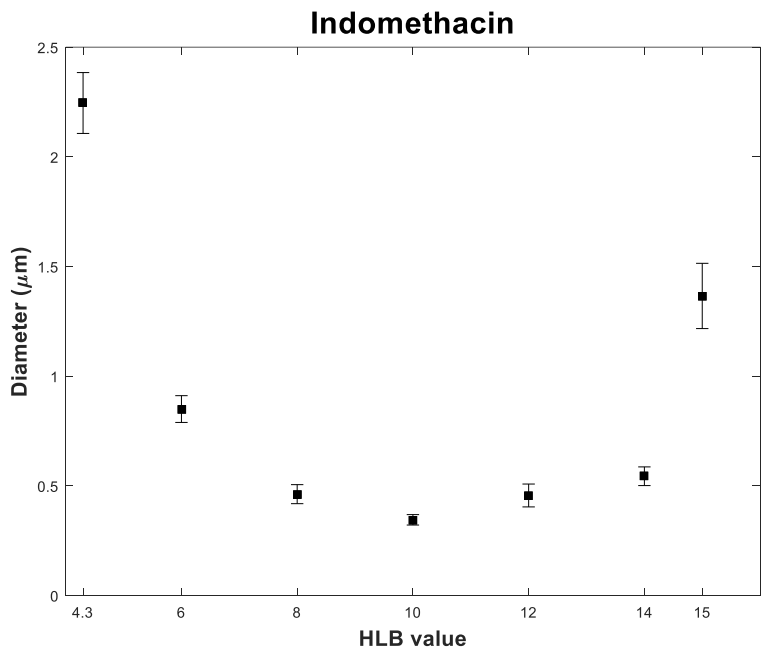
Indomethacin
Diameter (μm)
2.5
2
1.5
1
0.5
0
4.3
6
8
10
12
14
15
HLB value

(c)

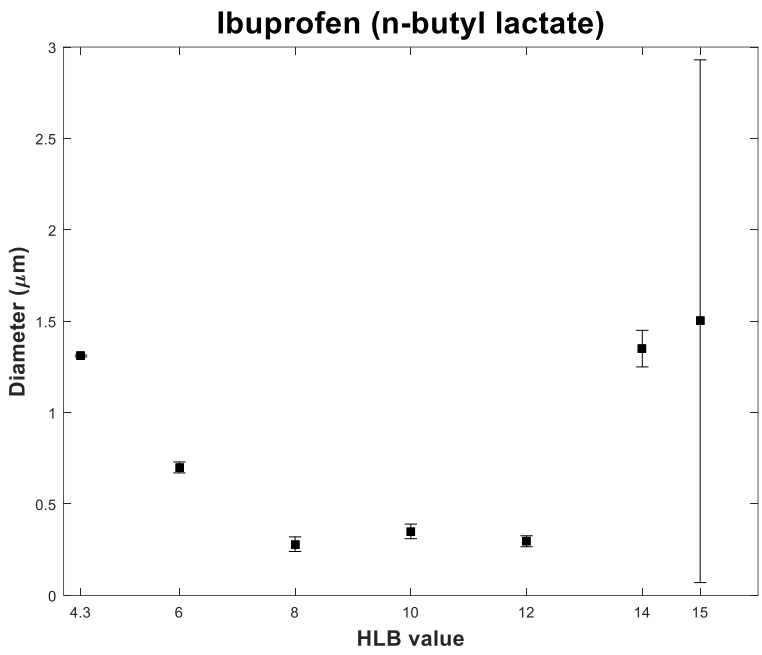

(d)

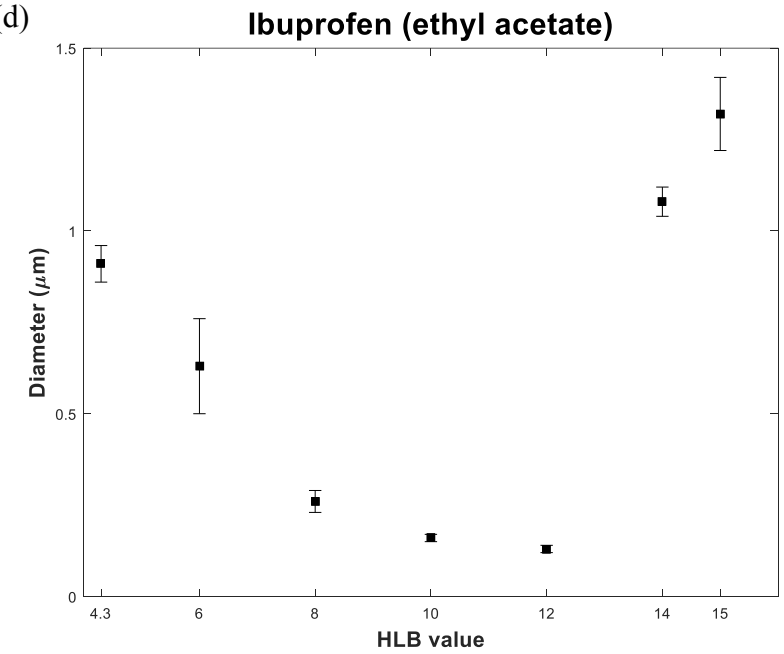

Figure 47: Mean particle diameter as a function of HLB value of a) fenofibrate nanosuspensions prepared from EA-in-water emulsions, b) indomethacin nanosuspensions prepared from MEK-in-water emulsions, c) ibuprofen nanosuspensions prepared from n-butyl lactate-in emulsions, and d) ibuprofen nanosuspensions prepared from ethyl acetate-in-water emulsions using Span 80/Tween 80 blends.

Ibuprofen, indomethacin, and fenofibrate suspensions were also prepared using Tween 65, which has an HLB value of 10.5. This allowed for a direct comparison of an

individual surfactant to a surfactant blend having the same HLB value. Results are shown in Figure 48. Similarly to the poloxamers, the Span 80/Tween 80 blend resulted in significantly smaller nanosuspensions than Tween 65. This further corroborates the assertion that the high success rate of surfactant blends is not solely attributable to HLB value. It is evident that the synergistic chemistry of certain surfactant mixtures is a large contributing factor to their superior performance over individual surfactants.

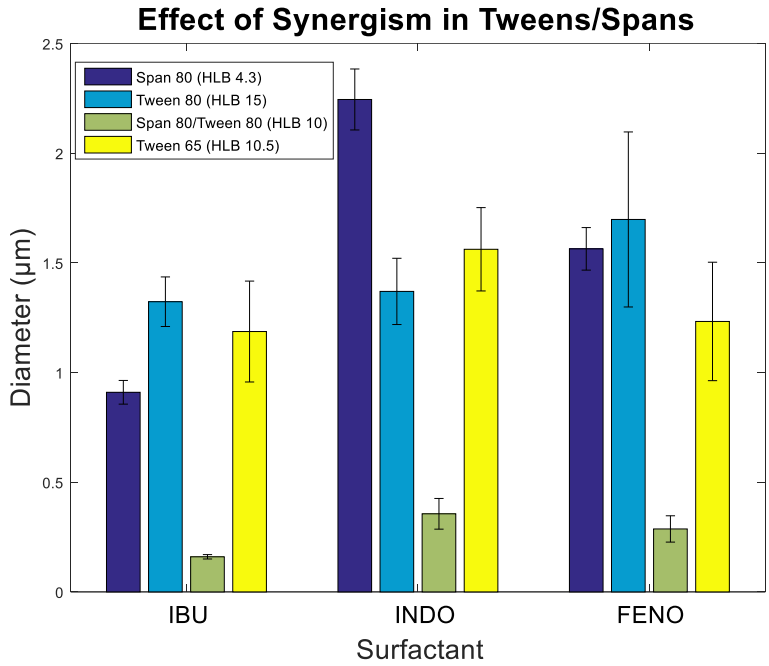

Figure 48:Comparison of mean particle diameter of suspensions prepared using Span 80 (HLB 4.3), Tween 80 (HLB 15), Tween 65 (HLB 10.5), or a Span 80/Tween 80 blend (HLB 10).

The synergism between Spans and Tweens in reducing interfacial tension has been previously reported in other applications including emulsion stabilization and oil recovery [188, 190]. The ability of Span 80/Tween 80 pairs to form small nanosuspensions despite having relatively low molecular weights ranging from 428.6 to 1310 g/mol is due to the fact that Tween 80 and Span 80 form a densely packed layer at the O/W interface as result of their similar chain lengths. Because Span 80 approaches the interface from the oil side and Tween 80 approaches from the water side, packing at the interface is optimized [191].

The hydrophobic oleate tail groups of the Span and Tween molecules anchor onto the drug crystal surface, while the hydrophilic polyoxyethylene chains of the Tween molecule provide steric hindrance against agglomeration.

For both the poloxamer series and the sorbitan esters, the optimal HLB value for producing nanosuspensions falls somewhere in the middle of the HLB range offered by the two surfactants. In general, size plotted as a function of HLB number resembles a U-shaped curve where the minimum particle size occurs around the mean HLB number. Therefore, for any combination of nonionic surfactants, it can be assumed that the smallest particle size will be achieved when equal parts of each surfactant are incorporated. This trend was observed for all model drugs regardless of their physicochemical properties (e.g. molecular weight, logP). Previous studies have also found no correlation between successful nanosuspension production and drug properties, indicating that our findings are applicable to a wide range of poorly water soluble compounds [180].

The smallest nanosuspensions were produced when the HLB value fell between 8 and 12 when the Span 80/Tween 80 blend was used, whereas Poloxamer 181/188 combinations resulted in the smallest nanosuspensions at HLB values of 12 through 28. The superior performance of the Poloxamer 181/188 blends over a wider range of HLB values is likely due to the high molecular weight of Poloxamer 188 as well as the large diffusion coefficients of the solvents used in the preparation of indomethacin and fenofibrate suspensions. The influence of solvent properties on nanosuspension formation will be discussed in the next section.

6.3.2 Effect of Solvent on Particle Size

The solvent plays an important role in crystal growth and morphology [192]

Ultimately, solvent selection is dictated by the solubility of the drug. Most poorly water soluble drugs exhibit high solubility in at least one partially water-miscible solvent suitable for emulsion-precipitation. If a drug is readily soluble in more than one partially water-miscible solvent, then the choice can be made based on the solvent diffusivity.

Solvent transport phenomenon has been shown to greatly affect the size of polymer nanoparticles and drug nanosuspensions prepared by the emulsion-diffusion method [193, 194]. The rate of solvent diffusion to the water phase (and counter-diffusion) depends on many factors, including the volume of water added, rate of water addition, temperature, and mixing speed. For this reason, all processing parameters were held constant except for the volume of water added in the dilution step, which was determined by the solubility of the solvent in water. Diffusion coefficients of binary liquids can be calculated by the Tyn-Calus equation [195]:

$D_{AB}^{\infty} = 8.93 \cdot 10^{-8} \left(\frac{V_A}{V_B^2}\right)^{\frac{1}{6}} \left(\frac{P_B}{P_A}\right)^{0.6} \frac{T}{\eta_B}$, where D_{AB} (cm^2/s) is the mutual diffusion coefficient at infinite dilution of solute A in solvent B, V_A and V_B (cm^3/g mol) are the molar volumes of A and B at their normal boiling points, P_A and P_B are saturation pressures of A and B, respectively, T (K) is the temperature, and η_B (cP) is the viscosity of solvent B.

The mutual diffusion coefficients of partially miscible solvent-water systems are displayed in Table 20 along with solvent properties used in the calculations. Ethyl acetate and MEK have the largest solvent-to-water diffusion coefficients. This corresponds to faster dissolution of emulsion droplets and rapid drug precipitation, resulting in smaller particles. Conversely, systems with small diffusion coefficients are susceptible to aggregation and Oswaldt ripening. The significantly smaller diffusion coefficient of n-butyl lactate is attributable to its higher viscosity, which inhibits the formation of small nanosuspensions by not only hindering diffusion during the solvent extraction step, but also providing resistance to the shear forces applied during emulsification.

Since diffusion between two phases is bidirectional, counter-diffusion of water into emulsion droplets must also be taken into consideration. The solvent exchange ratio R, a parameter used to quantify solvent diffusion from emulsion droplets and counter-diffusion of water into emulsion droplets, was calculated as follows [193]:

$$R = \frac{\text{Diffusion from solvent to water}}{\text{Diffusion from water to solvent}}.$$

N-butyl lactate has the highest exchange ratio among the solvents used, leading to the largest particle size. In a separate study, the diameter of PLGA nanoparticles prepared using emulsion-diffusion was found to increase exponentially with the increase of the solvent exchange ratio [193]. Rapid solvent exchange is implicated in the formation of local supersaturation regions, leading to aggregation.

Solvent	V_c (cm^3/g mol)	V_b (cm^3/g mol)	P	η (cP)	D_{AB} (cm^2/s)	D_{BA} (cm^2/s)	R
n-butyl lactate	466.5	178.57	358.27	3.58	8.910×10^{-6}	4.954×10^{-6}	1.798
Ethyl acetate	286	106.93	216.946	0.45	1.105×10^{-5}	3.460×10^{-5}	0.319
Methyl ethyl ketone	267	99.5	199.74	0.43	1.147×10^{-5}	3.530×10^{-5}	0.325

Table 20: Calculated mutual diffusion coefficients and exchange ratios (R) of partially water-miscible solvents in water at 20°C. V_b was calculated using the following relation [196]: $V_b = 0.285 \times V_c^{1.048}$. For water as solute, V_A = 37.4 cm3/g mol and P_A = 105.2 [197].

These calculations are in good agreement with experimental results. Indomethacin nanosuspensions produced using MEK and fenofibrate and ibuprofen nanosuspensions produced using ethyl acetate with the Poloxamer 181/188 series were mostly in the submicron range (Figure 45). Ibuprofen suspensions prepared using ethyl acetate as the solvent were smaller and more monodisperse than those prepared under identical conditions with n-butyl lactate with Span 80/Tween 80 (Figure 47c and d). Figure 49 shows a comparison of the particle size distributions of ibuprofen suspensions prepared using n-butyl lactate and ethyl acetate as the dispersed phase for four different surfactants.

Therefore, smaller particles are obtained with solvents that have large solvent-to-water diffusion coefficients and small exchange ratios.

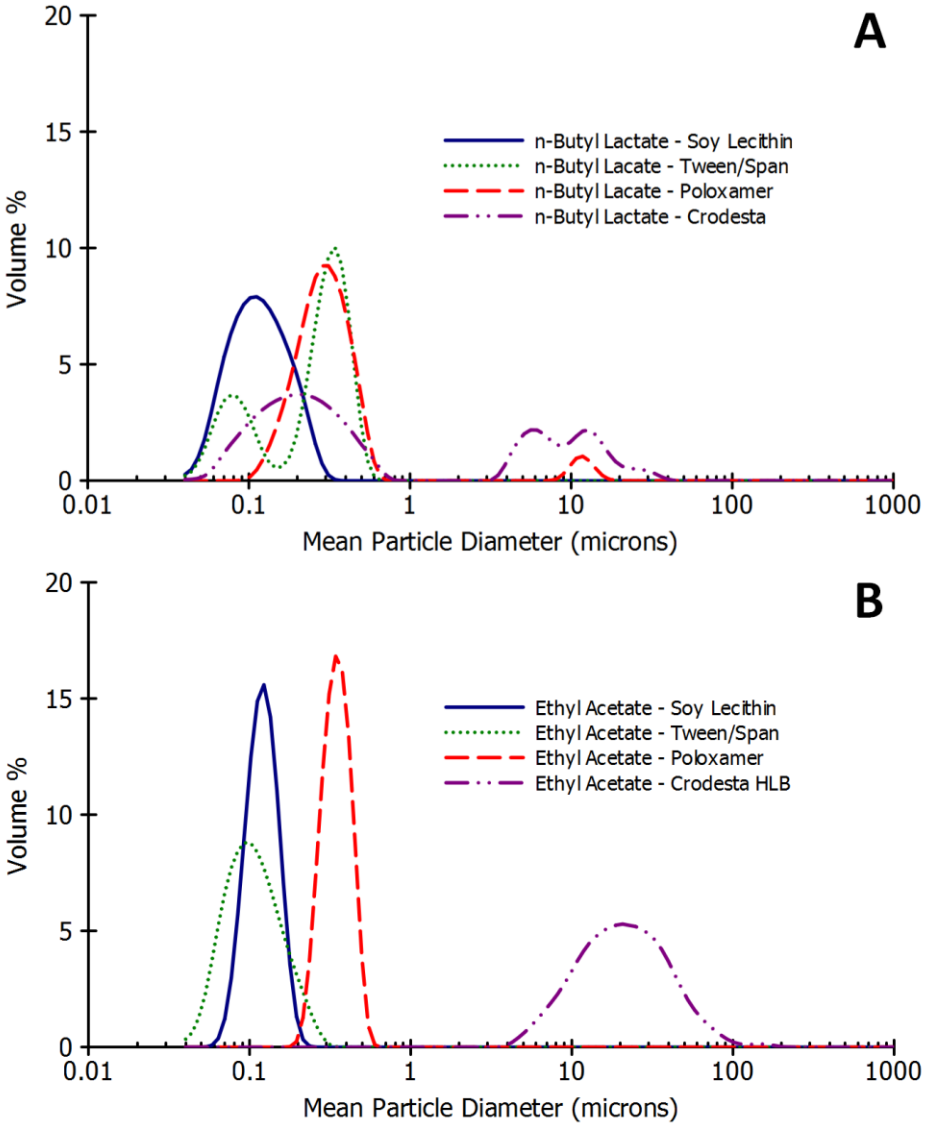

Figure 49: A comparison of representative particle size distributions of ibuprofen suspensions prepared from a) n-butyl lactate-in-water and b) ethyl acetate-in-water emulsions.

6.3.3 Zeta Potential of Nanosuspensions

The optimized nansosuspensions were further tested for stability using zeta potential. Zeta potential is often used as a predictor of long term stability and shelf life of colloidal systems. All formulations exhibited zeta potentials greater than 20 mV in absolute value, indicating good physical stability [171]. Formulations were stable for two weeks

under ambient conditions and no appreciable particle growth or aggregation was noted during this time. Results are shown in Table 21.

Drug	Oil Phase	Surfactants	HLB	Zeta Potential (mV)
Ibuprofen	EA	P181/P188	16	-27.43 ± 0.33
	n-butyl lactate	Span 80/Tween 80	10	-20.67 ± 0.21
	EA	Span 80/Tween 80	10	-25.50 ± 0.46
Indomethacin	MEK	P181/P188	16	-24.97 ± 1.22
	MEK	Span 80/Tween 80	10	-21.39 ± 1.01
Fenofibrate	EA	P181/P188	16	-25.87 ± 0.83
	EA	Span 80/Tween 80	10	-22.68 ± 0.97

Table 21: Zeta potential of nanosuspensions prepared at optimal HLB values for each respective surfactant mixture.

6.4 Conclusions

This study demonstrates the effect of surfactant synergism, HLB, and solvent properties on nanosuspension formation from the emulsion-diffusion technique using pharmaceutically acceptable solvents. There is a wide range of pharmaceutically acceptable nonionic surfactants to choose from with little guidance for formulators. In particular, the widely used sorbitan esters (Spans and Tweens) and high molecular weight PEO-PPO-PEO block copolymers (Poloxamers) yielded stable nanosuspensions. Blending these surfactants in equal proportions results in smaller and more stable nanosuspensions than using individual surfactants of the same HLB value. This is due to the optimal interfacial packing provided by chemically similar surfactants with contrasting hydrophilicities. The importance of favorable interactions between the two surfactants is highlighted by comparing the performance of surfactant blends to that of individual surfactants of the same HLB and similar chemical structures. Particle size plotted against HLB number exhibits U-shaped trajectory, indicating that the system reaches a point of maximum efficiency around the mean HLB value of the surfactant mixture. Thus, for any set of low HLB and high HLB surfactant, the most efficient combinations for producing

nanosuspensions are obtained by using combinations near the mid-point of HLB values. All nanosuspensions prepared using surfactant mixtures at the mean HLB value had excellent physical stability.

In addition, it was shown that an important consideration for utilizing the emulsion-diffusion method is the choice of solvent. Ultimately, the selection of solvent is dictated by the solubility of the drug. If the drug is readily soluble in more than one partially water-miscible solvent, then the choice can be made based on the solvent diffusivity. Next, it is important to choose a solvent with a large diffusion coefficient and small exchange ratio in order to promote rapid diffusion from O/W droplets and therefore decreased particle size. Overall, these results indicate that the emulsion-diffusion method yields stable nanosuspensions of poorly water soluble drugs with vastly different physicochemical properties given the right preparation conditions.

CHAPTER 7: CONCLUSIONS AND FUTURE WORK

7.1 Conclusions

7.1.1 Synthesis and Characterization of Janus Particles from Emulsions

Biphasic Janus particles were prepared from biodegradable materials using a modified emulsion solvent evaporation technique. Incompatible polymers (or polymer and lipid) undergo phase separation within surfactant-stabilized emulsion droplets. FDA-approved polymers and lipids PLGA, PCL, Precirol®, and Compritol ATO 888 successfully produced Janus particles. Other polymers such as poly(vinylpiridine), poly(t-butyl methacrylate), and poly(methyl methacrylate) were unable to form Janus particles in combination with one another or PLGA and PCL. Therefore, immiscibility is the first, but not only, condition for Janus particle formation. The inability of these polymers to form Janus particles is believed to be the result of vastly different polymer-water interfacial tensions of each of the polymers; if the interfacial tension between one of the polymers and water is significantly higher than that of the other polymer and water, core-shell particles will form.

During synthesis, the two polymers are initially homogeneously dispersed in solution. As solvent evaporation proceeds, the volume of the droplets decreases. The resulting increase in total polymer concentration induces phase separation of the two polymers. Upon complete solvent removal, Janus particles are obtained. Janus particles were fully characterized using standard particle characterization techniques, including optical and scanning electron microscopy, laser diffraction, photon correlation spectroscopy, powder X-Ray diffraction, and Raman spectroscopy. Microscopy revealed a biphasic structure, while XRD and Raman spectroscopy confirmed different chemistry

on each side of the particles. Both polymeric and hybrid polymer-lipid Janus particles exhibit compartmentalization and electrical anisotropy.

7.1.2 Factors Affecting the Size and Shape of Janus Particles

The effect of formulation and process variables such as O/W phase volume ratio, polymer concentration, surfactant type and concentration, solvent type, solvent evaporation rate, and emulsification shear rate on final particle characteristics were explored. As expected for an emulsion-based process, the particle size of Janus particles is determined by the shear rate, polymer concentration, and surfactant efficiency. Solvents with lower vapor pressure such as ethyl acetate left holes on the surface of the particle due to the longer residence time of the solvent.

Many different Janus particle morphologies ranging from crescent moon to snowman like to acorn-like are attainable by simply altering the type and concentration of ionic surfactant. Nonionic surfactants had no effect on particle morphology. Ultimately, particle morphology is determined by a delicate interplay between thermodynamics and kinetics. Thermodynamic factors determine the energetically favorable morphology, while kinetic factors determine whether the thermodynamic equilibrium morphology will be reached.

7.1.3 Thermodynamic Prediction of the Morphology of Janus Particles

A thermodynamic model for the prediction of Janus particle morphology has been developed based on the minimization of the free energy. For monophasic polymer particles, the configuration that gives the lowest free energy is a sphere because the only interfacial area that needs to be minimized is the one between the polymer and the water phase. However, when a second polymer is introduced into the system, there are three interfacial

areas of interest: 1) Polymer 1-Water, 2) Polymer 2-Water, and 3) Polymer 1-Polymer 2. Depending on the balance of interfacial tensions, phase separation of two polymers within emulsion droplets will result in either core-shell particles ($\gamma_{PLGA\text{-}W} >>> \gamma_{PCL\text{-}W}$ or $\gamma_{PCL\text{-}W} >>> \gamma_{PLGA\text{-}W}$), two separated droplets ($\gamma_{PLGA\text{-}PCL} >>> \gamma_{PLGA\text{-}W}$ and $\gamma_{PLGA\text{-}PCL} >>> \gamma_{PCL\text{-}W}$), or composite "Janus" particles ($\gamma_{PLGA\text{-}W} \approx \gamma_{PCL\text{-}W}$). Many different Janus morphologies are attainable by changing the interfacial tensions between each of the polymers and the water phase, which is easily achieved by changing the type and concentration of surfactant.

The Janus particle was modeled as two overlapping spheres, and the geometry was solved for in terms of measurable lengths instead of radii of curvature like previous models. The free energy of the system was minimized with respect to the two volume constraints of the polymers. The result is a system of equations that can be used to explicitly calculate the particle geometry from interfacial tension measurements. In reverse, if any one of the three interfacial tensions is known, the other two can be calculated based on measurements obtained from standard microscopy.

The interfacial tension between the two polymers is relatively low in comparison to those between the polymer phase and water, and is not expected to change with the addition of surfactant [50]. Because of this, our model was able to accurately predict Janus particle morphology based on experimentally measured $\gamma_{PLGA\text{-}W}$ and $\gamma_{PCL\text{-}W}$ values despite discrepancies in our calculated $\gamma_{PLGA\text{-}PCL}$ values. The model was used to calculate $\gamma_{PLGA\text{-}PCL}$ based on particle geometry obtained from microscopy and surface tension measurements for three different surfactants, PVA, SDS, and SDBS. Theoretically, all calculated $\gamma_{PLGA\text{-}PCL}$ values should be identical. The $\gamma_{PLGA\text{-}PCL}$ values calculated from PVA and SDBS were relatively consistent within the margin of error, ranging from 8.63-11.85 mN/m, and close

to the literature value of 7.48 mN/m [104]. The large error (~10-20%) in the $\gamma_{PLGA\text{-}PCL}$ calculations is due to the error in contact angle measurements used to calculate $\gamma_{PLGA\text{-}W}$ and $\gamma_{PCL\text{-}W}$, and the error in particle geometry measurements. When $\gamma_{PLGA\text{-}PCL}$ was calculated from SDS measurements, the result was 3.49 and 3.65 mN/m. This suggests that SDS is adsorbing onto the PLGA-PCL interface, thereby causing a reduction in $\gamma_{PLGA\text{-}PCL}$.

7.1.4 Co-encapsulation of Two Drugs in Janus Particles

Janus particles hold great promise in the field of drug delivery due to their capacity for multi-drug release of synergistic compounds [198]. Because drug release from polymeric nanoparticles is governed by the rate of polymer degradation and drug diffusion from the polymer matrix, bicompartmental Janus particles offer differential release of multiple payloads [199]. Another major advantage of Janus particles in drug delivery is the ability to co-encapsulate compounds of widely disparate solubility.

The single O/W emulsion method is suitable for encapsulating two hydrophobic compounds into Janus particles. The location of the drugs within Janus particles depends on drug-drug and drug-polymer interactions; in some cases, drugs will be evenly dispersed and in other cases they will segregate to separate compartments. Incorporation of a hydrophilic compound into Janus particles was achieved using the following strategies: single oil-in-water (O/W) emulsion containing a partially water-miscible solvent, O/W emulsion using a co-solvent (O/W-S), and double water-in-oil-in-water (W/O/W) emulsion. The W/O/W emulsion method resulted in a significantly higher encapsulation efficiency than both the O/W and O/W-S emulsion methods. However, the W/O/W double emulsion system is significantly more complex than O/W emulsions and as such requires special attention to formulation variables and experimental conditions. For example, it was found

that the diameter of the inner W/O emulsion droplets must be much less than that of the primary O/W emulsion droplets to avoid droplet rupture. Furthermore, inclusion of NaCl in the outer aqueous phase was required to balance the osmotic gradient in order to prevent diffusion of the innermost water phase into the outer water phase.

7.1.5 Advantages of Janus Particles in Drug Delivery: A Case Study

A case study aimed at treating lung cancer demonstrated the advantages of Janus particles in drug delivery. PLGA/Precirol® Janus particles containing DOX and CUR were evaluated for their efficacy in vitro and in vivo. Janus particles preferentially accumulated in the lungs (~60%) following administration via inhalation. PLGA/Precirol® Janus particles containing both drugs showed a nearly five-fold decrease in human lung cancer cell viability *in vitro*. This result was statistically significant when compared to free DOX, Janus particles containing DOX only, Janus particles containing CUR only, and empty Janus particles. However, Janus particles containing both DOX and CUR did not result in significantly higher cell killing than a mixture of Janus particles containing only DOX and Janus particles containing only CUR. In animal studies, Janus particles containing DOX and CUR nearly completely suppressed lung tumor growth. This time, Janus particles containing only DOX and Janus particles containing only CUR did not provide the same therapeutic benefit as the Janus particles containing both. The discrepancy between the *in vitro* and *in vivo* results attests to the importance of the drug delivery system; it is relatively easy to elicit a therapeutic effect when compounds are dumped directly onto cells, but achieving similar results *in vivo* requires the active agents to be delivered to the target site at a predetermined rate and time. Janus particles provide unified biodistribution of two drugs, which is necessary to achieve synergistic effects.

7.1.6 Pharmaceutical Nanosuspensions Prepared by Emulsion-Diffusion

Precipitation of drug crystals within O/W emulsions containing partially water-miscible solvents was proven a robust, simple, and effective method for producing pharmaceutical nanosuspensions. All of the solvents and surfactants used in this study possess low toxicity and are FDA-approved for use in pharmaceutical products. The emulsion-diffusion technique was applied to three model BCS Class II drugs, ibuprofen, indomethacin, and fenofibrate. Given the high success rate in nanosuspension production regardless of varying drug properties such as logP and molecular weight, it is expected that the findings from this study can be extended to the preparation of nanosuspensions of any drug compound belonging to BCS Class II or IV.

In order for a compound to be formulated as a nanosuspension by the emulsion-diffusion method, the only requirement is that it must be soluble in at least one partially water-miscible solvent and insoluble in water. This is not a limiting factor as there are many solvents to choose from, such as ethyl acetate, n-butyl lactate, methyl ethyl ketone (MEK), triacetin, and benzyl alcohol, all having different properties and dissolving capabilities. For example, triacetin can dissolve most high logP compounds, MEK can dissolve many drugs with strong lattice structures, n-butyl lactate is a protic polar solvent, and ethyl acetate is an aprotic polar solvent [200]. If the drug is soluble in more than one solvent, then the solvent should be selected on the basis of solvent diffusivity. Solvents with high diffusivities and low exchange ratios resulted in the smallest nanosuspensions.

Surfactants play a critical role in the formation and stabilization of pharmaceutical nanosuspensions and other nanotechnology-based drug delivery systems. A comprehensive screening study was performed in order to optimize the use of surfactants in

nanosuspension formulations. Nonionic surfactants representing two vastly different chemical classes were studied: PEO-PPO-PEO triblock copolymers (Poloxamers) and sorbitan esters (Spans and Tweens). Poloxamers, Spans, and Tweens offer a wide range of molecular weights and HLB values. Combinations of low- and high-HLB surfactants from each of the two surfactant classes were used to study the effects of HLB value on nanosuspension formation. Despite the fact that O/W emulsions generally require surfactants with an HLB value between 10 and 18, small, stable nanosuspensions were formed even when the HLB value of the surfactant mixture was well outside of the recommended HLB range. It is believed that blending two chemically similar surfactants with contrasting hydrophobicities provides a synergistic effect as result of the hydrophilic and hydrophobic surfactants approaching the O/W interface from opposing sides.

7.2 Future Work

7.2.1 Rational Design of Novel Janus Particles from Biodegradable Materials

In this work, biodegradable PLGA/PCL and PLGA/Precirol® Janus particles were synthesized and fully characterized. Several other polymers were tested to determine the feasibility of preparing Janus particles with different properties; however, these trials were largely unsuccessful. It is recommended that other biodegradable polymers based on poly(glycolic acid) (PGA), poly(lactic acid) (PLA), and PCL be applied to Janus particle production. PGA and PLA are the constituent polymers of PLGA. PGA is more hydrophilic, and PLA is more hydrophobic. Hence, PGA degrades faster than PLA. PLGA copolymers are available in PLA:PGA ratios ranging from 50:50 to 90:10, resulting in a wide range of degradation rates. As a general rule, the higher the PGA content, the faster the rate of degradation [201]. The exception to this is PLGA 50:50, which has the fastest degradation

rate [75]. Molecular weight is also an important factor in the degradation rate of polymers; the rate of degradation is inversely related to molecular weight. Finally, PLA, PGA and PLGA are available with different end groups, namely a free carboxylic acid end group and an ester-terminated group [202]. End groups affect the degradation rate of the polymer as well as the strength of drug-polymer interactions [203]. The abundance of PLA, PGA and PLGA polymers with different properties can be utilized to broaden the physicochemical characteristics and anisotropy of Janus particles. It would be interesting to produce Janus particles from PLA/PLGA combinations, and even PLGA/PLGA Janus particles using PLGA polymers with different PLA:PGA ratios (i.e., PLGA 50:50/PLGA 90:10 Janus particles). PLA, PGA and the different types of PLGA copolymers can also be combined with PCL to produce Janus particles. Poly(ethylene-co-vinyl acetate), polyhydroxyalkanoate (PHA), polyhydroxybutyrate (PHB), polyhydroxyvalerate (PHV), polydioxanone (PDS), polyanhydride, poly(ortho ester), polyphosphazene, poly(propylene fumarate), and poly(glutamic acid) are other biodegradable polymers frequently used in drug delivery that should be explored for feasibility in Janus particle synthesis [204]. The library of biodegradable polymers and thus possibilities for Janus particle composition is constantly expanding; for example, a quick search revealed the development of novel poly(L-lactic-co-caprolactone) copolymers. The use of natural polymers such as chitosan, gelatin, fibrin, collagen, and alginate is another avenue that should be explored for the production of new and exciting Janus particles. However, because these polymers are hydrophilic, the W/O emulsion method would have to be used instead of the O/W emulsion method. Furthermore, a W/O/W emulsion can be used as a template to produce Janus particles from a hydrophobic and hydrophilic polymer (e.g., PLGA/alginate Janus

particles). The resulting particles would contain a true hydrophilic face and hydrophobic face unlike the PLGA/PCL Janus particles, which merely comprise varying degrees of hydrophobicity. Such a hydrophobic-hydrophilic dichotomy would provide not only interesting drug release and drug loading properties, but also the capacity for emulsion stabilization.

7.2.2 Surface Functionalization of Janus Particles

As mentioned previously, many polymers have end groups that can be exploited for surface functionalization with biocompatibility enhancers or targeting ligands. Coating nanoparticles with PEG and other hydrophilic polymers including chitosan, dextran, or heparin is a strategy frequently used to impart stealth characteristics and reduce clearance by the reticuloendothelial system (RES). Such coatings can increase the circulation half-life of nanoparticles to greater than 40 hours by preventing the adsorption of opsonins [205]. Long plasma residence time critical to the success of nanoparticles that rely on passive tumor targeting via the enhanced permeability and retention (EPR) effect. The EPR effect describes the phenomenon whereby nanoparticles preferentially accumulate in solid tumors due to abnormalities in tumor vasculature, predominantly hypervascularization, which accounts for "enhanced permeatbility," and lack of lympathic drainage, which accounts for "enhanced retention" [206]. In order to exploit the EPR effect, however, nanoparticles must stay in circulation long enough to reach the tumor site.

While passive targeting is considered the gold standard for tumor targeting, only an estimated 20% of passively-targeted nanoparticles ultimately accumulate in tumors [207]. Moreover, passively-targeted nanoparticles are not readily internalized by cancer cells and oftentimes end up releasing their payload into the tumor microenvironment rather than

within cancer cells. To address these shortcomings, targeting ligands aimed at surface molecules or receptors overexpressed in cancer cells can be attached to the surface of nanoparticles. Targeting ligands include antibodies, aptamers, proteins, peptides, sugars, and small molecules [208]. The most commonly used targeting ligands in cancer therapy are the Herceptin antibody, vascular endothelial growth factor (VEGF) and epidermal growth factor receptor (EGFR) antibodies, the RGD peptide, and folic acid [209, 210]. Ligand binding to the cell surface receptors promotes cellular internalization of the nanocarrier via receptor-mediated endocytosis.

The effectiveness of actively-targeting nanoparticles is diminished by the fact that target receptors are not exclusively overexpressed in cancer cells alone (e.g., folate receptor) [211]. To achieve higher specificity and affinity, dual-ligand targeting schemes have been developed [212, 213]. Recent studies show that dual-ligand targeted nanoparticles achieve enhanced cell recognition and uptake compared to single-ligand approaches, leading to reduced toxicity and higher therapeutic efficacy [208, 211]. However, targeting ligands on a single surface could potentially interact with one another, resulting in unwanted adverse effects [214]. Janus particles are ideally suited for multivalent targeting because they offer two opposing surfaces with different chemistries. This inherently allows for the attachment of a different targeting ligand onto each face of the Janus particle, thus preventing unwanted interactions and providing greater binding affinity. In addition to increasing the binding affinity using two different ligands, Janus particles have been shown to increase the binding affinity by virtue of their shape alone. Dissipative particle dynamics simulations showed that Janus particles have a faster and stronger attachment than their isotropic counterparts [215].

Another targeting strategy often used in cancer therapy is stimuli-responsive drug release. The intrinsic abnormalities in the tumor microenvironment can be exploited by designing nanocarriers that trigger drug release upon exposure to variations in local temperature or pH. In addition to internal stimuli, triggered targeting drug delivery systems can also be programmed to respond to external stimuli such as UV light, ultrasound, or magnetic fields [216]. Janus particles are the only types of particles that can be designed to simultaneously respond to more than one stimulus. External stimuli triggered release could be coupled with internal stimuli triggered release. Such a dual-stimuli-responsive system could enhance particle localization and provide site-specific release. For instance, using a UV-responsive polymer as one compartment would promote Janus particle delivery to the general area of the tumor and a pH-responsive polymer as the other compartment would ensure drug release in the tumor microenvironment.

7.2.3 Drug Conjugation to Polymer Matrix Material for Independent Release

Up until this point, biphasic Janus particles have largely been synthesized using non-biodegradable polymers such as PS and PMMA which would not be suitable for drug delivery applications. Because of this, there is not much research in the way of drug release from Janus particles. It is expected that Janus particles will offer unique degradation and drug release profiles due to their bicompartmental and anisotropic nature. There is one report of pH-dependent, decoupled release of two compounds from Janus particles comprised of poly(acrylamide-co-acrylic acid) mixed with PEO on one side and cross-linked to dextran on the other side [23]. The PEO-containing compartment is pH-dependent and exhibited typical first-order release at physiological pH, while the dextran-containing compartment remained intact for the duration of the study. This composition allows for

staggered release of two compounds, where complete release from one compartment is followed by the onset of release from the other compartment.

Drug release from polymeric nanoparticles occurs via four main mechanisms: diffusion through water-filled pores, diffusion through the polymer matrix, osmotic pumping, and erosion [199]. Drug solubility in the receptor medium and the polymer matrix as well as the biodegradation rate of the polymer determine the drug release rate [217]. Drug release from PLGA/PCL Janus particles is expected to occur simultaneously barring any strong interactions between a drug and one of the polymers. Although PCL is crystalline, more hydrophobic, and thus much slower degrading than PLGA, the two drugs would escape out of the PLGA side. In order to achieve truly independent release kinetics of two compounds, the drugs should be chemically conjugated to each of the polymers comprising the Janus particle. This way, Janus particles could be designed to enable either simultaneous release of two compounds at approximately the same rate, simultaneous release at different rates, or sequential release.

APPENDIX

Calibration curves for curcumin and quercetin in 50:50 methanol/water are provided below.

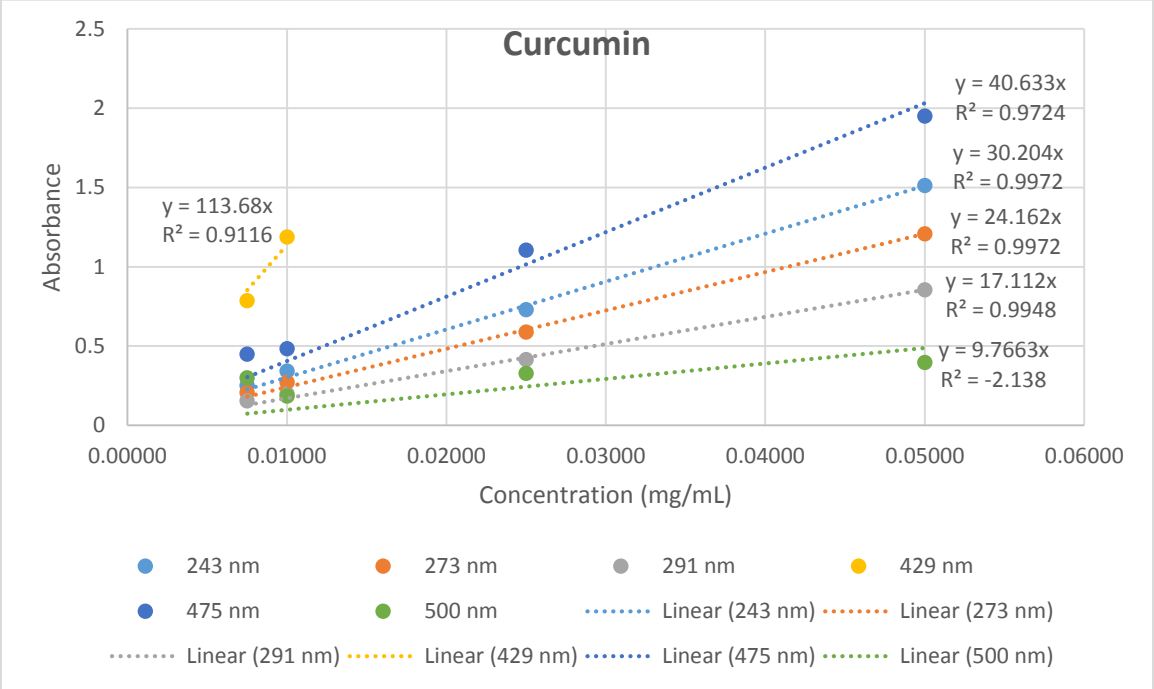

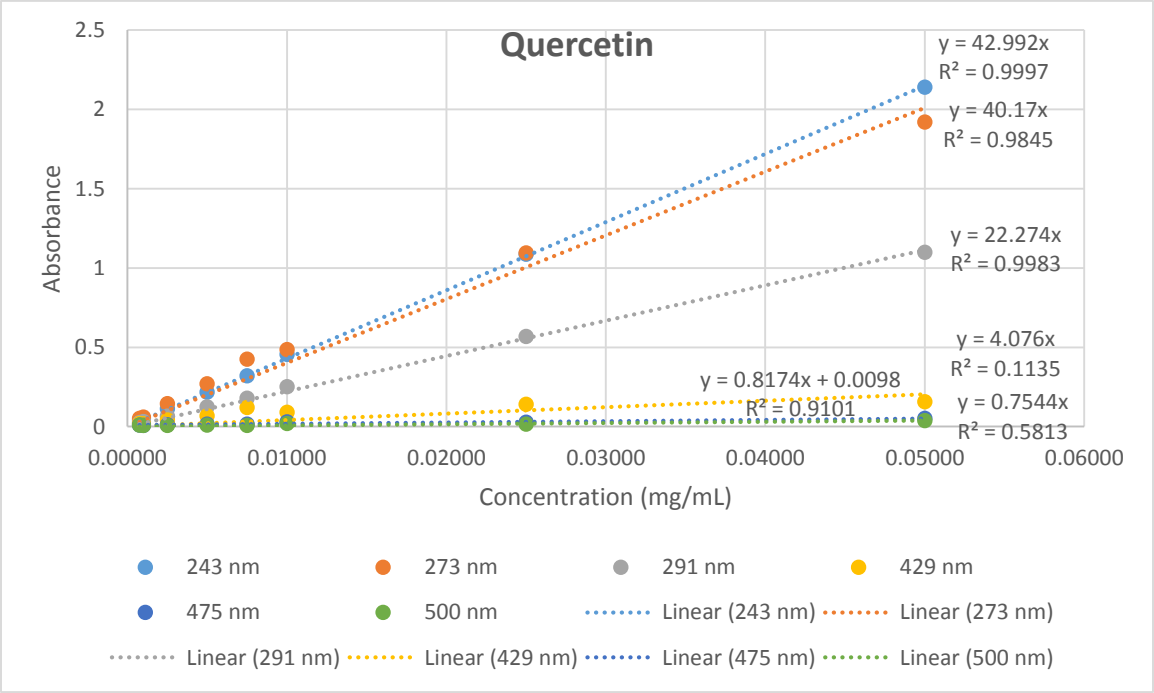

Calibration curves for curcumin and quercetin in THF are provided below.

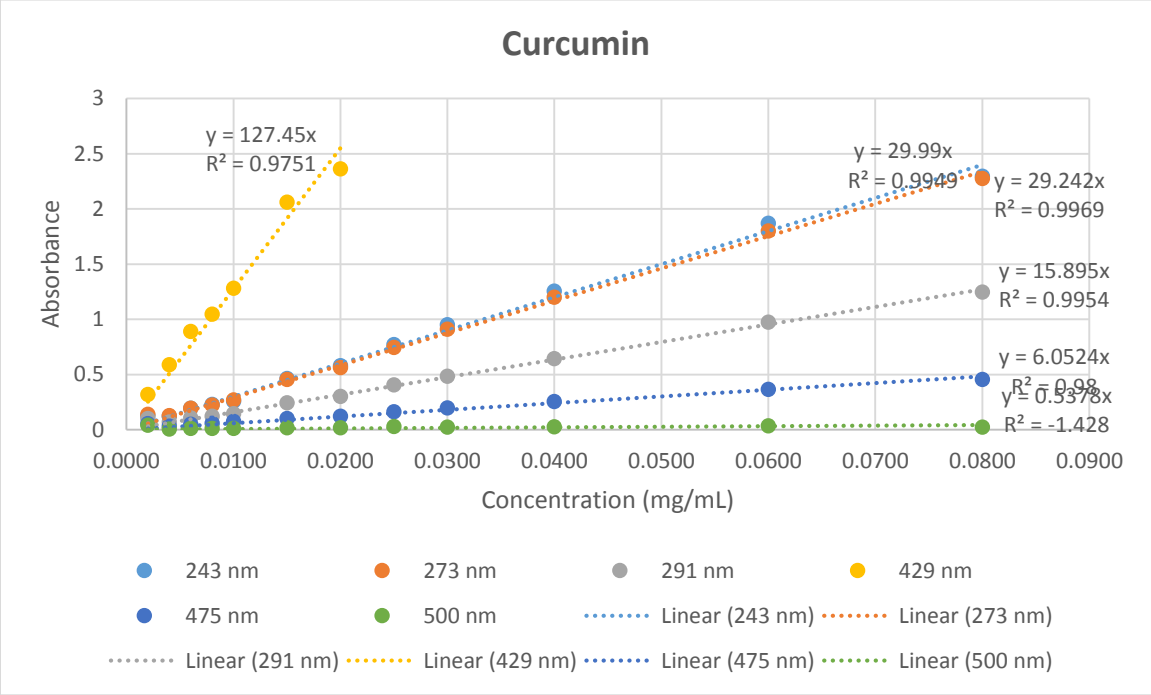

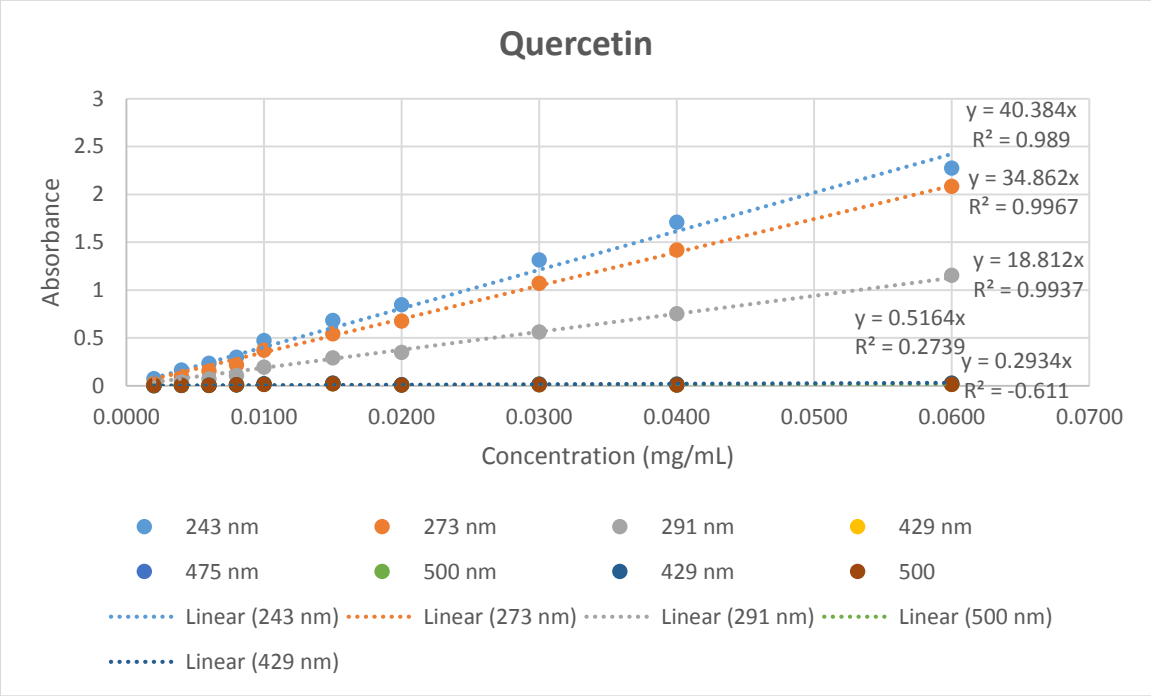

Calibration curves for acetaminophen and naproxen in 50:50 methanol/water are provided below.

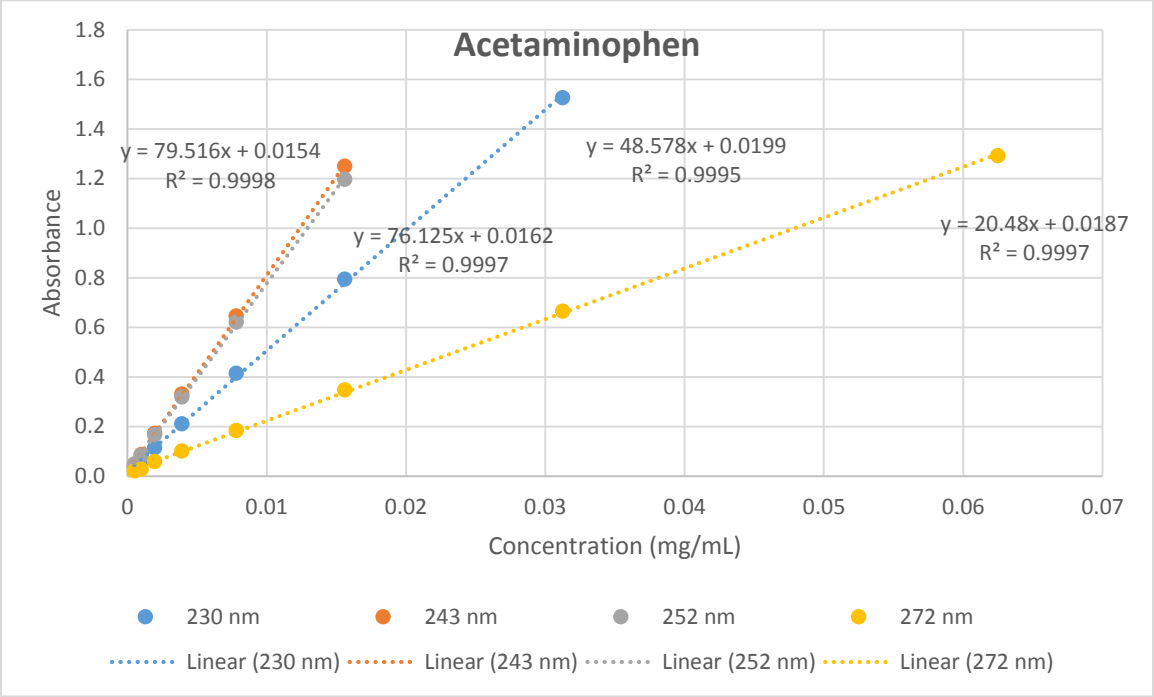

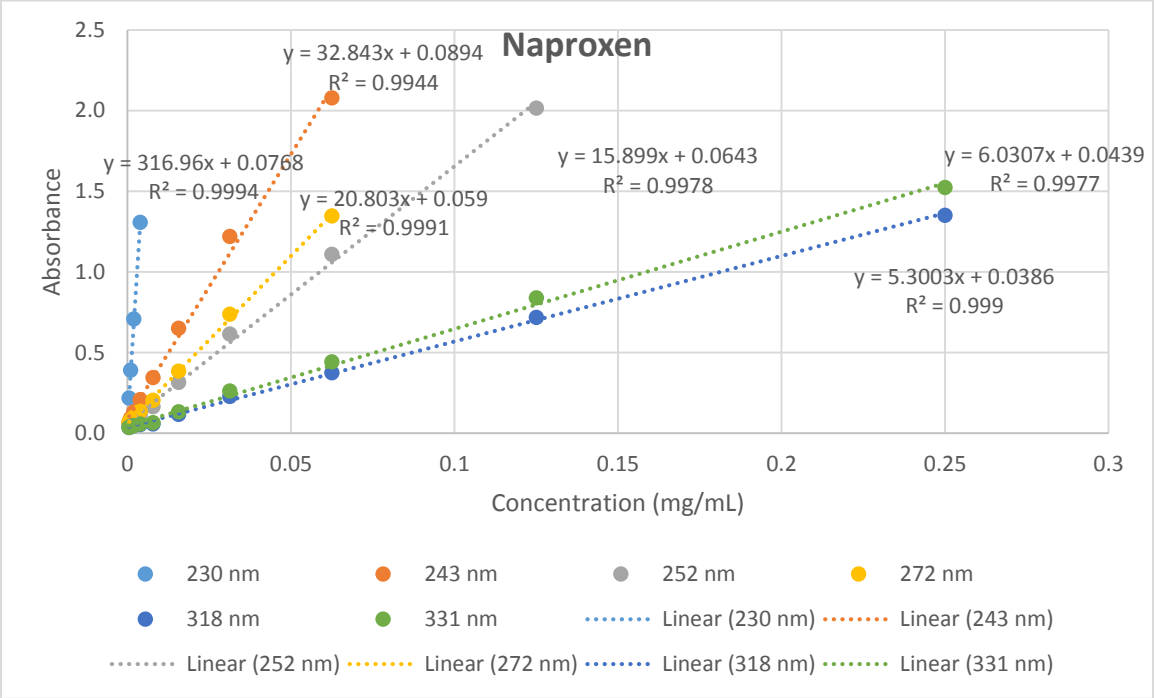

REFERENCES

1. de Gennes, P.G., *Soft matter.* Reviews of Modern Physics, 1992. **64**(3): p. 645-648.
2. Liu, B., et al., *Facile method for large scale synthesis of magnetic inorganic–organic hybrid anisotropic Janus particles.* Journal of Colloid and Interface Science, 2012. **385**(1): p. 34-40.
3. Hu, J., et al., *Fabrication, properties and applications of Janus particles.* Chemical Society Reviews, 2012. **41**(11): p. 4356-4378.
4. Perro, A., et al., *Design and synthesis of Janus micro- and nanoparticles.* Journal of Materials Chemistry, 2005. **15**(35-36): p. 3745-3760.
5. Du, J. and R.K. O'Reilly, *Anisotropic particles with patchy, multicompartment and Janus architectures: preparation and application.* Chemical Society Reviews, 2011. **40**(5): p. 2402-2416.
6. Lee, K.J., J. Yoon, and J. Lahann, *Recent advances with anisotropic particles.* Current Opinion in Colloid & Interface Science, 2011. **16**(3): p. 195-202.
7. Sacanna, S. and D.J. Pine, *Shape-anisotropic colloids: Building blocks for complex assemblies.* Current Opinion in Colloid & Interface Science, 2011. **16**(2): p. 96-105.
8. Yang, S., et al., *Microfluidic synthesis of multifunctional Janus particles for biomedical applications.* Lab on a Chip, 2012. **12**(12): p. 2097-2102.
9. Lipinski, C.A., et al., *Experimental and computational approaches to estimate solubility and permeability in drug discovery and development settings.* Advanced Drug Delivery Reviews, 2012. **64, Supplement**(0): p. 4-17.
10. Lipinski, C.A., *Drug-like properties and the causes of poor solubility and poor permeability.* Journal of Pharmacological and Toxicological Methods, 2000. **44**(1): p. 235-249.
11. Savjani, K.T., A.K. Gajjar, and J.K. Savjani, *Drug Solubility: Importance and Enhancement Techniques.* ISRN Pharmaceutics, 2012. **2012**: p. 195727.
12. Morgen, M., et al., *Polymeric Nanoparticles for Increased Oral Bioavailability and Rapid Absorption Using Celecoxib as a Model of a Low-Solubility, High-Permeability Drug.* Pharmaceutical Research, 2012. **29**(2): p. 427-440.
13. Park, K., *Controlled drug delivery systems: past forward and future back.* J Control Release, 2014. **190**: p. 3-8.
14. Roller, C. and D. Maddalo, *The molecular chaperone GRP78/BiP in the development of chemoresistance: mechanism and possible treatment.* Frontiers in Pharmacology, 2013. **4**.
15. Hu, C.-M.J., S. Aryal, and L. Zhang, *Nanoparticle-assisted combination therapies for effective cancer treatment.* Therapeutic Delivery, 2010. **1**(2): p. 323-334.
16. Tabernero, J., *The role of VEGF and EGFR inhibition: implications for combining anti-VEGF and anti-EGFR agents.* Mol Cancer Res, 2007. **5**(3): p. 203-20.
17. Kruis, F.E. and R.K. Joshi, *Nanoparticle design and handling — challenges for engineers and particle technologists.* China Particuology, 2005. **3**(1–2): p. 99-104.
18. Lee, J.H. and A. Nan, *Combination Drug Delivery Approaches in Metastatic Breast Cancer.* Journal of Drug Delivery, 2012. **2012**: p. 17.
19. Song, X., et al., *Dual agents loaded PLGA nanoparticles: Systematic study of particle size and drug entrapment efficiency.* European Journal of Pharmaceutics and Biopharmaceutics, 2008. **69**(2): p. 445-453.
20. Song, X.R., et al., *Reversion of multidrug resistance by co-encapsulation of vincristine and verapamil in PLGA nanoparticles.* European Journal of Pharmaceutical Sciences, 2009. **37**(3–4): p. 300-305.
21. Huang, H.-Y., et al., *Co-delivery of anti-vascular endothelial growth factor siRNA and doxorubicin by multifunctional polymeric micelle for tumor growth suppression.* Journal of Biomedical Materials Research Part A, 2011. **97A**(3): p. 330-338.
22. Avgoustakis, K., *Pegylated poly(lactide) and poly(lactide-co-glycolide) nanoparticles: preparation, properties and possible applications in drug delivery.* Curr Drug Deliv, 2004. **1**(4): p. 321-33.
23. Hwang, S. and J. Lahann, *Differentially Degradable Janus Particles for Controlled Release Applications.* Macromolecular Rapid Communications, 2012. **33**(14): p. 1178-1183.
24. Champion, J.A., Y.K. Katare, and S. Mitragotri, *Particle shape: a new design parameter for micro- and nanoscale drug delivery carriers.* J Control Release, 2007. **121**(1-2): p. 3-9.
25. Champion, J.A. and S. Mitragotri, *Role of target geometry in phagocytosis.* Proceedings of the National Academy of Sciences of the United States of America, 2006. **103**(13): p. 4930-4934.

26. Gratton, S.E.A., et al., *The effect of particle design on cellular internalization pathways.* Proceedings of the National Academy of Sciences, 2008. **105**(33): p. 11613-11618.
27. Geng, Y., et al., *Shape effects of filaments versus spherical particles in flow and drug delivery.* Nat Nanotechnol, 2007. **2**(4): p. 249-55.
28. Yoo, J.W., N. Doshi, and S. Mitragotri, *Adaptive micro and nanoparticles: temporal control over carrier properties to facilitate drug delivery.* Adv Drug Deliv Rev, 2011. **63**(14-15): p. 1247-56.
29. Kaewsaneha, C., et al., *Preparation of Janus colloidal particles via Pickering emulsion: An overview.* Colloids and Surfaces A: Physicochemical and Engineering Aspects, (0).
30. Lattuada, M. and T.A. Hatton, *Synthesis, properties and applications of Janus nanoparticles.* Nano Today, 2011. **6**(3): p. 286-308.
31. Wurm, F. and A.F.M. Kilbinger, *Polymeric Janus Particles.* Angewandte Chemie International Edition, 2009. **48**(45): p. 8412-8421.
32. Wolf, A., A. Walther, and A.H.E. Müller, *Janus Triad: Three Types of Nonspherical, Nanoscale Janus Particles from One Single Triblock Terpolymer.* Macromolecules, 2011. **44**(23): p. 9221-9229.
33. Wurm, F., et al., *Janus Micelles Induced by Olefin Metathesis.* Journal of the American Chemical Society, 2008. **130**(18): p. 5876-5877.
34. Hilfiker, R., B. Chu, and Z. Xu, *Micelle forming properties of polystyrene/polyisoprene AB block copolymers.* Journal of Colloid and Interface Science, 1989. **133**(1): p. 176-184.
35. Yoon, J., K.J. Lee, and J. Lahann, *Multifunctional polymer particles with distinct compartments.* Journal of Materials Chemistry, 2011. **21**(24): p. 8502-8510.
36. Perro, A., et al., *Production of large quantities of "Janus" nanoparticles using wax-in-water emulsions.* Colloids and Surfaces A: Physicochemical and Engineering Aspects, 2009. **332**(1): p. 57-62.
37. Jiang, S., et al., *Solvent-Free Synthesis of Janus Colloidal Particles.* Langmuir, 2008. **24**(18): p. 10073-10077.
38. Lin, C.-C., et al., *Fabrication and Characterization of Asymmetric Janus and Ternary Particles.* ACS Applied Materials & Interfaces, 2010. **2**(11): p. 3185-3191.
39. Misra, A.C., et al., *Multicompartmental Particles for Combined Imaging and siRNA Delivery.* Advanced Materials, 2012. **24**(28): p. 3850-3856.
40. Chen, C.-H., et al., *Janus Particles Templated from Double Emulsion Droplets Generated Using Microfluidics.* Langmuir, 2009. **25**(8): p. 4320-4323.
41. Park, J.I., et al., *Microfluidic Synthesis of Polymer and Inorganic Particulate Materials.* Annual Review of Materials Research, 2010. **40**(1): p. 415-443.
42. Shah, R.K., J.-W. Kim, and D.A. Weitz, *Janus Supraparticles by Induced Phase Separation of Nanoparticles in Droplets.* Advanced Materials, 2009. **21**(19): p. 1949-1953.
43. Nie, L., et al., *One-Pot Synthesis of Amphiphilic Polymeric Janus Particles and Their Self-Assembly into Supermicelles with a Narrow Size Distribution.* Angewandte Chemie International Edition, 2007. **46**(33): p. 6321-6324.
44. Pawar, A.B. and I. Kretzschmar, *Fabrication, Assembly, and Application of Patchy Particles.* Macromolecular Rapid Communications, 2010. **31**(2): p. 150-168.
45. Bhaskar, S., et al., *Towards Designer Microparticles: Simultaneous Control of Anisotropy, Shape, and Size.* Small, 2010. **6**(3): p. 404-411.
46. Bhaskar, S., et al., *Spatioselective Modification of Bicompartmental Polymer Particles and Fibers via Huisgen 1, 3-Dipolar Cycloaddition.* Macromolecular Rapid Communications, 2008. **29**(24): p. 1973-1973.
47. Abate, A.R., et al., *Synthesis of Monodisperse Microparticles from Non-Newtonian Polymer Solutions with Microfluidic Devices.* Advanced Materials, 2011. **23**(15): p. 1757-1760.
48. Sheu, H.R., M.S. El-Aasser, and J.W. Vanderhoff, *Phase separation in polystyrene latex interpenetrating polymer networks.* Journal of Polymer Science Part A: Polymer Chemistry, 1990. **28**(3): p. 629-651.
49. Saito, N., Y. Kagari, and M. Okubo, *Revisiting the Morphology Development of Solvent-Swollen Composite Polymer Particles at Thermodynamic Equilibrium†.* Langmuir, 2007. **23**(11): p. 5914-5919.
50. Saito, N., et al., *Formation of "Snowmanlike" Polystyrene/Poly(methyl methacrylate)/Toluene Droplets Dispersed in an Aqueous Solution of a Nonionic Surfactant at Thermodynamic Equilibrium†.* Langmuir, 2007. **23**(23): p. 11506-11512.

51. Perro, A., et al., *Synthesis of hybrid colloidal particles: From snowman-like to raspberry-like morphologies.* Colloids and Surfaces A: Physicochemical and Engineering Aspects, 2006. **284–285**(0): p. 78-83.
52. Rahman, M.M., et al., *Anisotropic magnetic microparticles from ferrofluid emulsion.* Soft Matter, 2011. **7**(4): p. 1483-1490.
53. Mock, E.B., et al., *Synthesis of Anisotropic Nanoparticles by Seeded Emulsion Polymerization.* Langmuir, 2006. **22**(9): p. 4037-4043.
54. Astete, C.E., C.S.S.R. Kumar, and C.M. Sabliov, *Size control of poly(d,l-lactide-co-glycolide) and poly(d,l-lactide-co-glycolide)-magnetite nanoparticles synthesized by emulsion evaporation technique.* Colloids and Surfaces A: Physicochemical and Engineering Aspects, 2007. **299**(1–3): p. 209-216.
55. O'Donnell, P.B. and J.W. McGinity, *Preparation of microspheres by the solvent evaporation technique.* Advanced Drug Delivery Reviews, 1997. **28**(1): p. 25-42.
56. Jeffery, H., S.S. Davis, and D.T. O'Hagan, *The preparation and characterisation of poly(lactide-co-glycolide) microparticles. I: Oil-in-water emulsion solvent evaporation.* International Journal of Pharmaceutics, 1991. **77**(2–3): p. 169-175.
57. Song, C.X., et al., *Formulation and characterization of biodegradable nanoparticles for intravascular local drug delivery.* Journal of Controlled Release, 1997. **43**(2–3): p. 197-212.
58. Li, M., O. Rouaud, and D. Poncelet, *Microencapsulation by solvent evaporation: State of the art for process engineering approaches.* International Journal of Pharmaceutics, 2008. **363**(1–2): p. 26-39.
59. Hamishehkar, H., et al., *The effect of formulation variables on the characteristics of insulin-loaded poly(lactic-co-glycolic acid) microspheres prepared by a single phase oil in oil solvent evaporation method.* Colloids and Surfaces B: Biointerfaces, 2009. **74**(1): p. 340-349.
60. Freitas, S., H.P. Merkle, and B. Gander, *Microencapsulation by solvent extraction/evaporation: reviewing the state of the art of microsphere preparation process technology.* Journal of Controlled Release, 2005. **102**(2): p. 313-332.
61. Romanski, F.S., et al., *Production and Characterization of Anisotropic Particles from Biodegradable Materials.* Langmuir, 2012. **28**(8): p. 3756-3765.
62. Chemistry, R.S., et al., *Janus Particle Synthesis, Self Assembly and Applications*. 2012: ROYAL SOC OF CHEMISTRY.
63. Desgouilles, S., et al., *The Design of Nanoparticles Obtained by Solvent Evaporation: A Comprehensive Study.* Langmuir, 2003. **19**(22): p. 9504-9510.
64. Lee, S.C., et al., *Quantitative analysis of polyvinyl alcohol on the surface of poly(d,l-lactide-co-glycolide) microparticles prepared by solvent evaporation method: effect of particle size and PVA concentration.* Journal of Controlled Release, 1999. **59**(2): p. 123-132.
65. Obeidat, W.M. and J.C. Price, *Viscosity of polymer solution phase and other factors controlling the dissolution of theophylline microspheres prepared by the emulsion solvent evaporation method.* J Microencapsul, 2003. **20**(1): p. 57-65.
66. Mainardes, R.M. and R.C. Evangelista, *PLGA nanoparticles containing praziquantel: effect of formulation variables on size distribution.* International Journal of Pharmaceutics, 2005. **290**(1–2): p. 137-144.
67. Quintanar-Guerrero, D., et al., *Influence of stabilizing agents and preparative variables on the formation of poly(d,l-lactic acid) nanoparticles by an emulsification-diffusion technique.* International Journal of Pharmaceutics, 1996. **143**(2): p. 133-141.
68. Mahboubian, A., et al., *Preparation and In-vitro Evaluation of Controlled Release PLGA Microparticles Containing Triptoreline.* Iran J Pharm Res, 2010. **9**(4): p. 369-78.
69. Sahana, D.K., et al., *PLGA nanoparticles for oral delivery of hydrophobic drugs: Influence of organic solvent on nanoparticle formation and release behavior In Vitro and In Vivo using estradiol as a model drug.* Journal of Pharmaceutical Sciences, 2008. **97**(4): p. 1530-1542.
70. Jeon, H.-J., et al., *Effect of solvent on the preparation of surfactant-free poly(dl-lactide-co-glycolide) nanoparticles and norfloxacin release characteristics.* International Journal of Pharmaceutics, 2000. **207**(1–2): p. 99-108.
71. Okubo, M., N. Saito, and T. Fujibayashi, *Preparation of polystyrene/poly(methyl methacrylate) composite particles having a dent.* Colloid and Polymer Science, 2005. **283**(6): p. 691-698.
72. Saito, N., Y. Kagari, and M. Okubo, *Effect of Colloidal Stabilizer on the Shape of Polystyrene/Poly(methyl methacrylate) Composite Particles Prepared in Aqueous Medium by the*

Solvent Evaporation Method†. Langmuir, 2006. **22**(22): p. 9397-9402.
73. Misra, R., et al., *Sustained antibacterial activity of doxycycline-loaded poly(D,L-lactide-co-glycolide) and poly(ε-caprolactone) nanoparticles.* Nanomedicine, 2009. **4**(5): p. 519-530.
74. Hiep, N.T. and B.T. Lee, *Electro-spinning of PLGA/PCL blends for tissue engineering and their biocompatibility.* J Mater Sci Mater Med, 2010. **21**(6): p. 1969-78.
75. Makadia, H.K. and S.J. Siegel, *Poly Lactic-co-Glycolic Acid (PLGA) as Biodegradable Controlled Drug Delivery Carrier.* Polymers, 2011. **3**(3): p. 1377-1397.
76. Kumari, A., S.K. Yadav, and S.C. Yadav, *Biodegradable polymeric nanoparticles based drug delivery systems.* Colloids and Surfaces B: Biointerfaces, 2010. **75**(1): p. 1-18.
77. Sonaje, K., et al., *Development of Biodegradable Nanoparticles for Oral Delivery of Ellagic Acid and Evaluation of Their Antioxidant Efficacy Against Cyclosporine A-Induced Nephrotoxicity in Rats.* Pharmaceutical Research, 2007. **24**(5): p. 899-908.
78. Hung, L.-H., et al., *PLGA micro/nanosphere synthesis by droplet microfluidic solvent evaporation and extraction approaches.* Lab on a Chip, 2010. **10**(14): p. 1820-1825.
79. Cai, Q., J. Bei, and S. Wang, *Synthesis and characterization of polycaprolactone (B)–poly(lactide-co-glycolide) (A) ABA block copolymer.* Polymers for Advanced Technologies, 2000. **11**(4): p. 159-166.
80. Sanna, V., et al., *Novel docetaxel-loaded nanoparticles based on poly(lactide-co-caprolactone) and poly(lactide-co-glycolide-co-caprolactone) for prostate cancer treatment: formulation, characterization, and cytotoxicity studies.* Nanoscale Research Letters, 2011. **6**(1): p. 260.
81. Tang, Z.G., N.P. Rhodes, and J.A. Hunt, *Control of the Domain Microstructures of PLGA and PCL Binary Systems: Importance of Morphology in Controlled Drug Release.* Chemical Engineering Research and Design, 2007. **85**(7): p. 1044-1050.
82. Amiji, M.M., *Nanotechnology for Cancer Therapy*. 2006: Taylor & Francis.
83. Müller, R.H., K. Mäder, and S. Gohla, *Solid lipid nanoparticles (SLN) for controlled drug delivery – a review of the state of the art.* European Journal of Pharmaceutics and Biopharmaceutics, 2000. **50**(1): p. 161-177.
84. Müller, R.H., et al., *Oral bioavailability of cyclosporine: Solid lipid nanoparticles (SLN®) versus drug nanocrystals.* International Journal of Pharmaceutics, 2006. **317**(1): p. 82-89.
85. Pardeike, J., A. Hommoss, and R.H. Müller, *Lipid nanoparticles (SLN, NLC) in cosmetic and pharmaceutical dermal products.* International Journal of Pharmaceutics, 2009. **366**(1–2): p. 170-184.
86. Kaur, T. and R. Slavcev, *Solid Lipid Nanoparticles: Tuneable Anti-Cancer Gene/Drug Delivery Systems*. Novel Gene Therapy Approaches. 2013.
87. Souto, E.B. and S. Doktorovová, *Chapter 6 - Solid Lipid Nanoparticle Formulations: Pharmacokinetic and Biopharmaceutical Aspects in Drug Delivery*, in *Methods in Enzymology*, D. Nejat, Editor. 2009, Academic Press. p. 105-129.
88. Zhang, L., et al., *Self-Assembled Lipid−Polymer Hybrid Nanoparticles: A Robust Drug Delivery Platform.* ACS Nano, 2008. **2**(8): p. 1696-1702.
89. Sah, H., et al., *Concepts and practices used to develop functional PLGA-based nanoparticulate systems.* Int J Nanomedicine, 2013. **8**: p. 747-65.
90. Clawson, C., et al., *Synthesis and Characterization of Lipid–Polymer Hybrid Nanoparticles with pH-Triggered Poly(ethylene glycol) Shedding.* Langmuir, 2011. **27**(17): p. 10556-10561.
91. Moghimi, S.M. and A.C. Hunter, *Poloxamers and poloxamines in nanoparticle engineering and experimental medicine.* Trends in Biotechnology, 2000. **18**(10): p. 412-420.
92. Research, F.C.f.D.E.a., *Inactive Ingredient Search for Approved Drug Products*. 2013: http://www.accessdata.fda.gov/scripts/cder/iig/index.Cfm.
93. Sahoo, S.K., et al., *Residual polyvinyl alcohol associated with poly (D,L-lactide-co-glycolide) nanoparticles affects their physical properties and cellular uptake.* J Control Release, 2002. **82**(1): p. 105-14.
94. Bala, I., S. Hariharan, and M.N.V.R. Kumar, *PLGA Nanoparticles in Drug Delivery: The State of the Art.* 2004. **21**(5): p. 36.
95. Kulshreshtha, A.K., O.N. Singh, and G.M. Wall, *Pharmaceutical Suspensions: From Formulation Development to Manufacturing*. 2009: Springer New York.
96. Yaszemski, M.J., et al., *Tissue Engineering And Novel Delivery Systems*. 2003: CRC Press.
97. Mainardes, R.M. and R.C. Evangelista, *PLGA nanoparticles containing praziquantel: effect of*

formulation variables on size distribution. Int J Pharm, 2005. **290**(1-2): p. 137-44.
98. Niwa, T., et al., *In vitro drug release behavior of D,L-lactide/glycolide copolymer (PLGA) nanospheres with nafarelin acetate prepared by a novel spontaneous emulsification solvent diffusion method.* J Pharm Sci, 1994. **83**(5): p. 727-32.
99. Ubrich, N., et al., *Preparation and characterization of propranolol hydrochloride nanoparticles: a comparative study.* J Control Release, 2004. **97**(2): p. 291-300.
100. Schenderlein, S., M. Luck, and B.W. Muller, *Partial solubility parameters of poly(D,L-lactide-co-glycolide).* Int J Pharm, 2004. **286**(1-2): p. 19-26.
101. Aragón, D.M., J.E. Rosas, and F. Martínez, *Thermodynamic study of the solubility of ibuprofen in acetone and dichloromethane.* Brazilian Journal of Pharmaceutical Sciences, 2010. **46**: p. 227-235.
102. Shah, N., et al., *Amorphous Solid Dispersions: Theory and Practice*. 2014: Springer New York.
103. Li, H., *Synthesis, Characterization and Properties of Vinyl Ester Matrix Resins*. 1998, Virginia Polytechnic Institute and State University.
104. Cao, X., et al., *One-step fabrication of polymeric hybrid particles with core-shell, patchy, patchy Janus and Janus architectures via a microfluidic-assisted phase separation process.* RSC Advances, 2015. **5**(97): p. 79969-79975.
105. Bordes, C., et al., *Determination of poly(ε-caprolactone) solubility parameters: Application to solvent substitution in a microencapsulation process.* International Journal of Pharmaceutics, 2010. **383**(1–2): p. 236-243.
106. Harris, M., G. Appel, and H. Ade, *Surface Morphology of Annealed Polystyrene and Poly(methyl methacrylate) Thin Film Blends and Bilayers.* Macromolecules, 2003. **36**(9): p. 3307-3314.
107. Xiang, T.-X. and B.D. Anderson, *Molecular Dynamics Simulation of Amorphous Indomethacin-Poly(Vinylpyrrolidone) Glasses: Solubility and Hydrogen Bonding Interactions.* Journal of Pharmaceutical Sciences. **102**(3): p. 876-891.
108. Rimai, D.S., L.P. DeMejo, and K.L. Mittal, *Fundamentals of Adhesion and Interfaces*. 1995: Taylor & Francis.
109. Wohlfarth, C., *Solubility parameter of poly(tert-butyl acrylate-b-methyl methacrylate)*, in *Polymer Solutions: Physical Properties and their Relations I (Thermodynamic Properties: pVT data and miscellaneous properties of polymer solutions)*, M.D. Lechner and K.F. Arndt, Editors. 2010, Springer Berlin Heidelberg: Berlin, Heidelberg. p. 1527-1527.
110. Wu, S., *Calculation of interfacial tension in polymer systems.* Journal of Polymer Science Part C: Polymer Symposia, 1971. **34**(1): p. 19-30.
111. Sinha, V.R. and A. Trehan, *Formulation, characterization, and evaluation of ketorolac tromethamine-loaded biodegradable microspheres.* Drug Deliv, 2005. **12**(3): p. 133-9.
112. Shiny, J., et al., *Development and evaluation of a novel biodegradable sustained release microsphere formulation of paclitaxel intended to treat breast cancer.* International Journal of Pharmaceutical Investigation, 2013. **3**(3): p. 119-125.
113. Sa, M.-W. and J.Y. Kim, *Effect of various blending ratios on the cell characteristics of PCL and PLGA scaffolds fabricated by polymer deposition system.* International Journal of Precision Engineering and Manufacturing, 2013. **14**(4): p. 649-655.
114. Baker, S.C., et al., *The relationship between the mechanical properties and cell behaviour on PLGA and PCL scaffolds for bladder tissue engineering.* Biomaterials, 2009. **30**(7): p. 1321-8.
115. Wang, Y., et al., *Preparation and assembly of concave polymer microparticles.* RSC Advances, 2015. **5**(46): p. 36680-36686.
116. Kryszewski, M., A. Galeski, and E. Martuscelli, *Polymer Blends: Volume 2: Processing, Morphology, and Properties*. 2013: Springer US.
117. Okubo, M., et al., *Incorporation of Nonionic Emulsifiers Inside Particles in Emulsion Polymerization: Mechanism and Methods of Suppression†.* Langmuir, 2006. **22**(21): p. 8727-8731.
118. Higuchi, T., et al., *Spontaneous formation of polymer nanoparticles with inner micro-phase separation structures.* Soft Matter, 2008. **4**(6): p. 1302-1305.
119. Müller, R.H. and C. Jacobs, *Buparvaquone mucoadhesive nanosuspension: preparation, optimisation and long-term stability.* International Journal of Pharmaceutics, 2002. **237**(1–2): p. 151-161.
120. Naha, P.C., H.J. Byrne, and A.K. Panda, *Role of Polymeric Excipients on Controlled Release Profile of Glipizide from PLGA and Eudragit RS 100 Nanoparticles.* Journal of Nanopharmaceutics and Drug Delivery, 2013. **1**(1): p. 74-81.

121. Tkachenko, N.H., et al., *The influence of ionic and nonionic surfactants on aggregative stability and electrical surface properties of aqueous suspensions of titanium dioxide.* J Colloid Interface Sci, 2006. **299**(2): p. 686-95.
122. Crowley, M.M., et al., *Pharmaceutical applications of hot-melt extrusion: part I.* Drug Dev Ind Pharm, 2007. **33**(9): p. 909-26.
123. Cheng, D., et al., *Engineering PLGA doped PCL microspheres with a layered architecture and an island-sea topography.* RSC Advances, 2014. **4**(18): p. 9031-9038.
124. Moorthi, C. and K. Kathiresan, *Curcumin–Piperine/Curcumin–Quercetin/Curcumin–Silibinin dual drug-loaded nanoparticulate combination therapy: A novel approach to target and treat multidrug-resistant cancers.* Journal of Medical Hypotheses and Ideas, 2013. **7**(1): p. 15-20.
125. Jackson, J.K., et al., *The antioxidants curcumin and quercetin inhibit inflammatory processes associated with arthritis.* Inflamm Res, 2006. **55**(4): p. 168-75.
126. Seideman, P., *Additive effect of combined naproxen and paracetamol in rheumatoid arthritis.* Br J Rheumatol, 1993. **32**(12): p. 1077-82.
127. Seideman, P., P. Samuelson, and G. Neander, *Naproxen and paracetamol compared with naproxen only in coxarthrosis. Increased effect of the combination in 18 patients.* Acta Orthop Scand, 1993. **64**(3): p. 285-8.
128. Yang, Y.-Y., T.-S. Chung, and N. Ping Ng, *Morphology, drug distribution, and in vitro release profiles of biodegradable polymeric microspheres containing protein fabricated by double-emulsion solvent extraction/evaporation method.* Biomaterials, 2001. **22**(3): p. 231-241.
129. Lamprecht, A., et al., *Influences of process parameters on nanoparticle preparation performed by a double emulsion pressure homogenization technique.* International journal of pharmaceutics, 2000. **196**(2): p. 177-182.
130. Li, Y.-P., et al., *PEGylated PLGA nanoparticles as protein carriers: synthesis, preparation and biodistribution in rats.* Journal of Controlled Release, 2001. **71**(2): p. 203-211.
131. Bilati, U., E. Allémann, and E. Doelker, *Poly (D, L-lactide-co-glycolide) protein-loaded nanoparticles prepared by the double emulsion method-processing and formulation issues for enhanced entrapment efficiency.* Journal of microencapsulation, 2005. **22**(2): p. 205-214.
132. Zambaux, M., et al., *Influence of experimental parameters on the characteristics of poly (lactic acid) nanoparticles prepared by a double emulsion method.* Journal of Controlled Release, 1998. **50**(1): p. 31-40.
133. Granberg, R.A. and Å.C. Rasmuson, *Solubility of Paracetamol in Pure Solvents.* Journal of Chemical & Engineering Data, 1999. **44**(6): p. 1391-1395.
134. Fude, C., et al., *Preparation and characterization of melittin-loaded poly (dl-lactic acid) or poly (dl-lactic-co-glycolic acid) microspheres made by the double emulsion method.* Journal of Controlled Release, 2005. **107**(2): p. 310-319.
135. Pistel, K.F. and T. Kissel, *Effects of salt addition on the microencapsulation of proteins using W/O/W double emulsion technique.* J Microencapsul, 2000. **17**(4): p. 467-83.
136. Umeyor, E.C., et al., *Preparation of novel solid lipid microparticles loaded with gentamicin and its evaluation in vitro and in vivo.* J Microencapsul, 2012. **29**(3): p. 296-307.
137. Tamjidi, F., et al., *Nanostructured lipid carriers (NLC): A potential delivery system for bioactive food molecules.* Innovative Food Science & Emerging Technologies, 2013. **19**(0): p. 29-43.
138. Hadinoto, K., A. Sundaresan, and W.S. Cheow, *Lipid–polymer hybrid nanoparticles as a new generation therapeutic delivery platform: A review.* European Journal of Pharmaceutics and Biopharmaceutics, 2013. **85**(3, Part A): p. 427-443.
139. Mandal, B., et al., *Core–shell-type lipid–polymer hybrid nanoparticles as a drug delivery platform.* Nanomedicine: Nanotechnology, Biology and Medicine, 2013. **9**(4): p. 474-491.
140. Duan, J., et al., *Reversion of multidrug resistance by co-encapsulation of doxorubicin and curcumin in chitosan/poly(butyl cyanoacrylate) nanoparticles.* International Journal of Pharmaceutics, 2012. **426**(1–2): p. 193-201.
141. Misra, R. and S.K. Sahoo, *Coformulation of Doxorubicin and Curcumin in Poly(d,l-lactide-co-glycolide) Nanoparticles Suppresses the Development of Multidrug Resistance in K562 Cells.* Molecular Pharmaceutics, 2011. **8**(3): p. 852-866.
142. Severino, P., et al., *Current State-of-Art and New Trends on Lipid Nanoparticles (SLN and NLC) for Oral Drug Delivery.* Journal of Drug Delivery, 2012. **2012**: p. 750891.
143. Basu, S., et al., *Nanoparticle-mediated targeting of MAPK signaling predisposes tumor to*

chemotherapy. Proceedings of the National Academy of Sciences, 2009.
144. Shah, V., et al., *Genotoxicity of different nanocarriers: possible modifications for the delivery of nucleic acids.* Curr Drug Discov Technol, 2013. **10**(1): p. 8-15.
145. Taratula, O., et al., *Nanostructured lipid carriers as multifunctional nanomedicine platform for pulmonary co-delivery of anticancer drugs and siRNA.* J Control Release, 2013. **171**(3): p. 349-57.
146. Shah, V., et al., *Genotoxicity of Different Nanocarriers: Possible Modifications for the Delivery of Nucleic Acids.* Current drug discovery technologies, 2013. **10**(1): p. 8-15.
147. Garbuzenko, O.B., et al., *Inhibition of lung tumor growth by complex pulmonary delivery of drugs with oligonucleotides as suppressors of cellular resistance.* Proceedings of the National Academy of Sciences, 2010. **107**(23): p. 10737-10742.
148. Roa, W.H., et al., *Inhalable nanoparticles, a non-invasive approach to treat lung cancer in a mouse model.* Journal of Controlled Release, 2011. **150**(1): p. 49-55.
149. Walther, A. and A.H.E. Müller, *Janus Particles: Synthesis, Self-Assembly, Physical Properties, and Applications.* Chemical Reviews, 2013. **113**(7): p. 5194-5261.
150. Tanaka, T., et al., *Effect of Molecular Weight on the Morphology of Polystyrene/Poly(methyl methacrylate) Composite Particles Prepared by the Solvent Evaporation Method†.* Langmuir, 2008. **24**(21): p. 12267-12271.
151. Yamashita, N. and M. Okubo, *Preparation of hemispherical particles by cleavage of micrometer-sized, spherical polystyrene/poly(methyl methacrylate) composite particles with Janus structures: effect of polystyrene-b-poly(methyl methacrylate).* Polym J, 2014.
152. Wang, Y., et al., *Janus-like polymer particles prepared via internal phase separation from emulsified polymer/oil droplets.* Polymer, 2009. **50**(14): p. 3361-3369.
153. Sundberg, D.C., et al., *Morphology development of polymeric microparticles in aqueous dispersions. I. Thermodynamic considerations.* Journal of Applied Polymer Science, 1990. **41**(7-8): p. 1425-1442.
154. Lamour, G., et al., *Contact Angle Measurements Using a Simplified Experimental Setup.* Journal of Chemical Education, 2010. **87**(12): p. 1403-1407.
155. Luo, X. and P.T. Mather, *Preparation and Characterization of Shape Memory Elastomeric Composites.* Macromolecules, 2009. **42**(19): p. 7251-7253.
156. Atala, A. and R.P. Lanza, *Methods of Tissue Engineering*. 2002: Academic Press.
157. Briddick, A., et al., *Surfactant and Plasticizer Segregation in Thin Poly(vinyl alcohol) Films.* Langmuir, 2016. **32**(3): p. 864-72.
158. Bahri, M.A., et al., *Investigation of SDS, DTAB and CTAB micelle microviscosities by electron spin resonance.* Colloids and Surfaces A: Physicochemical and Engineering Aspects, 2006. **290**(1–3): p. 206-212.
159. Chaudhuri, R.G. and S. Paria, *Dynamic contact angles on PTFE surface by aqueous surfactant solution in the absence and presence of electrolytes.* Journal of Colloid and Interface Science, 2009. **337**(2): p. 555-562.
160. Croll, T.I., et al., *Controllable Surface Modification of Poly(lactic-co-glycolic acid) (PLGA) by Hydrolysis or Aminolysis I: Physical, Chemical, and Theoretical Aspects.* Biomacromolecules, 2004. **5**(2): p. 463-473.
161. Good, R.J., *Contact angle, wetting, and adhesion: a critical review.* Journal of Adhesion Science and Technology, 1992. **6**(12): p. 1269-1302.
162. Kwok, D.Y. and A.W. Neumann, *Contact angle measurement and contact angle interpretation.* Advances in Colloid and Interface Science, 1999. **81**(3): p. 167-249.
163. Saito, N., Y. Kagari, and M. Okubo, *Effect of Colloidal Stabilizer on the Shape of Polystyrene/Poly(methyl methacrylate) Composite Particles Prepared in Aqueous Medium by the Solvent Evaporation Method.* Langmuir, 2006. **22**(22): p. 9397-9402.
164. Ge, X., et al., *Effects of concentration of nonionic surfactant and molecular weight of polymers on the morphology of anisotropic polystyrene/poly(methyl methacrylate) composite particles prepared by solvent evaporation method.* Colloid and Polymer Science, 2009. **287**(7): p. 819-827.
165. Kong, T., et al., *Engineering polymeric composite particles by emulsion-templating: Thermodynamics versus Kinetics.* Soft Matter, 2013.
166. CHINGUNPITUK, J., *Nanosuspension Technology for Drug Delivery.* 2011, 2011. **4**(2): p. 15.
167. Kesisoglou, F., S. Panmai, and Y. Wu, *Nanosizing — Oral formulation development and biopharmaceutical evaluation.* Advanced Drug Delivery Reviews, 2007. **59**(7): p. 631-644.

168. Teeranachaideekul, V., et al., *Development of ascorbyl palmitate nanocrystals applying the nanosuspension technology.* International Journal of Pharmaceutics, 2008. **354**(1–2): p. 227-234.
169. Verma, S., B.D. Huey, and D.J. Burgess, *Scanning Probe Microscopy Method for Nanosuspension Stabilizer Selection.* Langmuir, 2009. **25**(21): p. 12481-12487.
170. Zhu, W., et al., *Atomistic simulation study of surfactant and polymer interactions on the surface of a fenofibrate crystal.* Eur J Pharm Sci, 2011. **42**(5): p. 452-61.
171. Verma, S., R. Gokhale, and D.J. Burgess, *A comparative study of top-down and bottom-up approaches for the preparation of micro/nanosuspensions.* International Journal of Pharmaceutics, 2009. **380**(1–2): p. 216-222.
172. Patel, V.R. and Y.K. Agrawal, *Nanosuspension: An approach to enhance solubility of drugs.* Journal of Advanced Pharmaceutical Technology & Research, 2011. **2**(2): p. 81-87.
173. Wang, Y., et al., *Stability of nanosuspensions in drug delivery.* Journal of Controlled Release, 2013. **172**(3): p. 1126-1141.
174. Feng, T., S. Bates, and M.T. Carvajal, *Toward understanding the evolution of griseofulvin crystal structure to a mesophase after cryogenic milling.* International Journal of Pharmaceutics, 2009. **367**(1-2): p. 16-19.
175. Trotta, M., R. Cavalli, and D. Chirio, *Griseofulvin nanosuspensions from triacetin-in-water emulsions.* Stp Pharma Sciences, 2003. **13**(6): p. 423-426.
176. Zhu, W., et al., *Atomistic simulations of aqueous griseofulvin crystals in the presence of individual and multiple additives.* Chemical Engineering Science, 2012. **73**(0): p. 218-230.
177. Donoso, M.D., R.J. Haskell, and R.R. Schartman, *Surfactant choice and the physical stability of nanosuspensions as a function of pH.* International Journal of Pharmaceutics, 2012. **439**(1–2): p. 1-7.
178. Davis, H.T., *Factors determining emulsion type: Hydrophile—lipophile balance and beyond.* Colloids and Surfaces A: Physicochemical and Engineering Aspects, 1994. **91**(0): p. 9-24.
179. Huibers, P.D.T. and D.O. Shah, *Evidence for Synergism in Nonionic Surfactant Mixtures: Enhancement of Solubilization in Water-in-Oil Microemulsions.* Langmuir, 1997. **13**(21): p. 5762-5765.
180. Van Eerdenbrugh, B., et al., *A screening study of surface stabilization during the production of drug nanocrystals.* Journal of Pharmaceutical Sciences, 2009. **98**(6): p. 2091-2103.
181. Hong, C., et al., *Effects of stabilizing agents on the development of myricetin nanosuspension and its characterization: an in vitro and in vivo evaluation.* Int J Pharm, 2014. **477**(1-2): p. 251-60.
182. Lestari, M.L., R.H. Muller, and J.P. Moschwitzer, *Systematic screening of different surface modifiers for the production of physically stable nanosuspensions.* J Pharm Sci, 2015. **104**(3): p. 1128-40.
183. Hanafy, A., et al., *Pharmacokinetic evaluation of oral fenofibrate nanosuspensions and SLN in comparison to conventional suspensions of micronized drug.* Advanced Drug Delivery Reviews, 2007. **59**(6): p. 419-426.
184. Ma, J.K.H. and B. Hadzija, *Basic physical pharmacy*. 2013, Burlington, MA: Jones & Bartlett Learning.
185. Shinoda, K. and H. Saito, *The Stability of O/W type emulsions as functions of temperature and the HLB of emulsifiers: The emulsification by PIT-method.* Journal of Colloid and Interface Science, 1969. **30**(2): p. 258-263.
186. Wantanabe, A., *A Trial Production of a Table of the Optical Crystallographic Characteristics of Crystalline Drugs Including Crystal Habits.* Yakugaku Zasshi, 2002. **122**: p. 595-606.
187. Lee, J., J.Y. Choi, and C.H. Park, *Characteristics of polymers enabling nano-comminution of water-insoluble drugs.* International Journal of Pharmaceutics, 2008. **355**(1–2): p. 328-336.
188. Posocco, P., et al., *Interfacial tension of oil/water emulsions with mixed non-ionic surfactants: comparison between experiments and molecular simulations.* RSC Advances, 2016. **6**(6): p. 4723-4729.
189. Müller, R.H., *Colloidal Carriers for Controlled Drug Delivery and Targeting: Modification, Characterization and in Vivo Distribution*. 1991: Wiss. Verlag-Ges.
190. Fang, L., T. Wang, and B. Lamsal, *Synergistic effect of surfactants and silica nanoparticles on oil recovery from condensed corn distillers solubles (CCDS).* Industrial Crops and Products, 2015. **77**: p. 553-559.
191. Morpeth, F., *Preservation of Surfactant Formulations*. 2012: Springer Netherlands.
192. Li, T., B. Li, and M.S. Tomassone, *Surface characterization of aspirin crystal planes using*

molecular dynamics simulations. Chemical Engineering Science, 2006. **61**(15): p. 5159-5169.
193. Choi, S.-W., et al., *Thermodynamic parameters on poly(d,l-lactide-co-glycolide) particle size in emulsification–diffusion process.* Colloids and Surfaces A: Physicochemical and Engineering Aspects, 2002. **201**(1–3): p. 283-289.
194. Song, K.C., et al., *The effect of type of organic phase solvents on the particle size of poly(d,l-lactide-co-glycolide) nanoparticles.* Colloids and Surfaces A: Physicochemical and Engineering Aspects, 2006. **276**(1–3): p. 162-167.
195. Tyn, M.T. and W.F. Calus, *Diffusion coefficients in dilute binary liquid mixtures.* Journal of Chemical & Engineering Data, 1975. **20**(1): p. 106-109.
196. Hsu, J.P., *Interfacial Forces and Fields: Theory and Applications*. 1999: Taylor & Francis.
197. Gmehling, J., et al., *Chemical Thermodynamics for Process Simulation*. 2012: Wiley.
198. Cao, H., et al., *Intelligent Janus nanoparticles for intracellular real-time monitoring of dual drug release.* Nanoscale, 2016. **8**(12): p. 6754-6760.
199. Kamaly, N., et al., *Degradable Controlled-Release Polymers and Polymeric Nanoparticles: Mechanisms of Controlling Drug Release.* Chemical Reviews, 2016. **116**(4): p. 2602-2663.
200. Romanski, F.S., *The Production and Stabilization of Pharmaceutical Nanosuspensions*, in *Chemical and Biochemical Engineering*. 2011, Rutgers, the State University of New Jersey.
201. Gentile, P., et al., *An Overview of Poly(lactic-co-glycolic) Acid (PLGA)-Based Biomaterials for Bone Tissue Engineering.* International Journal of Molecular Sciences, 2014. **15**(3): p. 3640-3659.
202. Sah, H., et al., *Concepts and practices used to develop functional PLGA-based nanoparticulate systems.* International Journal of Nanomedicine, 2013. **8**: p. 747-765.
203. Budhian, A., S.J. Siegel, and K.I. Winey, *Production of haloperidol-loaded PLGA nanoparticles for extended controlled drug release of haloperidol.* J Microencapsul, 2005. **22**(7): p. 773-85.
204. Varshosaz, J., S. Taymouri, and H. Hamishehkar, *Fabrication of polymeric nanoparticles of poly(ethylene-co-vinyl acetate) coated with chitosan for pulmonary delivery of carvedilol.* Journal of Applied Polymer Science, 2014. **131**(1): p. n/a-n/a.
205. Amoozgar, Z. and Y. Yeo, *Recent advances in stealth coating of nanoparticle drug delivery systems.* Wiley Interdisciplinary Reviews. Nanomedicine and Nanobiotechnology, 2012. **4**(2): p. 219-233.
206. Greish, K., *Enhanced permeability and retention (EPR) effect for anticancer nanomedicine drug targeting.* Methods Mol Biol, 2010. **624**: p. 25-37.
207. Lorenzer, C., et al., *Going beyond the liver: Progress and challenges of targeted delivery of siRNA therapeutics.* Journal of Controlled Release, 2015. **203**: p. 1-15.
208. Bertrand, N., et al., *Cancer nanotechnology: The impact of passive and active targeting in the era of modern cancer biology.* Advanced Drug Delivery Reviews, 2014. **66**: p. 2-25.
209. Chang, J., et al., *Characterization of endocytosis of transferrin-coated PLGA nanoparticles by the blood–brain barrier.* International Journal of Pharmaceutics, 2009. **379**(2): p. 285-292.
210. Daniels, T.R., et al., *The transferrin receptor and the targeted delivery of therapeutic agents against cancer.* Biochimica et Biophysica Acta (BBA) - General Subjects, 2012. **1820**(3): p. 291-317.
211. Saul, J.M., A.V. Annapragada, and R.V. Bellamkonda, *A dual-ligand approach for enhancing targeting selectivity of therapeutic nanocarriers.* Journal of Controlled Release, 2006. **114**(3): p. 277-287.
212. Bhattacharyya, S., et al., *Efficient Delivery of Gold Nanoparticles by Dual Receptor Targeting.* Advanced Materials, 2011. **23**(43): p. 5034-5038.
213. Li, X., et al., *Enhancement of cell recognition in vitro by dual-ligand cancer targeting gold nanoparticles.* Biomaterials, 2011. **32**(10): p. 2540-5.
214. Wang, F., et al., *Dual Surface-Functionalized Janus Nanocomposites of Polystyrene/Fe3O4@SiO2 for Simultaneous Tumor Cell Targeting and Stimulus-Induced Drug Release.* Advanced Materials, 2013. **25**(25): p. 3485-3489.
215. Djohari, H. and E.E. Dormidontova, *Kinetics of Nanoparticle Targeting by Dissipative Particle Dynamics Simulations.* Biomacromolecules, 2009. **10**(11): p. 3089-3097.
216. Domb, A.J. and W. Khan, *Focal Controlled Drug Delivery*. 2014: Springer US.
217. Singh, R. and J.W. Lillard, *Nanoparticle-based targeted drug delivery.* Experimental and molecular pathology, 2009. **86**(3): p. 215-223.